ELSEVIER

Prog. Polym. Sci. 28 (2003) 261–302

PROGRESS IN POLYMER SCIENCE

www.elsevier.com/locate/ppolysci

Wetting at polymer surfaces and interfaces

Mark Geoghegan[a,*], Georg Krausch[b]

[a]*Department of Physics and Astronomy, University of Sheffield, Hounsfield Road, Sheffield S3 7RH, UK*
[b]*Lehrstuhl für Physikalische Chemie II, Bayreuther Institut für Kolloid- und Grenzflächenforschung (BZKG), Universität Bayreuth, D-95440 Bayreuth, Germany*

Received 4 February 2002; revised 2 August 2002; accepted 3 August 2002

Abstract

Experimental research on wetting in polymer films is a subject that is reaching maturity. We review progress from the past few years in research into the influence of a boundary in polymer blends, concentrating largely on the wetting transition, and the growth of wetting layers, where we pay particular attention to blends in which hydrodynamic flow plays a dominant role. A summary of work over the same period concerning the dewetting of polymer films is also included, along with a discussion of the role of pattern formation caused by dewetting and topographically and chemically patterned substrates. We conclude by summarising some experiments that we believe may inspire future research. © 2002 Elsevier Science Ltd. All rights reserved.

Keywords: Polymer films; Wetting; Dewetting; Pattern formation; Polymer blends; Wetting transition

Contents

* Corresponding author.
E-mail addresses: mark.geoghegan@sheffield.ac.uk (M. Geoghegan), georg.krausch@uni-bayreuth.de (G. Krausch).

PII: S0079-6700(02)00080-1

1. Introduction

The study of wetting phenomena at polymer surfaces and interfaces is a rapidly maturing subject since the first quantitative studies of surface segregation at the end of 1980s [1,2]. The wetting behaviour of thin polymer films is of great importance not only because of the applications of polymers for various industrial uses but also because of the importance of polymers as model systems to test mean field theories. Industrially, issues of wetting are clearly important in coatings. Indeed, wherever a stable film is necessary an understanding of wetting is required. The factors determining film stability, i.e. ensuring that the polymer wets the surface, require that the opposite phenomenon (dewetting) be also well understood. Wetting is also relevant for the study of pattern formation and other aspects of soft lithography. Finally, wetting phenomena are of interest in the rapidly growing field of biophysics. Here, applications range from the issue of biocompatibility, to the need for 'smart' surfaces that are capable of responding to the properties of the surrounding medium such as pH, ion concentration, or temperature.

Aside from its technological relevance, wetting behaviour at polymer surfaces and interfaces has proven to be important for the understanding of mean field theories of wetting in general. This is due to the variable length of polymer chains, the relatively small density fluctuations, and the relatively slow motion of the long chain molecules. Although the respective theories are generally not limited to polymers, polymer physics often offers the best test of the theory. A good example along this line is the theory of spinodal decomposition [3], which was developed to describe phase-separation processes in binary metal alloys. Very convincing observations of the early stages of phase separation have been described for polymeric systems [4], due to the possibility of observing the kinetics over longer time scales. Another benefit of working with polymers is that the size of the individual chains, typically a few nanometres in length, can be tailored by altering the molecular weight. In terms of wetting phenomena, this was well exemplified by the observation of surface-directed spinodal decomposition in polymer blends [5]. Here, phase separation does not proceed isotropically as it would like to in the bulk but is directed by the surface, and a layered structure is observed with a phase of the lower surface energy wetting the surface, with the second component forming a sub-layer below the surface. In the absence of thermal noise, the layered structure would proceed deep into the film. As it is, the layering is eventually broken up by thermal noise. Altering the molecular weight enables one to alter the miscibility of the mixture by adjusting the entropy of mixing, but without changing any thermodynamic parameters, and this has enabled a study of wetting as a function of miscibility [6].

The purpose of this review is to consider recent developments in wetting phenomena at surfaces. There have been several other reviews on this and related subjects that may be of interest to the reader. For example, earlier experiments on wetting in polymer films are reviewed in detail by Krausch [7]. We shall also not give too much consideration to segregation and wetting phenomena at buried interfaces because this has been more than adequately covered in a recent review by Budkowski [8]. An earlier review by Stamm may also be of interest here [9]. Stamm covers work on polymer interfaces but devotes most of his review to the techniques available for their study. For an overview of the relevant and important theory, the interested reader is advised to consult the review by de Gennes [10], which, though not recent, still contains much to recommend it. A later discussion of various theories and theoretical methods by Binder [11] is particularly useful because it compares experiment and theory from a theoretician's perspective. A discussion of the role of Monte Carlo simulations and self-consistent field theory in the structure of thin polymer blend films has recently been published [12]. On a related subject, Puri and Frisch published a shorter review concerning modelling in phase separating systems [13]. We exclude here most of the recent results on block copolymer thin films, which have been reviewed both by Krausch [7] and more recently by Fasolka and Mayes [14]. The science underpinning much of the research in this review is covered in the book by Jones and Richards [15].

The rest of the paper is organised as follows. We first discuss the progress that has been made in the work on wetting of the surface from one component of a polymer blend before we consider the complementary effects of spreading and dewetting. We conclude our review with a

Nomenclature

A_H	Hamaker constant
a	polymer segmental length
b	Flory–Huggins lattice parameter
D	diffusion coefficient
d-	deuterated-
$\Delta f'$	energy cost in having different surface composition from bulk
FReS	forward recoil spectrometry
F8BT	poly(9,9′-dioctylfluorene-*alt*-benzothiadiazole)
G	Gibbs free energy
G_{bulk}	Flory–Huggins free energy of mixing of a polymer blend
$\Delta G_{surface}$	surface contribution to Gibbs free energy
g	'squared gradient' term in the free energy of a polymer blend
h-	protonated- (non-deuterated)
ITO	indium tin oxide
k_B	Boltzmann's constant
L	layer, film thickness
l	size of prewetting layer
$l_{d,SAM}$	size of layer at SAM interface
LED	light emitting diode
LE-FReS	low energy forward recoil spectrometry
M_w	molecular weight
N, N_A, N_B	chain length (number of segments), and length of polymers A and B
NEXAFS	near edge X-ray absorption fine structure
NR	neutron reflectometry
NRA	nuclear reaction analysis
PB	polybutadiene
PCL	poly(ε-caprolactone)
PEDOT	poly(3,4-ethylene dioxythiophene)
PEO	poly(ethylene oxide)
PEP	poly(ethylene propylene)
PFB	poly(9,9′-dioctylfluorene-*alt*-bis-*N*,*N*′-(4-butylphenyl)-bis-*N*,*N*′-phenyl-1,4-phenylenediamine)
PFO	poly(9,9′-dioctylfluorene)
PI	polyisoprene
PMMA	poly(methyl methacrylate)
PS	polystyrene
PSS	poly(4-styrene sulphonic acid)
PS_xBrS_{1-x}	poly(styrene-*co*-bromostyrene)
PtBMA	poly(*tert*-butyl methacrylate)
PVDF	poly(vinylidene fluoride)
PVME	poly(vinyl methyl ether)
PVP	poly(2-vinyl pyridine)
PαMS	poly(α-methyl styrene)
R_g	polymer radius of gyration
S	spreading coefficient
s	surface interaction parameter
SAM	self-assembled monolayer
SAN	poly(styrene-*co*-acrylonitrile)
SBS	polystyrene-*block*-polybutadiene-*block*-polystyrene
SEM	scanning electron microscopy
SIMS	secondary ion mass spectrometry
SFM	scanning force microscopy
SNOM	scanning near-field optical microscopy

t	time
T	absolute temperature
t_{av}	average thickness of polymer film on topographically rough substrate
TEM	transmission electron microscopy
ToF	time of flight
t_{peak}	smallest thickness of polymer film on topographically rough substrate
W_{vdW}	energy due to van der Waals interactions
x	distance, film thickness
XPS	X-ray photoelectron spectroscopy
z	depth
z^*	surface excess
χ	Flory–Huggins interaction parameter
χ_s	Flory–Huggins interaction parameter evaluated on the spinodal
$\Delta\gamma$	surface energy (tension) difference
$\Delta\mu_{\alpha,\infty}$	$\partial G/\partial\phi$, evaluated at $\phi = \phi_\alpha$ or ϕ_∞
ε	quench depth
γ, γ_A, γ_B, γ_{AB}	surface energy (polymer film surface, substrate surface, film–substrate interface)
Γ	molecular surface excess
Φ	surface energy
ϕ	volume fraction
ϕ_s	surface volume fraction
ϕ_∞ and ϕ_d	bulk and depletion layer volume fractions
ϕ_α, ϕ_β	lower and upper coexistence volume fractions
λ	characteristic wavelength of dewetting or phase separation
μ, μ_s, μ_1	chemical potential, surface chemical potential, surface chemical potential difference
Θ_A, Θ_B	contact angles for a film A dewetting a deformable substrate, B
ρ	density
σ	surface free energy
ξ	bulk correlation length
ζ	thickness of surface segregated/wetting layer

discussion of the present situation of wetting as a mean to obtain pattern formation on structured substrates, before briefly discussing the areas that we believe will contribute significantly in the years to come.

2. Experimental techniques

Although we do not wish to provide a comprehensive review of the experimental techniques available for the study of wetting in polymer films, it is necessary to briefly describe some of the more important techniques in order to aid the following discussion. There are two classes of techniques that are relevant: depth profiling techniques and different forms of microscopy, which provide information on the lateral distribution of material. Several techniques, such as infrared experiments, that are not discussed here may also be relevant in certain experimental situations, and we refer the reader to the review by Stamm [9] for a fuller list and description of the techniques of interest. Many of the techniques described below are covered in more detail in the earlier review by Krausch [7], as well as the more specific reviews for the individual techniques cited below.

2.1. Depth profiling techniques

Depth profiling is used to determine the composition of one or more components of a film as a function of depth (i.e. in the direction perpendicular to the film's surface). In general these techniques are not particularly useful at providing lateral information on the composition of films but there is progress being made in this area. Ion scattering techniques and reflection experiments are the primary tools used for depth profiling.

Depth profiling is particularly important, when one requires information on the wetting properties of multi-component polymer mixtures. These mixtures are often unstable, and the component with the lower surface energy will segregate preferentially to the surface. However, whether or not this segregation corresponds to a wetting layer can only be determined by knowing the composition profile as a function of depth. The same applies to the wetting of a buried interface, e.g. a substrate, from a polymer mixture. One way of tackling such problems is to

etch away at the film, and taking measurements as the below-surface region is revealed, layer by layer. This is the principle behind dynamic secondary ion mass spectrometry (dynamic SIMS) [16]. With this technique a beam of ions, typically O_2^+ or Ar^+, etches the film, and the emitted fragments are analysed with a mass spectrometer. For known etching rates, it is possible to reveal a detailed profile of the composition of most elements in the film as a function of depth. SIMS can also be used in scanning and dynamic modes to obtain three-dimensional images, with a lateral resolution down to between 0.1 and 1 μm, either by scanning the image at each etching step [17], or by using an ion microscope [18].

Another method of direct depth profiling is MeV ion beam scattering [19,20]. Here, a beam of ions, produced by a van de Graaff or other accelerator is incident on the sample. These ions are scattered at the surface, or within the sample, and the particles emitted from nuclear reactions or fragments from collisions are detected. Scattering within the sample is due to collisions with the electron clouds, which act to reduce the incident energy of the ion. Such techniques can be used for depth profiling because the energy of the detected particles depends primarily on the energy of the incident particles, which, because of the inelastic collisions, in turn depends on the depth in the sample at which the scattering event took place.

Three MeV ion beam techniques are of particular importance and are worth mentioning separately. The first of these is Rutherford backscattering. An ion beam, usually of $^4He^{++}$, is backscattered by collisions with heavier elements in the sample. In wetting experiments, the technique is rarely used because of the need for a heavy element not usually found in polymer systems, although a form of contrast can be introduced by selectively staining one component of a mixture [21].

The ion beam technique with historically the greatest impact has probably been forward recoil spectrometry (FReS) [19,22], also referred to as elastic recoil detection analysis. Here, a $^4He^{++}$ beam scatters deuterium and hydrogen in the sample, which can both be detected in the forward scattering direction. With care a depth profile can be built up for both hydrogenated and deuterated components in a blend. Data accumulation in this technique is particularly rapid, but there have also been several developments of this technique to improve the depth resolution which is typically ~80 nm depending on the angle of incidence of the beam to the sample, such as the optimisation of energy (LE- or low energy FReS [23]), the use of a time-of-flight (ToF) apparatus [24], or the use of different ions [25,26] instead of $^4He^{++}$. However, each of these techniques has its drawbacks and, although not impossible, resolutions of better than ~10 nm are difficult to achieve.

The final ion beam technique worth mentioning is ^3He nuclear reaction analysis (NRA) [27,28]. Here, $^3He^{++}$ ions undergo a nuclear reaction with deuterons in the sample to give off α-particles and protons. Either of these can be detected, and their energy corresponds to the depth in the sample at which the reaction took place. As with FReS therefore, deuterium is used for contrast but the experimental arrangement is quite simple and a resolution of better than 20 nm can be routinely obtained.

The depth profiling techniques mentioned above obtain information about the composition in real space. By contrast, methods such as X-ray [29] and neutron reflectometry (NR) [29–31] offer depth information in reciprocal or momentum space. In these techniques, neutrons or X-rays are reflected from the sample, and the reflected radiation is detected as a function of the incident beam intensity. As with light, the amount reflected is dependent on the refractive index of the medium (we do not talk of a neutron refractive index, but rather the scattering length density of a material). The de Broglie wavelength of neutrons, cooled to a temperature of a little over 20 K by a liquid hydrogen moderator, is of the order of a few Angstroms, and similar to that of X-rays. As a result, these techniques reveal information on much shorter length scales compared to those of the real-space depth profiling techniques discussed above. A resolution of better than 1 nm is routinely achieved. NR is perhaps better suited to polymer depth profiling because of the ready availability of deuterium for contrast. X-ray reflectometry requires the presence of heavy elements for successful depth profiling. Since many materials are transparent to neutrons and X-rays, these techniques are particularly well suited for studies of buried interfaces. A difficulty with reflection techniques is the absence of real-space information because reflectivity is a function of neutron momentum and does not provide a unique one-to-one correspondence with a depth profile. Often the user will need to use a complementary technique, such as an ion scattering technique, in order to have enough information to fit the reflectivity data.

2.2. Microscopy techniques

In case information on the lateral distribution of material is required, alternative techniques are indispensable. In the field of wetting, optical and scanning force microscopy (SFM) have proven to be quite helpful. As long as the characteristic lengths are of the order of microns, optical microscopy is by far the easiest technique to obtain information on the lateral distribution of material in thin films. Reflection white light interference microscopy can provide sufficient contrast between lateral areas of different film thickness and/or optical beam paths. If smaller features are to be revealed, SFM is the method of choice. Topographical features are easily revealed and material contrast can be established either by differences in the mechanical properties of the materials [32,33] or by selective removal of one of the two phases in a selective solvent [34]. Care must, however, be taken when topographical features are imaged by TappingMode™

SFM in case the different phases have strongly different mechanical properties [35]. Here, differences in tip indentation into the surface may interfere with real topographical features and the interpretation of the apparent surface topography may be non-trivial.

As an alternative technique, scanning near-field optical microscopy (SNOM or NSOM) combines the aspects of both optical microscopy and SFM [36,37]. By use of a nanoscopically sized optical aperture, which is usually a tapered optical fibre, kept some nanometres above the sample surface by a non-contact force measurement ('shear force' distance control), the diffraction limit of conventional optics can be circumvented. The technique has been applied to the early stage of lateral phase separation in polymer blends [38]. It is fair to say, however, that SNOM is still subject to technical problems and has not played the role anticipated in the early 1990s [39].

A recent and quite powerful alternative to SFM measurements is the use of a scanning electron microscope (SEM) equipped with a field emission electron source. Due to the small source size, rather low acceleration voltages are sufficient to achieve the desired lateral resolution. In consequence, many thin polymer films—though non-conductive in bulk—can be imaged without coverage by a conducting material (metals, carbon, etc.). Different polymeric materials can often be distinguished without heavy metal staining by virtue of work function differences. Indeed, field emission SEM can also be operated in transmission mode to circumvent problems associated with normal transmission electron microscopy (TEM), such as poor contrast [40]. Compared to SFM, fast large area scans and fast zoom ups are possible and even a chemical contrast can often be realised. However, height differences cannot quantitatively be mapped.

Finally, we point to a recent extension of SFM to bulk imaging [41]. Magerle has shown that high spatial resolution volume images can be created by an iteration of SFM and suitable removal of a thin surface layer, e.g. by plasma etching. In case of multiphase materials, where the different phases can be distinguished, e.g. by their mechanical properties, the bulk structure of the material can be reconstructed from a stack of SFM topography and phase images by suitable image processing. This technique is referred to as *nanotomography*. Konrad et al. have applied this technique to unravel the thin film structure of a PS-*block*-PB-*block*-PS triblock copolymer (SBS, where PS refers to polystyrene and PB refers to polybutadiene) [42]. Spatial resolution of some few nanometres along all three spatial axes was demonstrated.

Surface analysis by ion scattering is also possible, although usually fails to provide the lateral resolution offered by the scanning probe techniques. However, both SIMS and X-ray photoelectron spectroscopy (XPS) can provide lateral chemical information. XPS is probably the more commonly used given its relatively simple principle. In XPS experiments [43], X-rays are incident on the sample. Photoelectrons are emitted from the first few nanometres of the sample, and their energy is not only characteristic of the elemental composition of the sample, but also of the bonding, which can provide important molecular information. The principle behind SIMS has already been mentioned above. Probably, the best method of using 'static' SIMS to obtain quantitative surface information is by using a ToF spectrometer [44], whereby large mass fragments of several kDa can be detected and sensitivity in the detection of the emitted ions is maximised.

There have also been improvements in the microscopy of surfaces using X-rays. The main contribution has come from workers using the near edge X-ray absorption fine structure (NEXAFS) technique [45]. The NEXAFS technique requires the use of an X-ray microscope on a synchrotron source. Despite demanding requirements, the ability of NEXAFS to provide chemical contrast with a spatial resolution of much better than 0.1 μm has ensured its use in a number of studies on polymer blends [46–48]. Both X-ray and NR can reveal in plane information such as roughness but both X-ray and neutrons also have the capacity to seek out lateral length scales by either analysing diffuse scattering with X-rays [49–51] or by considering off-specular neutron reflection [52].

3. Polymer blends

3.1. A brief historical introduction

Early work on the surface of polymer blends was concerned with the characterisation of the near-surface composition by techniques such as XPS or attenuated total reflection–Fourier transform infrared (ATR-FTIR) spectroscopy [53]. A particularly important example of early work pertinent to the material covered in the present review was light scattering and optical microscopy measurements characterising the formation of domains in phase separating thin films of PS and poly(vinyl methyl ether) (PVME) [54]. In another PS/PVME blend (although this one was miscible), XPS was used to show that PVME preferentially adsorbs to the surface [1]. By varying the angle at which the photoelectrons were ejected, a depth profile was obtained. This enabled the authors to obtain the characteristic length for the surface-enriched layer, which was seen to be of the order of the chain size.

A few years before these pioneering XPS measurements, important theoretical work was being developed to describe surface effects in a polymer blend film [55]. This work extended the applicability of the mean field theory of wetting [56] to include polymer mixtures. Importantly, it allowed the experimentalist to easily predict the shape of the depth profile, provided there was sufficient knowledge of relevant material parameters (molecular weight, Flory–Huggins χ-parameter [57,58], and the surface energy difference between the two

components). The first experiment describing a test of this theory was published by Jones et al. in 1989 [2]. Taking advantage of the small difference in surface energies between the components of isotopic polymer mixtures, the authors used FReS to quantify the surface segregation of deuterated polystyrene (d-PS) from a mixture with normal (non-deuterated) PS. The lower surface energy of the d-PS is believed to lie in the small difference in polarisability in the C–H and C–D bonds, respectively.

The next major step, also from Jones et al., was the demonstration of self-assembly in thin films of an immiscible polymer blend of an isotopic mixture of poly(ethylene propylene) (PEP) [5]. In this case the mixture would normally phase separate without an energy barrier via spinodal decomposition leading to a spatially isotropic domain structure. However, the preferential accumulation of the lower surface energy component leads to one-dimensional composition waves in the direction perpendicular to the plane of the surface. In the experiments described, these composition waves met and interfered in the centre of the film.

Progress in this field was rapid, with various authors next considering the effect of the chemical nature of the substrate [59], the film thickness [60], and the growth rate of the surface-wetting layer [61,62].

Although there have been more recent experiments relating to the development of some of the above, we first turn our attention to the historically important quest for the observation of the wetting transition in a polymer blend film.

3.2. Wetting transition

As we have mentioned, the framework for discussing wetting phenomena in binary mixtures derives from the first paper by Cahn in 1977 [56]. A few years later, it was realised that polymer mixtures are ideal for the study of wetting, first by Nakanishi and Pincus [63], and then by Schmidt and Binder [55]. However, as should be apparent from earlier comments in this review, these two papers were somewhat ahead of their time because the experimental techniques at the beginning of the 1980s were not suitable for the indisputable observation of a wetting transition. Indeed, it was not until the year 2000 that the first observations in polymer mixtures were published.

A wetting transition occurs when the free energies of a partially wetting film is the same as that of a completely wetting film. The transition can be viewed by altering relevant experimental parameters. For a first order phase transition hysteresis is expected while this is not the case for a second order transition. The mathematics of the wetting transition is discussed in Appendix A.

In the purest sense, observation of a wetting transition requires the demonstration of the transition from a partially wetted surface to a macroscopically thick wetting layer. It has been argued that, because of the long diffusion times of polymers, a macroscopically thick wetting layer would be very difficult to achieve [11], meaning that the wetting transition could not be observed in polymer blend films. In this case the experiments that are described in this section merely *locate* the wetting transition rather than present an *observation* of it. However, this is an issue of semantics and so we do not consider it further.

3.2.1. Experimental tests

In a polymer blend, there are three experimental parameters that can be varied to observe the wetting transition: temperature, composition, and molecular weight. In the two studies identifying the wetting transition, Rysz et al. [64] varied temperature and composition, while Geoghegan et al. [6] varied the molecular weight, M_w.

The polymer blend chosen by Rysz and co-workers was a mixture of random polyolefin copolymers of poly(ethylene-*co*-ethylethylene) with differing ratios of ethylene to ethylethylene in the components of the blend. A mixture of 75% deuterated ethylethylene characterised by degree of polymerisation, $N = 1625$, with a copolymer containing 66% ethylethylene (non-deuterated, $N = 2030$) was used for the studies. The depth profiling techniques of dynamic SIMS and NRA were used for these studies; hence the need for deuterium to give contrast. The approach of Rysz et al. was to observe both equilibrium profiles and the dynamics of wetting. The necessity for the dynamics is clear; a wetting layer must grow indefinitely, whereas a layer corresponding to partial wetting will stop growing when it achieves equilibrium. However, the equilibrium profile is useful as it provides a conformation that the Cahn model describes the system. As the binodal is approached, the adsorbed amount increases asymptotically. The adsorbed amount is often denoted by the surface excess, z^* (Fig. 1), which is defined by

$$z^* = \int_0^\infty (\phi(z) - \phi_\infty)\mathrm{d}z, \tag{1}$$

where $\phi(z)$ is the fraction of material by volume (volume fraction) at a depth, z and ϕ_∞ is the bulk volume fraction ($z = \infty$). If a depletion layer ($\phi < \phi_\infty$) exists between the wetting layer and the bulk, then the surface excess is defined with respect to the height of the depletion layer and not the bulk material. Rysz et al. were able to observe the increase in surface excess as a function of bulk volume fraction. The phase diagram was measured previously [65] and is shown

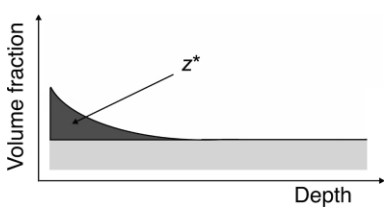

Fig. 1. Schematic diagram illustrating the measured adsorbed amount or surface excess (z^*).

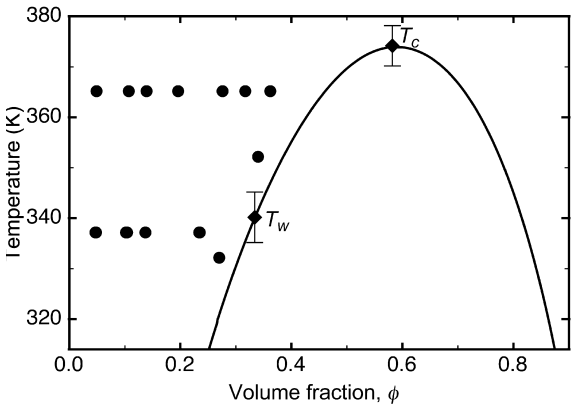

Fig. 2. Phase diagram for the polyolefin blend studied by Rysz et al. [64]. The circles represent the samples for which measurements were taken, and the diamonds correspond to the points on the coexistence curve corresponding to the wetting transition, T_w and the critical point, T_c. Reprinted with permission from Europhys Lett 2000;50:35. © 2000 EDP Sciences [64].

in Fig. 2 along with the samples measured. In Fig. 3 we show their results for two temperatures, 365 and 337 K, respectively, above and below the wetting transition temperature, ($T_w = 340 \pm 5$ K). The data are plotted as a function of distance from coexistence (i.e. ϕ_∞/ϕ_α). Samples measured at 365 K exhibit larger equilibrium surface excess, as they are nearer to coexistence in comparison with the blends at the lower temperature. By measuring the adsorbed amount, it is possible to determine the surface energy difference between the two components, and thus calculate the surface chemical potential, $-\mathrm{d}\Phi/\mathrm{d}\phi_s$. The details of this calculation are shown in Appendix A, and further discussion of the surface energy of these polyolefin blends has been presented elsewhere [65,66]. In Fig. 4 we show $-\mathrm{d}\Phi/\mathrm{d}\phi_s$ plotted with the corresponding bulk term $2\sqrt{(g\Delta f'(\phi))}$ (g and $\Delta f'(\phi)$ are defined in Appendix A). The

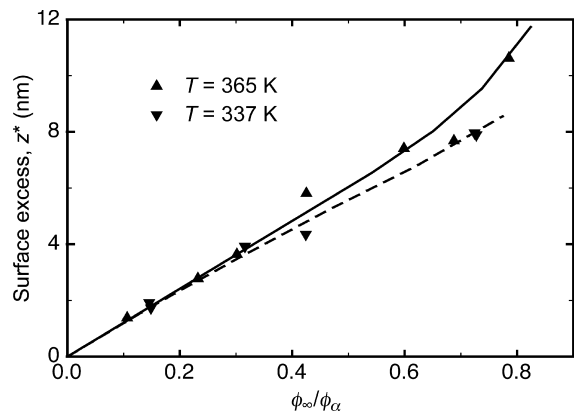

Fig. 3. Two adsorption isotherms as a function of ϕ_∞/ϕ_α for the polyolefin mixture [64] at temperatures above and below T_w. Reprinted with permission from Europhys Lett 2000;50:35. © 2000 EDP Sciences [64].

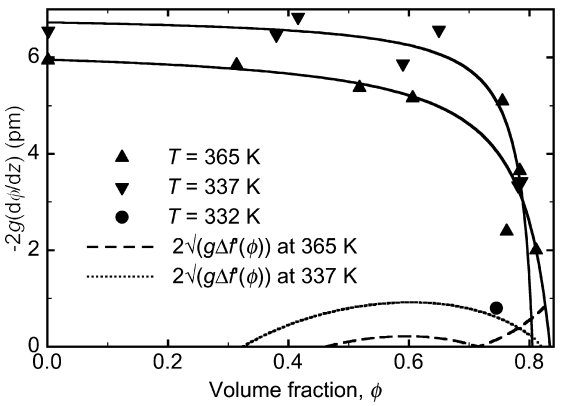

Fig. 4. Phase portraits for the blends used by Rysz et al. [64]. The intersection of $2\sqrt{(g\Delta f'(\phi))}$ (broken lines) with $-\mathrm{d}\Phi/\mathrm{d}\phi_s$ (solid lines and symbols) occurs on either side of the wetting transition. The mathematics of such phase portraits is discussed in Appendix A. Reprinted with permission from Europhys Lett 2000;50:35. © 2000 EDP Sciences [64].

$-\mathrm{d}\Phi/\mathrm{d}\phi_s$ term represents the benefit in having the component of the lower surface energy at the surface, whereas the $2\sqrt{(g\Delta f'(\phi))}$ term corresponds to the cost in having a composition gradient and a surface composition different to that in the bulk. If the curve for $-\mathrm{d}\Phi/\mathrm{d}\phi_s$ does not intersect the bulk term, $2\sqrt{(g\Delta f'(\phi))}$, then only total wetting can occur. If these lines do intersect then the free energy minimum is governed by whichever term dominates, and this is discussed in Appendix A. The fit to $-\mathrm{d}\Phi/\mathrm{d}\phi_s$ intersects $2\sqrt{(g\Delta f'(\phi))}$ in the region of partial wetting at the lower temperature (i.e. between the two values of surface volume fraction ϕ_s, where $2\sqrt{(g\Delta f'(\phi))} = 0$), and in the region of complete wetting at 365 K (i.e. the intersection occurs at a value of ϕ_s greater than where $2\sqrt{(g\Delta f'(\phi))} = 0$), demonstrating that these two temperatures straddle the wetting transition.

Although the surface segregation measurements discussed above demonstrate the existence of a wetting transition, there is little difference between partial and complete wetting. To remove any doubt that they had located the wetting transition, Rysz and co-workers performed measurements on the dynamics of wetting [64]. A difficulty in measuring wetting dynamics is that, as the surface layer grows, the bulk is depleted of material. This means that, unless the film is very thick, a continuously growing wetting layer is difficult to observe. However, this problem can be circumvented following an idea of Steiner and co-workers [67–69]. Two coexisting layers are placed in contact with each other. On annealing, the wetting layer should grow with a continuous supply of material from the lower film, which is rich in the wetting component. This is shown in Fig. 5. Indeed, if the two layers are not particularly thick, the layers will eventually invert [69]. By annealing these films for periods of more than 2 months, it becomes possible to distinguish which layers had reached equilibrium,

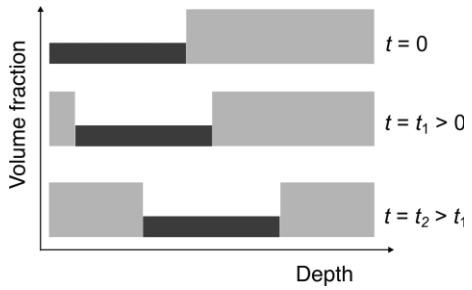

Fig. 5. Schematic diagram showing how a film of two coexisting phases will wet the surface layer. At $t = 0$ the lower coexisting phase is at the surface, with the upper coexisting phase underneath. However, with the upper coexisting phase favouring the surface, material will flow through the film from the substrate layer to the surface. The net effect of this is to shift the lower coexisting phase towards the substrate.

and which grew continuously; we show representative data in Fig. 6. The bilayer film annealed for 73.2 days at 332 K is unchanged from a profile obtained after annealing for 12.6 days and so has reached equilibrium but the one annealed for 3.4 days at 352 K exhibits a wetting layer that is still growing. Scaling the temperature of the wetting film to 332 K gives an annealing time of 18.8 days [70], so the different wetting behaviour must lie in the films being annealed on either side of a wetting transition.

Another route to the observation of the wetting transition utilises the two-phase region of the phase diagram. The surface layer should be stable for shallow quenches into the two-phase region, but is expected to break-up into droplets for deeper quenches. This was exploited by Geoghegan et al. [6], who looked at partially miscible blends of d-PS and poly(α-methylstyrene) (PαMS) in the unstable region of the phase diagram. In an earlier study, it was observed that the

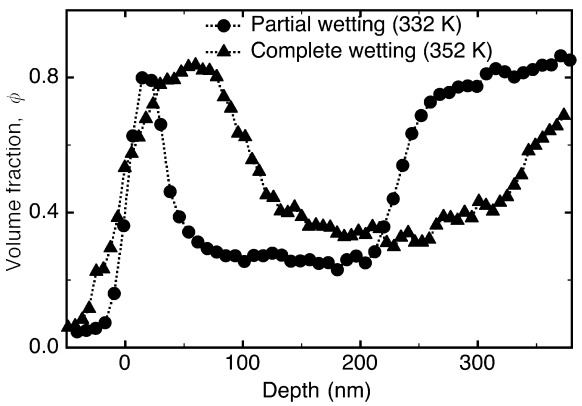

Fig. 6. Dynamic SIMS data for polyolefin films annealed for 73.2 days at 332 K and 3.4 days at 352 K. See text for molecular parameters. These films were initially bilayers at their coexisting compositions at the required temperatures as described in Fig. 5. The sample annealed at 332 K has reached equilibrium, whilst that at 352 K consists of a growing wetting layer.

wetting layer in this blend grows logarithmically with time [62], an observation previously associated with wetting at coexistence [68]. Puri and Frisch later suggested that the d-PS/PαMS blend represented a good example of a low noise system [13], which in turn meant that the more common $t^{1/3}$ growth of the surface layer should be achieved by deeper quenches. By changing the molecular weight, deeper quenches were accessible, and NRA measurements on the growth law showed that there was indeed a transition to a faster growth law. The $t^{1/3}$ growth is indicative of the coarsening of droplets at the surface. SFM measurements on these films showed that there was a change in the roughness of the film. The logarithmic growth corresponded to surfaces that remained flat (r.m.s. roughness remained below 1 nm), whereas the deeper quenches corresponded to much rougher films (r.m.s. roughness of typically ~4 nm).

The identification of a wetting transition by both sets of workers completes what we believe to be the final major task concerning the fundamental physics of wetting in polymer blends. However, there are still many important goals for the interested experimentalist to achieve. Hysteresis in the location of the transition between partial and complete wetting was not observed in any of the experiments discussed above even though hysteresis is inherent in any first order transition. Another interesting challenge is the observation of a second order wetting transition [56,71], although there are theoretical arguments suggesting that this might be very difficult to achieve experimentally [71,72] (see also Appendix A).

3.3. Other polymer blend film depth profiling experiments

3.3.1. Kinetics of wetting layer growth

The growth of surface layers is largely, but not exclusively, dependent on thermodynamic factors, with the miscibility of the polymer blend being a crucial example. First experiments were performed on mixtures of polyisoprene (PI) and PEP [73]. Using light scattering two length scales of phase separation were observed; a bulk length scale growing linearly with time, t, and a wetting layer that grew with $t^{3/2}$. The bulk behaviour is to be expected from hydrodynamic flow, but the explanation of the 'fast mode' of surface growth is still something of a mystery. Explanations for the fast mode include a coarsening-related effect [74], but most workers believe it to be of hydrodynamic origin [75,76] although as yet no theory has been fully tested. We shall turn to hydrodynamic wetting layer growth later in this review. However, measurements on a less immiscible isotopic mixture of PEP revealed a $t^{1/3}$ growth law [61]. Although it is not a trivial matter to identify the growth law with the nature of the wetting layer, the authors observed dynamic scaling, meaning that the shape of the depth profiles becomes independent of time when the profiles are scaled to the thickness of the wetting layer. Since the wetting layer is growing as $t^{1/3}$ and dynamic

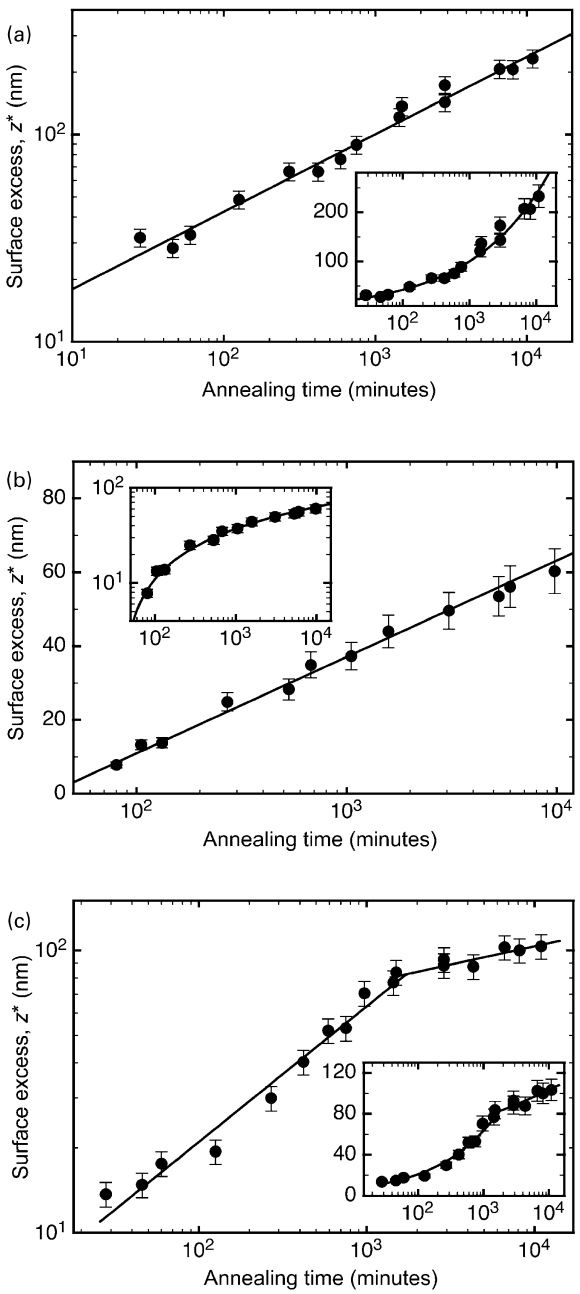

Fig. 7. Wetting layer growth for a d-PS-rich phase from a mixture with PαMS for three different molecular weight pairs [6]. (a) A very immiscible blend (M_w(d-PS) = 163 kDa, M_w(PαMS) = 108 kDa, and $\phi_\infty = 0.43$) with $\varepsilon = 2.4$ exhibits a $t^{0.37}$ growth of the surface excess. (b) A blend with $\varepsilon = 0.44$ (M_w(d-PS) = 80 kDa, M_w(PαMS) = 41.7 kDa, and $\phi_\infty = 0.37$) has a wetting layer that grows logarithmically in time. (c) The wetting layer for a shallow quench (M_w(d−PS) = 35 kDa, M_w(PαMS) = 41.7 kDa, and $\phi_\infty = 0.52$), with $\varepsilon = 0.06$, grows initially with $t^{0.47}$ before slowing to $t^{0.13}$. This growth at later times may well be logarithmic. Reprinted with permission from Phys Rev E 2000;62:940. © 2000 American Physical Society [6].

scaling is observed, bulk phase separation also exhibits a $t^{1/3}$ behaviour. Other measurements on polyolefin blends found growth laws slower than the $t^{1/3}$, which were explained in terms of long-range forces. Steiner and Klein [67] observed the wetting layer to grow as $t^{0.20}$, but a logarithmic growth law could fit the data equally well. Because the logarithmic growth is a signature of a short-range surface potential, the authors estimated a decay length for an exponentially decaying surface field to some 31 nm. This rather large value led the authors to question the role of short-range forces. In truth other short-range surface fields will give a logarithmic growth [77,78], so the validity of this decay length is not clear. However, to extinguish any doubt concerning the importance of long-range forces for the growth of the wetting layers in their system, Steiner and Klein calculated a Hamaker constant from their power law growth to be in the order of 10^{-21}–10^{-20} J in agreement with the expectation for such non-polar mixtures.

Later measurements on a blend of PS and poly(α-methylstyrene) (PαMS) showed a logarithmic growth of the surface layer as well [62]. A power law growth of $t^{0.14}$, which also could provide a good fit to the data, cannot be readily explained in terms of long-range forces. However, in the same study, a layer near, but not at, the substrate exhibited a $t^{1/3}$ growth. This implies that, like the earlier measurements on the mixture of PI and PEP [73], not all systems demonstrate the same behaviour in the bulk and at the surface. A more detailed study of mixtures of PS and PαMS revealed three growth laws as the molecular weight wa changed, thereby changing the immiscibility [6]. The quench depth, ε, is a measure of immiscibility and is given by

$$\varepsilon = \frac{\chi - \chi_s}{\chi_s}, \tag{2}$$

where χ_s is the value of the Flory–Huggins interaction parameter, χ on the spinodal. The results for the surface excess as a function of annealing time for three of the quench depths studied are shown in Fig. 7, taken from Ref. [6]. For the shallowest quench inside the two-phase region ($\varepsilon = 0.06$, corresponding to M_w(d-PS) = 35 kDa and M_w(PαMS) = 41.7 kDa) a $t^{1/2}$ growth law was observed (Fig. 7(c)), which slowed down at later times. For slightly deeper quenches ($\varepsilon = 0.44$, corresponding to M_w(d-PS) = 80 kDa and M_w(PαMS) = 41.7 kDa) a region of logarithmic growth was observed (Fig. 7(b)). At the deepest quenches ($\varepsilon = 2.4$; M_w(d-PS) = 163 kDa and M_w(PαMS) = 108 kDa), the $t^{1/3}$ behaviour was recovered (Fig. 7(a)). The crossover from logarithmic to $t^{1/3}$ surface growth corresponds to the crossover from complete to partial wetting, and it is therefore between these quench depths that the wetting transition discussed above lies (Section 3.2).

In Fig. 8 we schematise the growth of wetting layers for the different quench depths. At the bottom we show a surface layer that is rich in the wetting component, but for which the wetting layer is not stable, and droplets are

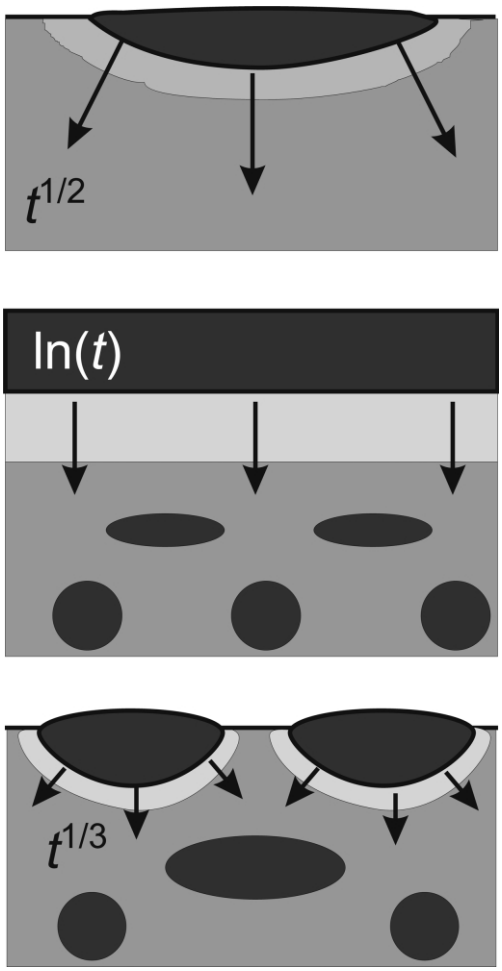

Fig. 8. Schematic diagram of the growth of the wetting layer as a function of quench depth. For the shallowest quench, wetting begins with a $t^{1/2}$ growth law as the surface-favoured component diffuses to the surface to form surface droplets. Slightly deeper quenches have a wetting layer growing with bulk phase separation occurring simultaneously. Here, the surface layer growth is logarithmic. For the deepest quench, the behaviour at the surface is similar to that in the bulk, with phase-separated droplets coarsening. The growth of the surface layer is then $t^{1/3}$.

formed on the surface. The wetting layer is not stable because the χ-parameter is so large that a growing wetting layer cannot survive and breaks up. Here, there are also droplets in the bulk, and both surface and bulk droplets are growing with $t^{1/3}$ behaviour because they are both exhibiting Lifshitz–Slyozov-like coarsening ($t^{1/3}$) [79].

For shallower quenches (middle diagram of Fig. 8), the surface-wetting layer is stable and grows continuously. At the same time, there are domains growing in the bulk. As these domains grow, there is less material to be supplied to the wetting layer and so the wetting layer cannot grow with a diffusion-limited $t^{1/2}$ growth, but instead grows logarithmically with time.

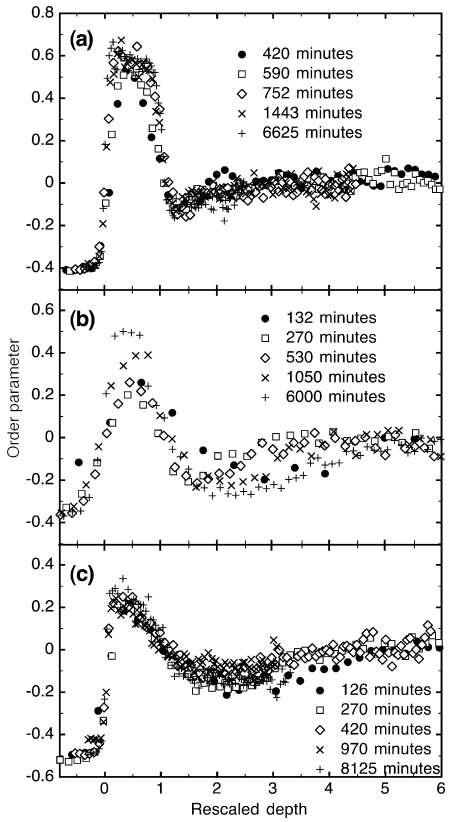

Fig. 9. Dynamic scaling plots corresponding to the same blends as in Fig. 7 [6]. The order parameter is given by $\phi - \phi_\infty$ and the wetting layer is scaled to a thickness of 1. Dynamic scaling is *not* exhibited only where logarithmic growth is observed (b).

The most surprising growth law is the $t^{1/2}$ behaviour. The $t^{1/2}$ growth itself suggests a simple diffusive growth. However, if the bulk were not being depleted in the component which wets the surface, a $t^{1/2}$ growth would be possible. The authors assumed that droplets were forming on the surface, and because no phase separation was (yet) occurring in the bulk, the bulk was behaving like a semi-infinite reservoir for the surface layer. This is illustrated schematically in the top diagram of Fig. 8. At later times, this was not the case and the surface layer became starved of material, eventually slowing down the wetting layer growth (middle diagram of Fig. 8).

To test these hypotheses, dynamic scaling was used. Here, the wetting layer is assumed to have constant thickness with time, and the depth profile is normalised so that the wetting layer thickness does not change. If there is no phase separation in the bulk, as we supposed for the $t^{1/2}$ growth, then dynamic scaling should occur as there is only one length scale present in the system, i.e. the thickness of the wetting layer. For the logarithmic growth, dynamic scaling should fail because the wetting layer is growing logarithmically but Lifshitz–Slyozov-like coarsening ($t^{1/3}$) [79] is expected to be occurring in the bulk. Finally, the

region of $t^{1/3}$ growth should exhibit dynamic scaling for the same reasons as in the earlier experiments of Krausch et al. [61], i.e. a surface layer and bulk phase separation are both occurring with a $t^{1/3}$ behaviour. As can be seen from Fig. 9 this is indeed what was observed.

In closing this discussion we note that, although the arguments noted above are relatively simple, theoretical work is ongoing and may shed some further light on the interpretation of this, and similar, work [80].

In this section, we have described the kinetics of the growth of wetting layers, and we have given some indication of how wetting layers may form by describing experiments on very shallow quenches [6], but the question as to what precedes the wetting layer is still an open one. It may well be the case that before logarithmic growth there may well be a small region of $t^{1/2}$ growth, but there are as yet no data on how the wetting layer is formed in films which are expected to exhibit $t^{1/3}$ or hydrodynamic ($\propto t$) growth. We expect that future research will consider this problem in more detail, but a related problem as to how the surface layer forms in systems prior to phase separation has been achieved, and we turn to this next.

3.3.2. The approach to phase separation

In a miscible polymer blend, the time scale for the surface layer formation is controlled by how long it takes for the polymer with the lower surface energy to diffuse to the surface. This diffusion-limited surface layer growth was discussed by Jones and Kramer [81] in terms of a simple model. The model consists of the depth profile of a polymer blend controlled by three compositions: the surface volume fraction, ϕ_s, the volume fraction of the depletion layer underneath the surface layer, ϕ_d, and the volume fraction in the bulk material, ϕ_∞. The assumption underpinning the three-layer model is that the layers are continuously in equilibrium with each other [82]. Then one can set the surface excess, z^* to be given by

$$z^* = (\phi_\infty - \phi_d(t))\sqrt{Dt}, \tag{3}$$

where D is the interdiffusion diffusion coefficient. Since the size of the surface layer in an undersaturated system (i.e. $\phi_\infty < \phi_\alpha$) grows logarithmically with the distance from the binodal ($\phi_\alpha - \phi_d$), we obtain (see Appendix A for details of the calculation and the inherent assumptions)

$$z^* = -\zeta \ln\left(\frac{\phi_\alpha - \phi_d}{\phi_\alpha}\right), \tag{4}$$

where ζ is a length representing the size of the surface segregated layer. Eliminating ϕ_d, we obtain

$$z^* = (\phi_\infty - \phi_\alpha(1 - \exp(-z^*/\zeta)))\sqrt{Dt}. \tag{5}$$

As phase separation is approached, the logarithmic term in the surface excess becomes important. Geoghegan et al. tested this kinetics on an isotopic PS blend using NR [83]. In these experiments, the surface excess was measured as a function of annealing time at a constant measurement temperature of 457 K. In Fig. 10 we show this growth as a function of $\sqrt{t}$ for the two blends measured. The agreement with the model is reasonable. The simulations (solid lines) were produced by least square fits varying the values of ζ and D. The mutual diffusion coefficient obtained from these results was also compared with previous measurements [84–86], and agreement was found to be acceptable (within an order of magnitude). The surface energy difference between the two components was obtained from ϕ_s (Appendix A) to 0.12 mJ/m^2 for the miscible blend. For the partially miscible blend, a somewhat larger value of 0.21 mJ/m^2 was found. This is a significant variation, given that the surface energy of high polymers is only a weak function of molecular weight [87]. Nevertheless, the values obtained are in reasonable agreement with other similar studies [2,26,88]. Despite minor discrepancies it is possible to conclude that standard mean-field theory may be used to explain the behaviour of polymer blends as the coexistence curve is approached. We now contrast these results with a related experiment, in which the standard theory, as outlined above, cannot be used.

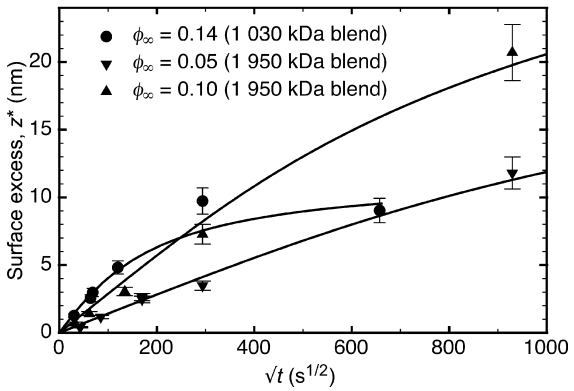

Fig. 10. Measurements of surface excess as a function of annealing time for the two blends of d-PS and h-PS [83]. In each case the d-PS and h-PS have the same molecular weight: 1.03×10^6 Da for a completely miscible blend (with $\phi_\infty = 0.14$), and 1.95×10^6 Da for a partially miscible blend (with $\phi_\infty = 0.05$ and 0.10). The solid lines are simulations obtained from the simple theory discussed in the text. Reprinted with permission from Macromolecules 1997;30:4220. © 1997 American Chemical Society [83].

In a different approach to study surface segregation at the onset to phase separation, Genzer and Composto studied thin films of PS (with $N_A = 1650$ chain segments) and a random copolymer of styrene and bromostyrene (PS_xBrS_{1-x}, with $N_B = 1670$ chain segments and $x = 0.92$) as the critical point was approached [89]. The thickness of the surface layer in such experiments was found to be smaller than the values predicted by the standard mean field theory discussed above, suggesting that bulk parameters such as χ were playing an increasingly important role in the size of the surface layer. In these experiments, LE-FReS was used to measure the surface excess as T_c was approached from the

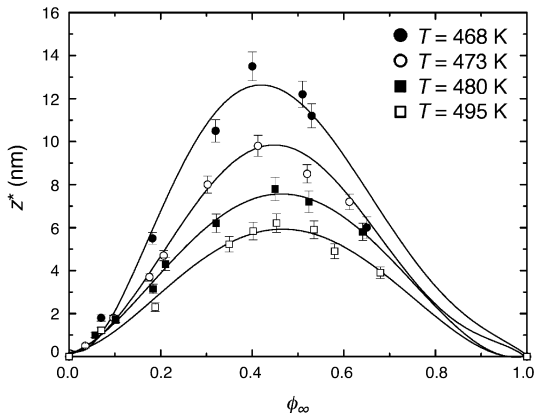

Fig. 11. Equilibrium surface excess of d-PS ($N = 1650$) mixed with PS_xBrS_{1-x} ($x = 0.92$, $N = 1670$) for various values of ϕ_∞ at various temperatures approaching the critical point ($T_c = 462$ K) [89]. The symbols are the LE-FReS data and the solid lines are guides to the eye. Reprinted with permission from Europhys Lett 1997;38:171. © 1997 EDP Sciences [89].

one phase region ($T_c \approx 462$ K). In Fig. 11 the values of surface excess determined for four different temperatures are shown as a function of ϕ_∞ (the system was symmetric with a critical volume fraction of 0.502). From these data, one sees that the surface excess increases as the critical point is approached. However, it is also possible to calculate the surface free energy from the off-critical data, and it was noted that the surface chemical potential, μ_s (Appendix A) remained constant except for the symmetric blends, where it decreased. The discrepancy was observed to be larger closer

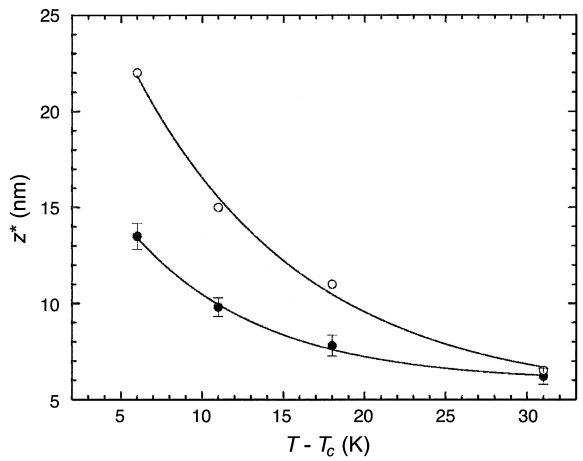

Fig. 12. Equilibrium surface excess as a function of $T - T_c$ for d-PS/PS_xBrS_{1-x} mixtures at $\phi_\infty \approx 0.5$ [89]. Solid circles represent the experimental low energy FReS data, whilst open circles show theoretical predictions obtained by using mean field theory to calculate the surface free energies. The solid lines are guides to the eye. Reprinted with permission from Europhys Lett 1997;38:171. © 1997 EDP Sciences [89].

to T_c. In Fig. 12 we show z^* for symmetric systems as the critical point is approached. The values calculated from the surface free energy are also shown; here they are considerably larger than the measured values. To explain this result, the bulk correlation length ξ was invoked as the size of the surface layer, with the approximation that

$$z^* \approx \xi(\phi_s - \phi_\infty). \tag{6}$$

The bulk correlation represents the length over which composition fluctuations remain significant and can be shown for symmetric systems to be [90]

$$\xi = \frac{a}{6\sqrt{\phi_\infty(1-\phi_\infty)(\chi_s - \chi)}}, \tag{7}$$

where χ_s corresponds to the value of χ at the critical point. Using a form for the surface tension derived from the Gibbs adsorption equation [91]:

$$-\frac{d\gamma}{d\phi_s} = 2k_B T z^* \rho(\chi_s - \chi)\left(\frac{d\phi_s}{d\phi_\infty}\right)^{-1} \tag{8}$$

as well as Eqs. (6) and (7), it can readily be shown that

$$\mu_s \propto \sqrt{\chi_s - 4\chi\phi_\infty(1-\phi_\infty)}, \tag{9}$$

which, as T_c is approached, tends to zero for symmetric systems. This provides a plausible explanation of why the increase in surface excess is less than expected.

Although the above explanation is plausible, there are other possible contributions to the depressed values of z^* near the critical point. A rigorous understanding of the temperature dependence of the surface free energy and the surface energy difference between the components would be particularly useful. Related experiments on the temperature dependence of surface energy have been performed using ion scattering from polyolefin blends [8,92,93]. It has been suggested, for example, that finite size effects, not accounted for in the above explanation, will play an important role [11]. Another reason concerns the location of T_c itself. Fluctuations tend to decrease T_c slightly, because slight variations in composition in the two-phase region close to the critical point will move the blend into the miscible region of the phase diagram [94]. Therefore, it is possible that fluctuations will contribute to the depressed value of z^*. In general, however, it is hard to see how such bulk effects cannot play a role in the growth of a wetting layer close to T_c, although whether or not this is a large effect is as yet untested experimentally. One aspect that is likely to prove interesting is the kinetics of segregation close to T_c, where the correlation length has been seen to affect the diffusion of polymer chains [95]. When the correlation length is of the same size as the segregating polymer, it is expected that the approach to equilibrium will be significantly impeded, providing an interesting test of whether or not such segregation near T_c is diffusion-limited.

3.3.3. Hydrodynamic flow

A phase-separated medium can either consists of many

domains dissolved in a majority component, or as a bicontinuous structure. In the former case, coarsening is driven by the Laplace pressure exerted by the domains on the surrounding matrix, which forces the domains to grow in size and can even force the volume fraction of the majority component in the domain to be slightly greater than the coexistence value. These domains may well meet, and the formation of a new, larger domain is no longer governed by coarsening, but is driven by the surface tension between the phases and the viscosity of the components. This is hydrodynamic flow. A simple scaling law for flow-driven growth of these bulk domains has been described by Siggia [96], who predicts a crossover from a $t^{1/3}$ behaviour to a linear growth law. Marko extended this analysis to the growth of surface domains [75]. The ideas developed by Marko were used to explain the behaviour of wetting layer growth in off-critical isotopic blends of PEP [97], which were linear in time, but exhibited a $t^{1/3}$ growth law for critical quenches. Although such explanations were convincingly backed up with computer (cell dynamical) simulations of hydrodynamic flow, evidence for the necessary interconnected structure (tubes) linking the bulk with the wetting layer was missing. In the case of a bicontinuous structure, the conditions for hydrodynamic flow are already present in that the interconnected structure allows the fast material transport that is its signature. The behaviour of a wetting layer from a film of a mixture in which droplets of one phase are dissolved in the other is not, however, the same as that from mixtures that exhibit a bicontinuous structure in the bulk [76].

Identifying systems that exhibit hydrodynamic flow means finding systems by which the conditions for fast material transport are available. This is generally achieved in the late stages of phase separation, when a mixture can break-up into a bicontinuous structure. Very early studies on hydrodynamic flow in polymeric mixtures were undertaken by Tanaka, who used optical microscopy to study a mixture of PS and PVME [98]. We concentrate here on work on a critical mixture of deuterated PMMA (d-PMMA) and a random copolymer of acrylonitrile and styrene (SAN) [99–102], which forms a bicontinuous morphology just below the wetting layer. Nevertheless, off-critical mixtures can also exhibit hydrodynamic flow, as has been shown for an isotopic PEP mixture, in which the majority d-PEP phase wetted the surface [103].

A method of identifying hydrodynamic flow is to use ion beam analysis to observe the growth of the surface layer, whilst accessing the bulk with SFM. This can be performed by dissolving the surface layer in a selective solvent. Two groups have performed such work; in one study a mixture of PS and a random copolymer of styrene and bromostyrene was studied [104]. The growth of the PS-rich surface layer was followed using dynamic SIMS and NRA. Dissolving the PS in cyclohexane enabled the random copolymer in the bulk to be studied by SFM. These authors were also able to vary the surface energy with the addition of a PS-*block*-PI diblock copolymer, which preferentially segregates to the surface [105].

The other series of experiments into the morphology of thin film blends exhibiting hydrodynamic flow is due to Wang and Composto using blends of PMMA and SAN [99–101]. The surface behaviour was measured using FReS, and the bulk was observed using SFM. In order to access the bulk of the material, the PMMA was selectively dissolved in acetic acid. Along with identifying hydrodynamic growth, these authors were able to follow the evolution of the film during each stage of growth.

The difficulties inherent in identifying hydrodynamic growth of wetting layers in polymer blend films stem from the different growth stages taking place during annealing. In a first stage, the lower surface energy component (A) of the phase-separated mixture will wet the surface, and in the case of the work by Wang and Composto, the substrate, too [99]. After this stage hydrodynamic flow of material to the surface is expected to occur. However, in a thin film, wetting of surface and substrate will cause a trilayer structure to occur. Such a structure will tend to break-up, with a third stage consisting of material flow from both the surface and the substrate. This flow will use the 'tubes', which fed the wetting layer growth, but will occur via a coarsening mechanism. Finally, the middle region (B-rich) will break-up, dewet from the A-rich region. Correspondingly, the interfacial roughness will increase.

In Fig. 13 we show low energy FReS data describing the growth of a wetting layer of deuterated PMMA from a blend with the SAN copolymer. In Fig. 14 the thickness, ζ, of the wetting layer is presented as a function of time. In the case of the data for the samples annealed at 458 K, it is clear that the surface layer thickness grows linearly in time over an order of magnitude in time. SFM was also used to image the samples, along with the selective dissolution of the PMMA in acetic acid. As can be seen n Fig. 15, the SAN surface is much rougher than the surface

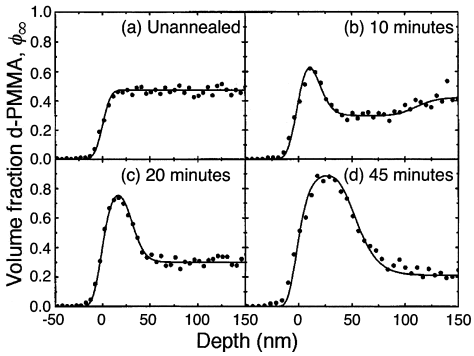

Fig. 13. Volume fraction profiles for d-PMMA ($M_w = 90$ kDa)/SAN ($M_w = 124$ kDa, 33% acrylonitrile by weight) blend films annealed at 463 K with $\phi_\infty = 0.47$ as measured by LE-FReS [100]. The rapidly increasing surface excess is indicative of hydrodynamic flow. Reprinted from Phys Rev E 2000;61:1659 with permission from RJ Composto [100].

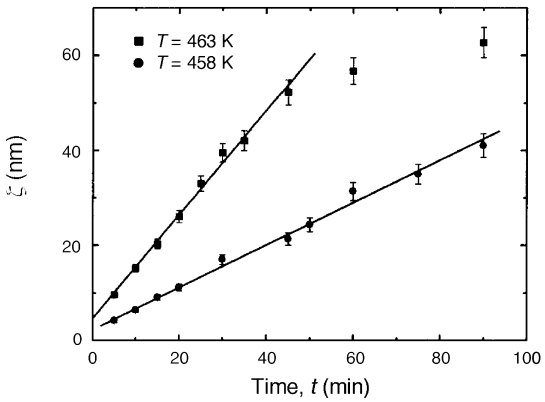

Fig. 14. Thickness of d-PMMA wetting layer (from a blend with SAN) plotted against time. The straight lines show linear fits indicating hydrodynamic flow [101]. In the sample annealed at 463 K, the growth of the wetting layer slows down after 1 h due to depletion of d-PMMA from the wetting layer. The d-PMMA has $M_w = 90$ kDa and $\phi_\infty \approx 0.5$ and the SAN has $M_w = 124$ kDa (with an acrylonitrile content of 33% by weight). Reprinted from J Chem Phys 2000;113:10386 with permission from RJ Composto [101].

of the PMMA wetting layer and exhibits a bicontinuous morphology.

Although hydrodynamic growth is revealed in the first hour or so of annealing, the film continues to develop long after that. In Fig. 16 the low energy FReS data show a rather dramatic phase evolution. The film first breaks up via an apparently homogenous phase to form a bilayer structure. Of course, such FReS depth profiles do not reveal the full three-dimensional morphology, and SFM was used to measure the lateral length scale and roughness dominating the films at each stage in the evolution of the structure [99, 101]. The SFM images, shown in Fig. 17, reveal both the surface morphology and the morphology of the near surface, which was exposed by acetic acid etching of the PMMA.

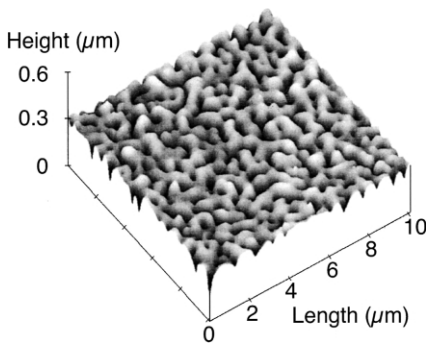

Fig. 15. SFM surface image of a d-PMMA/SAN blend film with the d-PMMA removed after being first annealed for an hour at 458 K [100]. The acetic acid treatment reveals the bicontinuous morphology of the SAN underneath the PMMA wetting layer. Reprinted from Phys Rev E 2000;61:1659 with permission from RJ Composto [100].

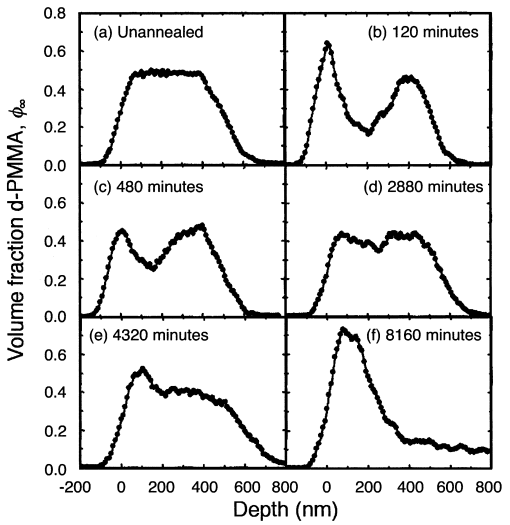

Fig. 16. Volume fraction-depth profile of d-PMMA as measured by FReS for a ~500 nm thick film of a blend with SAN annealed at 458 K [101]. The profile develops from a homogenous film to a bilayer, with d-PMMA wetting the surface. The path to equilibrium is interesting, with a trilayer morphology giving way to the final bilayer structure, via the apparently homogenous structure shown in (d). Reprinted from J Chem Phys 2000;113:10386 with permission from RJ Composto [101].

These images can be compared with the FReS data in Fig. 16. In Fig. 17(b), after 20 min annealing, a bicontinuous structure is visible in the below-surface scan, which is clearly not observable from the surface scan (Fig. 17(a)). The surface scans show a clear increase of the lateral length scale of the wetting layer, from sub-micron sizes (after 20 min) to ~20 μm (after 262 h). The same increase in length scale is happening to the near-surface morphology, except that smaller PMMA-rich holes are present and remain throughout annealing, although their size does change. As a result of these images, the authors were able to correlate the structures and roughnesses obtained by SFM, with phase separation at different locations in the film. The lateral length scale can be revealed from Fourier transforms of these SFM images and is seen (Fig. 18) to crossover from a linear growth to a Lifshitz–Slyozov-like $t^{1/3}$ coarsening behaviour. The Lifshitz–Slyozov behaviour does not start after the hydrodynamic regime, but rather starts during it, but is not observed because the much faster hydrodynamic flow is dominant. Nevertheless, one can see that the crossover to coarsening behaviour in the Fourier transforms occurs after only 15 min, whereas the wetting layer growth displays hydrodynamic behaviour beyond this to well over an hour (Fig. 14). This means that the trilayer structure breaks up because of the coarsening occurring parallel to the surface. However, as well as this coarsening, another mechanism of break-up is occurring. A film rich in SAN sandwiched between the PMMA-rich layers is thermodynamically unstable and will dewet by spinodal

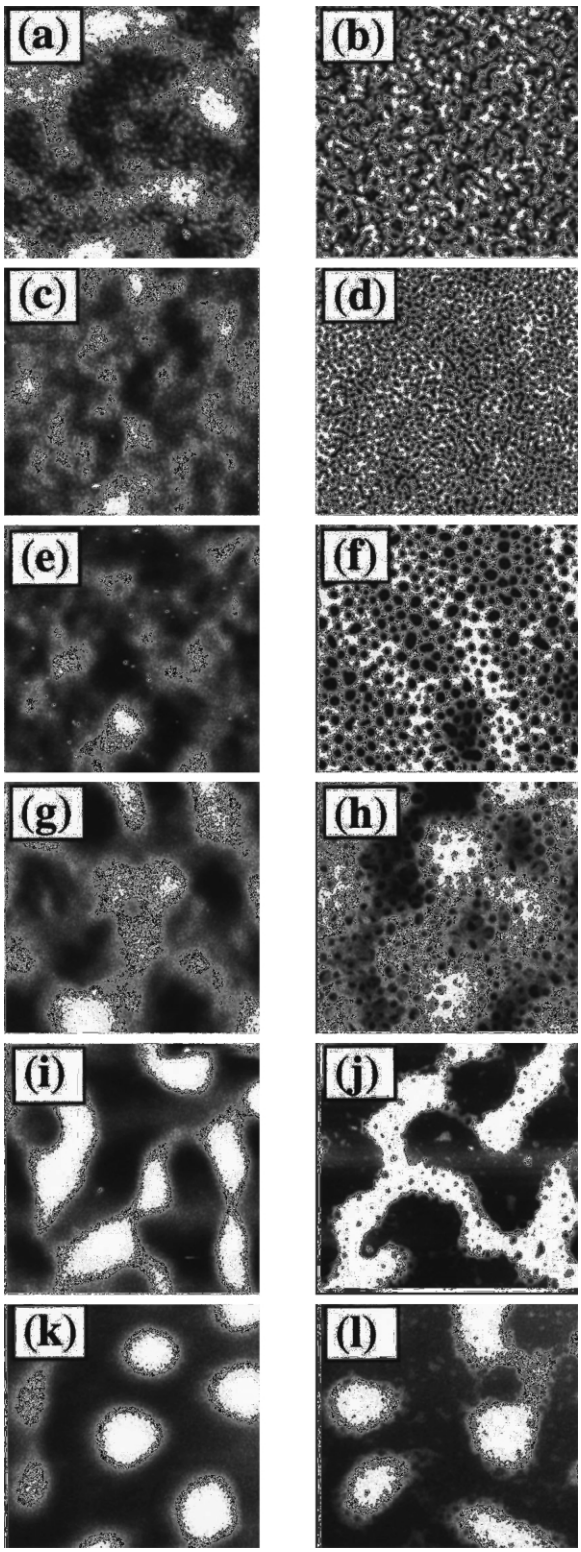

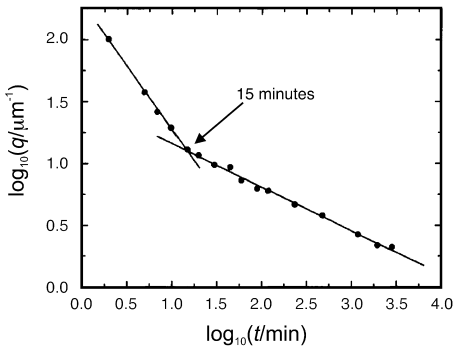

Fig. 18. Lateral characteristic wave number ($q = 2\pi/\lambda$) of the phase separation of films of d-PMMA and SAN annealed at 458 K [101]. The gradients reveal hydrodynamic flow (for $t < 15$ min, the slope is -1.02) and Lifshitz–Slyozov coarsening (for $t > 15$ min, the slope is -0.35). The beginning of the coarsening mechanism is not observed here because it is obscured by much more rapid hydrodynamic flow. Reprinted from J Chem Phys 2000;113:10386 with permission from RJ Composto [101].

dewetting due to long-range forces [106]. This mechanism of rupture, convolved with the coarsening is responsible for the particular sample morphology observed here [101] and explains why the final structure is a series of droplets. Further detailed discussion of these rupture mechanisms is discussed in a later publication [102].

We show in Fig. 19 a schematic diagram displaying the early, intermediate, and late stages of phase evolution of the films. However, to briefly summarise here, the film morphology develops in a three-stage process, which begins with hydrodynamic wetting of the surface and substrate by d-PMMA. The component wetting the surfaces (d-PMMA) flows back into the bulk of the film, whilst the phases in the middle layer coarsen. Capillary fluctuations in this middle layer cause its rupture and eventually break-up into a final dewetted droplet morphology.

Although the above work using solvents to selectively remove one component from the mixture represents a major contribution to the study of hydrodynamic flow in polymer blend films, much has also been deduced about hydrodynamic flow from ion beam depth profiling and SFM [103] or optical phase interference microscopy [107].

Fig. 17. SFM images of d-PMMA/SAN blend films showing the surface (left column) and sub-surface morphology after dissolving the d-PMMA with acetic acid (right column) of films with $\phi_\infty = 0.47$ annealed at 458 K [101]. The images are (length scale and annealing time): (a and b) 10 μm × 10 μm, 20 min; (c and d) 50 μm × 50 μm, 240 min; (e and f) 50 μm × 50 μm, 2880 min; (g and h) 50 μm × 50 μm, 4320 min; (i and j) 80 μm × 80 μm, 8160 min; (k and l) 80 μm × 80 μm, 15 720 min. Reprinted from J Chem Phys 2000;113:10386 with permission from RJ Composto [101].

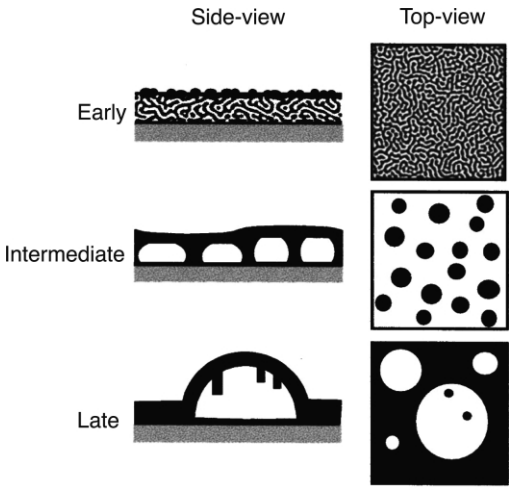

Fig. 19. Model for the d-PMMA (dark)/SAN (light) blend film evolution as a function of time [101]. At the earliest time, there is a layered structure with bulk phase separation and short-wavelength surface roughening. In an intermediate stage, a SAN-rich phase is formed, surrounded by PMMA-rich surface and substrate wetting layers. The SAN-rich layer is perforated with d-PMMA, visible from the top view. Here, the lateral wavelength is observed to increase from the short-wavelength roughening in the early stage. In the late stage, these droplets grow, causing the film to break-up, although they remain covered by a PMMA-rich layer. Reprinted from J Chem Phys 2000;113:10386 with permission from RJ Composto [101].

3.3.4. Surface segregation

The large size of polymer molecules means that surface layers can alter material properties quite significantly. In many small molecule systems, surface layers can be ignored, but this is not the case for polymer systems even far away from the phase boundary. Deep inside the one phase region of a phase diagram, the polymer of the lower surface energy in a blend will segregate to the surface, and this segregated layer will persist over approximately one polymer radius of gyration, R_g into the bulk.

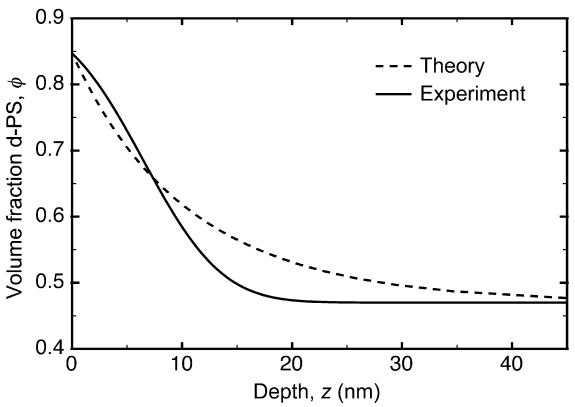

Fig. 20. Volume fraction-depth profile for a blend of d-PS ($\phi_\infty = 0.484$, $M_w = 49$ kDa) with PαMS ($M_w = 50$ kDa) after annealing for a day at 453 K as obtained from NR experiments (solid line) [109]. The broken line is the volume fraction-depth profile as predicted by mean field theory. Reprinted with permission from Phys Rev E 1996;53:825. © 1996 American Physical Society [109].

First experiments showed that surface segregation occurs in polymer blends, and that the composition of the segregated layer depends on the bulk composition [1]. Subsequent experiments [2] demonstrated how mean field theory [55] could be used to analyse the amount of surface segregated polymer. Later the limits of mean field theory were discussed based upon the exact shape of the surface segregated layer [108]. In thin films of isotopic PS blends, NR experiments demonstrated that the near surface region was significantly more enriched than theoretically expected, and that the segregated layer tended to decay faster than predicted by the simple mean field theory (given by Eq. (A19) in Appendix A). These results were backed up by further NR experiments on miscible thin films of blends of d-PS and PαMS [109] (see Fig. 20 for the comparison of data and theory). Various possibilities have been suggested to explain the disagreement between theory and experiment. The possibility of flattening close to the surface being due to long-range forces [88] has been dismissed by Jones, who included the effect of long-range forces into his calculations [110]. The mean field method was later improved by Genzer et al. [111], who noted that for any given surface free energy, the Schmidt and Binder approach [55] could predict either z^* or ϕ_s, but not both at the same time. They, therefore, extended the mean field model to be self-consistent and found much better agreement with data for isotopic PS blend thin films. The most complete study of the physics behind surface segregation has been by Norton et al. [91], who used NR to study segregation from isotopic PEP blends. As in the previous studies, the authors observed a flattening of the surface enriched component near the surface. They also noted that the approach of Genzer et al. [111] could not be used to explain the deviation from mean field theory observed in their profiles. To explain their results, they developed a new method involving the Gibbs adsorption equation [112] given by

$$\mathrm{d}\gamma = -\sum_i \Gamma_i \,\mathrm{d}\mu_i, \tag{10}$$

where Γ_i is the molecular surface excess and μ_i is the chemical potential of the ith component. In such measurements, the surface excess of the segregated component is equal to the loss of the other component at the surface ($z_d^* + z_h^* = 0$, where the subscripts indicate the deuterated and non-deuterated components, respectively). Substituting for the surface excesses, one may then write

$$\frac{\Gamma_d N_d}{\rho_d} + \frac{\Gamma_h N_h}{\rho_h} = 0, \tag{11}$$

where $\rho_{d,h}$ are the densities of the monomers of the two

components. The mathematics is described elsewhere [91,113], but in summary, the chemical potential is obtained from Flory–Huggins mean field theory, enabling one to calculate $d\mu$. Provided $d\phi_1/d\phi_\infty$ is known through experimental measurement, it is a simple matter to obtain Eq. (8) if we use the substitution

$$\frac{d\gamma}{d\phi_1} = \frac{d\gamma}{d\phi_\infty}\left(\frac{d\phi_1}{d\phi_\infty}\right)^{-1}. \quad (12)$$

Because $d\phi_1/d\phi_\infty$ is a measured parameter, this method of extracting the surface energy difference is model independent, and only requires knowledge of the bulk thermodynamics. Despite this progress a full understanding of the behaviour of the surface energy and surface composition profile of polymer blends is still lacking, not only because there are some differences in the theories discussed above, but because of the discrepancies between the results for polymer blends and for recent models of the interfacial tension in simple polymeric liquids [114].

Segregation from a binary polymer blend (B/C) to an interface of a homopolymer A is another subject that has been addressed theoretically [115] and experimentally [113,116]. This issue is important because the segregation of one component to the interface may have practical importance in compatibilising two films by lowering the interfacial tension. The authors used LE-FReS depth profiling on an interface between PS and a miscible blend of two random copolymers of PS and partially brominated PS (PS_xBrS_{1-x} and d-PS_yBrS_{1-y}, with different molecular weights and degrees of bromination x and y, respectively). Segregation was indeed observed and reached a maximum for a particular concentration of d-PS_yBrS_{1-y}, which corresponded to the best compatibilisation. Their results were found to agree well to self-consistent mean field theory calculations. In contrast to other means of interface compatibilisation involving block copolymers [117,118], this method circumvents the necessity for expensive block copolymer synthesis and may therefore be of technological relevance. It should, however, be noted that there are other methods of using polymers to compatibilise interfaces by, for example, the addition of random [119,120] copolymers to one of the components at either side of the interface, or by the use of grafted chains to form an interface, either with another polymer [121] or with an inorganic substrate [122,123].

Another practical use of surface segregation is found in applications where particular surface properties need to be established and eventually regenerated throughout the lifetime of the material. As an example, consider the problem of fouling the hulls of ships, where bio-resistant surfaces are of major economic importance. A particularly interesting study in this respect is the work by Hester et al. [124]. Here, an amphiphilic comb polymer with PEO side chains and a PMMA backbone is blended with poly(vinylidene fluoride) (PVDF). XPS measurements showed that the comb polymer segregates to the surface on annealing. Furthermore, these samples were exposed to a solution containing the plasma protein bovine serum albumin and found that the comb polymer imparted significant protein resistance when compared to the unannealed film or pure PVDF. Since significant amounts of the comb polymer segregate to the surface on annealing (the authors quote 45% surface coverage for only 3% bulk volume fraction), very little of the comb polymer is necessary in the bulk of the film, ensuring that the bulk properties of the material are largely unaffected by the additive. An additional bonus of this method is that, although the surface layer degrades on exposure to acidity, further annealing regenerates the surface, because there is still enough material left in the bulk to replenish the surface layer. This latter property is clearly not available with separate coating technologies. An understanding of the physics of these systems is only present at the qualitative stage, however, because of the complicated nature of the molecules involved. At present very little work involving surface segregation involving branched polymers [125] (such as combs) and networks [126] has been undertaken.

3.3.5. Variation of the segregated component

The importance of the substrate surface energy for the particular domain structure formed during thin film phase separation was already realised in the early experiments on this subject [59]. However, these studies were rather qualitative as they compared substrates of highly different surface energy. Quantitative studies were first performed by Genzer and Kramer, who used mixed self-assembled monolayers (SAMs) made from thiols with two different end groups [127,128]. In this case the surface energy of the SAM can be continuously varied via the SAM composition. Another means to the same end could be achieved by using random copolymers of varying composition as a substrate layer or coating [129].

Genzer and Kramer used SAM-coated substrates to cause a wetting reversal transition in an isotopic blend. They were able to alter a layering of d-PEP/PEP/d-PEP/SAM into d-PEP/PEP/SAM [127] by variation of the substrate surface energy. The kinetics of the transition is particularly interesting, because it demonstrates the effect of long-range forces in wetting in polymeric liquid mixtures. In Fig. 21 the structure of an isotopic PEP film for six different substrate energies is presented. As the substrate energy is raised, the thickness of the d-PEP wetting layer at the substrate, $l_{d,SAM}$ decreases. With only short-range forces present, this would not be possible, as is shown in their calculations in Fig. 22, where a remarkably abrupt transition in $l_{d,SAM}$ is predicted. This is not surprising because calculations have shown a dramatic increase in the effect of long-range forces as the phase boundary is approached [110].

Although changing the nature of the substrate is the most effective means of tailoring wetting properties, it is by no means the only way. Other experiments on surface

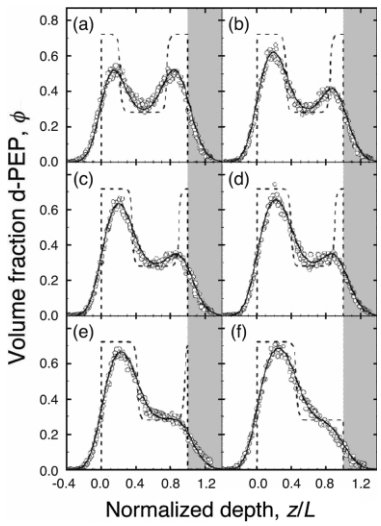

Fig. 21. FReS volume fraction profiles for d-PEP in a blend with h-PEP as the substrate surface energy is increased from (a) 20.5 to (f) 25.6 mJ/m^2 after annealing at 314 K for 2 weeks [128]. The broken lines represent the volume fraction profile before convolution with the instrumental resolution function. The shaded region underneath the film represents the location of the SAM. Reprinted with permission from Europhys Lett 1998;44:180. © 1998 EDP Sciences [128].

segregated layers of isotopic PS blends demonstrated a similar reversal. By varying the molecular weights of the polymers, neutron reflection experiments showed that the surface could be enriched in either d-PS or h-PS [130]. Later experiments on PS and PB blend films showed that the effect of M_w on wetting layer reversal was not restricted to isotopic polymer blends [21]. More recent work on a polyolefin blend has shown that either component of the blend can segregate to the surface if $-\mathrm{d}\Phi/\mathrm{d}\phi_s$ changes sign for $\phi < 0$

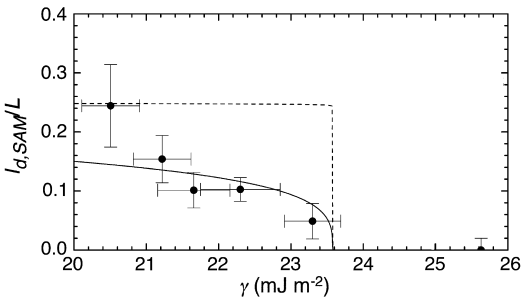

Fig. 22. The thickness of the d-PEP-rich wetting layer at the interface between the isotopic PEP blend and the SAM normalised by the total film thickness as a function of the substrate surface energy, γ [128]. The solid line represents the best fit utilising long-range van der Waals forces, and the broken line includes only short-range forces. This result clearly demonstrates that the behaviour observed in Fig. 21 is due to long-range forces. Reprinted with permission from Europhys Lett 1998;44:180. © 1998 EDP Sciences [128].

(enrichment-depletion duality) [8,131]. Although a wetting layer may be removed by changing the nature of the substrate, it is also possible to create a wetting layer only transiently as the route to a different phase-separated or dewetted morphology. Such transient wetting has been reported in different experiments [38,99,107].

3.4. Morphology of surface induced phase separation

One of the major themes concerning wetting in phase separating systems is the interplay of the surface phase with the bulk film. The experimental goal in such studies is to understand the final three-dimensional morphology of these mixtures. This has already been discussed above with respect to hydrodynamic flow (Section 3.3.3) but an equally interesting topic concerns very thin films, in which the substrate is also playing a role. Such films could also have useful applications in technology; in one study an immiscible polymer blend had one component removed using a selective solvent [132]. The resultant nanoporous film was observed not to reflect light, a property that might find application in solar cells, for example.

One of the first studies on phase-separated polymer blend films was undertaken by Bruder and Brenn [59], who looked at mixtures of PS and PS$_x$BrS$_{1-x}$ on silicon and chromium substrates. In another early work, as-cast mixtures of PS and PB were studied using NRA, NR, and TEM to reveal that a lamellar morphology could be obtained as the PS [133] (and in some cases PB [21]) wetted the surfaces. It should be pointed out that there are experiments dating from before the above that consider the morphology of phase-separated polymer blend films [54,134].

Blends of PS and PMMA are probably the most studied immiscible system [132,135–140]. In one study [135], thin films of blends of PS (M_w = 94.9 kDa) and PMMA (M_w = 100 kDa) were spin cast from a common solvent and the resultant morphology studied using SFM, where necessary with the selective dissolution by acetic acid or cyclohexane to remove the PMMA or PS, respectively, without disturbing the other component. Since it is very difficult to find a ternary system (polymer/polymer/solvent), whereby the solvent is equally good for both of the polymers, it was interesting to study the effect of different solvents on the film morphology. The authors also considered the effect of film thickness. Finally, three different surface treatments were used for the silicon substrates: the native oxide layer provided a high energy substrate, low energy substrates were produced by depositing an alkane SAM on the silicon, and a surface energy in between these two extremes was created by depositing a gold layer on the silicon via an intermediate chrome layer. The three solvents that were used were tetrahydrofuran (which is nearly a neutral solvent for the two polymers), toluene (which is a better solvent for PS) and methyl ethyl ketone (which prefers PMMA). To summarise the results where the surface energy and solvent were varied, rounded surface structures were obtained when

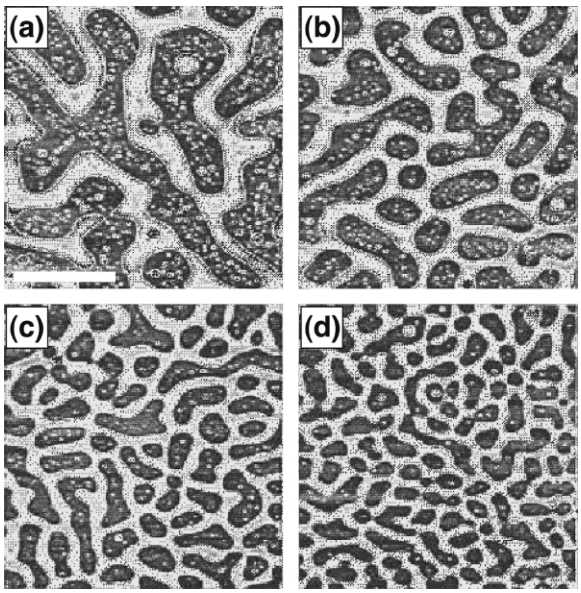

Fig. 23. Blends of PS (M_w = 94.9 kDa) and PMMA (M_w = 100 kDa) spin cast from toluene onto a gold surface [135]. The films are of thickness (a) 140, (b) 105, (c) 95 and (d) 80 nm. Clearly, the typical size of the phase-separated structure increases with film thickness. The scale bar is 10 μm and in all cases the PS concentration was 50% by weight. Data used from Ref. [135].

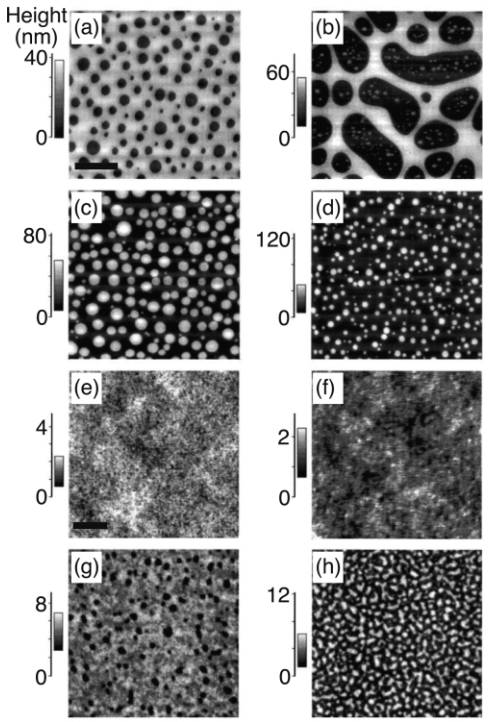

Fig. 24. SFM images (the scale bar is 5 μm) of films of blends of $PBr_{0.91}S_{0.09}$ (M_w = 393 kDa) and d-$PBr_{0.07}S_{0.93}$ (M_w = 253 kDa) with (a) $\phi = 0.93$, (b) 0.78, (c) 0.69, and (d) 0.39. In these films the blend is highly immiscible and phase separation is well defined. We also show SFM images (the scale bar is 1 μm) for $PBr_{0.91}S_{0.09}$ blended with d-$PBr_{0.67}S_{0.33}$ (M_w = 364 kDa) with (e) $\phi = 0.91$, (f) 0.72, (g) 0.62, and (h) 0.32 [144]. The deuteration in these blends is incidental to the physics behind the film morphology. Reproduced by permission of the Royal Society of Chemistry from Faraday Discuss 1999;112:285 [144].

the common solvent used for casting is better for the polymer with the greater surface energy. In the opposite case, the casting delivers surface structure with sharp, well-defined edges. Either the PMMA or the PS preferentially wetted the substrate, depending on the substrate treatment. In terms of controlling the morphology of the film, it was also observed that for thicker films, the lateral phase separation was considerably larger than is the case for thinner films. To illustrate this, SFM images of the morphology of such PS/PMMA blend films are shown in Fig. 23, whose thickness was varied by altering the spin-coating speed. In these films, phase separation starts during solvent evaporation and continues until the film reaches equilibrium or solvent evaporation has rendered the film glassy. However, during solvent evaporation the film thins and geometrical constraints also become important. For this reason the phase-separated structures become small for thinner films. As a final remark on this paper, it was noted that during solvent casting it was also possible that a dewetting mechanism also existed. The simultaneous existence of phase separation and dewetting in immiscible films is extremely difficult to quantify and it is only recently that workers have started to attempt to understand such phenomena [141–143].

Although it is accepted that quantitative analysis of spin-cast films is extremely difficult, there are other ways to manage this problem. One particularly promising route was shown in blends of PS_xBrS_{1-x} and PS_yBrS_{1-y} [144]. By tuning x and y, one can vary the miscibility of the blends as effectively by varying M_w and far more easily than by adjusting the temperature. When x and y are similar, these blends are quite miscible, but when $x \approx 1$ and $y \approx 0$, the mixture is highly immiscible. As an example we show in Fig. 24 SFM images of such films, which clearly reveal that there is much greater phase separation and much sharper interfaces between the domains when the difference between x and y is large.

The influence of the confining walls on the final morphology after annealing has also been studied using NRA [145]. A blend of random copolymers of ethylene and ethylethylene was used for these studies. One component was deuterated and this contained a greater fraction of ethylene. The films were either cast directly onto a gold covered silicon wafer, or floated onto a previously heavily cross-linked (by ion beam irradiation) polyolefin film. In the former case (on gold), the deuterated component preferentially wetted the vacuum interface and the non-deuterated

component preferred the substrate, whilst in the other case the deuterated component segregated to both surfaces. On annealing the films in the case where the boundaries favoured different components, a layered structure was observed, whereas in the case with the irradiated film-covered substrate (which favoured the same component as the vacuum surface), NRA revealed a profile that was constant with depth. The conclusion from this is that phase separation was occurring orthogonal to the plane of the film, demonstrating earlier theoretical predictions [146].

In addition to the above, there has also been work on blends of PS and PVME and the isotopic PEP system [147]. In these experiments, the same component preferentially wetted both interfaces. Provided the films were thin enough, droplets of one phase were formed, which protruded from the film but it is believed that these PVME (or h-PEP) droplets remain encapsulated within a film of d-PS (or d-PEP) in contrast to previous experiments where symmetric surface conditions did not apply [46,101,135,136,139,141].

Despite the difficulties involved due to the large number of experimental parameters, there are other phenomena in phase separating thin polymer films that would be worthy of further study. As an example, there have been experiments on blends in which one component is semi-crystalline. Here, the competition between phase separation and crystallisation is by no means obvious. Early measurements have been made on films of blends of SAN and poly(ε-caprolactone) (PCL) [148], although these experiments were precursors to later experiments to understand the SAN/PCL bulk system [149]. An example where both components are semi-crystalline concerns thick (~0.1 mm) films of mixtures of polyethylene and polypropylene compatibilised with a random copolymer of the two [150]. Such a system, when annealed, has been shown to create lamellar structures, developing deep into the film. However, there are important applications of polymer blends that incorporate semi-crystalline polymers so a fundamental understanding of their morphology is crucial. As an example, many of the polymers involved in the fabrication of organic semi-conductor devices are semi-crystalline, and we discuss some experiments in this particular field next.

3.5. Semi-conducting polymers

An area that has only just begun to be exploited is the study of blends of semi-conducting polymers for the improvement of electronic device performance. The use of polymer instead of silicon-based semi-conductors stems from the desire to create organic devices that are flexible and can be created on a large scale at low cost via novel synthetic routes [151] and simple production techniques such as solution processing or spin casting [152,153]. One of the obstacles to research in this area is that the two research communities (organic device physics and polymer films) have not interacted sufficiently, but these barriers are now being overcome [154]. To describe the importance of this area, we consider the basic components of an organic semi-conducting device such as a polymer light emitting diode (LED) or a photovoltaic device such as a photodiode or a solar cell, which we shall present in a simple form in order to communicate the principles of operation and explain why the behaviour of polymers at surfaces and interfaces is of importance.

Semi-conducting polymers are often termed conjugated and usually consist of alternating double and single bonds along their backbone (they consist of sp_2 and π covalent bonds). This makes these polymers relatively rigid molecules that are often quite difficult to dissolve. In conjugated polymers, the π electrons are delocalised over several monomers along the chain, enabling electron and hole transport.

The structure of an organic semi-conducting device is shown schematically in Fig. 25. It requires two electrodes, a substrate, and the semi-conducting polymer film. Because the devices operate either by emitting or by absorbing photons, one electrode must be transparent and for this reason (and its high work function), an indium tin oxide (ITO) anode is commonly used. The other electrode can be any suitable conducting material, provided that its work function enables efficient carrier injection into the adjacent semi-conducting material; it must also be stable and, unlike ITO, reflect light.

In the operation of a photovoltaic device, photon absorption will create excitons (electron–hole pairs). These will migrate through the material until they reach an interface between the two components where dissociation may occur, forming electrons and holes. In an efficient device, the electrons and holes will migrate towards the anode or cathode where charge can be collected. A small reverse bias is applied across the electrodes in order to enable efficient collection of charge. The goal is to collect these charges at the electrodes without recombination having occurred before the electrodes can be reached.

Single polymer layers, or polymer multi-layers, can be used in these devices but they have the disadvantage that excitons have a typical diffusion range in organic materials of a few nm; for example, an exciton has a range of 7 nm in

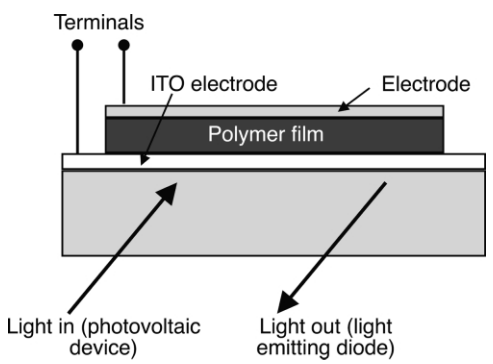

Fig. 25. Schematic diagram illustrating the components of an organic semi-conductor device.

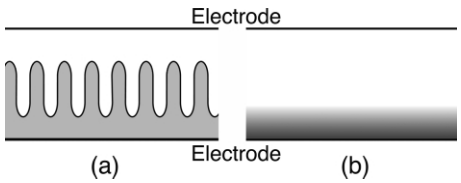

Fig. 26. Schematic diagrams showing *possible* morphologies which could be effectively used in the creation of (a) photovoltaic devices and (b) LEDs.

poly(*p*-phenylene vinylene), meaning that an interface should be no more than 7 nm from where the exciton is formed if it is to be successfully dissociated and the resultant charges separated [155]. Polymer blends typically give better performance than single layer structures [154] and are certainly less expensive and easier to fabricate than bilayer structures, and are very often more efficient too, especially in the case of photovoltaic devices. However, polymer blends can give rise to undesirable isolated phases rich in one component within the device. One therefore would like to create a large interface area between the two phases, each of which continuously connects towards the respective electrode. The large interfacial area is important because it will help to ensure that excitons are never too far from an interface, where dissociation can occur. A schematic diagram of the shape of such an interface is shown in Fig. 26(a); similar structures may be achievable via a dewetting mechanism or by a Mullins–Sekerka wetting instability [156], although neither of these phenomena are likely to achieve the narrow structures that would provide optimal device performance. Of course, by having a flat interface between two thin layers, one can achieve the requirement that the excitons are no more than one diffusion length from an interface, but another advantage of a structure such as that in Fig. 26(a) is that, compared to a flat interface, a larger proportion of the volume is within a diffusion length from an interface. This means that an exciton is less likely to reach and dissociate at an interface when the interface is flat. Another advantage of the structure shown in Fig. 26(a) is that the polymer layer can be thicker than for thin flat homopolymer layers. This is important because the thicker the layer, the greater the photon collection efficiency in a photovoltaic device.

For the operation of an LED, a forward bias is applied across the polymer blend film by the two electrodes. An electron from the donor polymer is injected into the conduction level (by analogy with traditional semi-conductors) at the metal electrode. At the ITO electrode, a hole is injected and these charges will migrate throughout the material until they recombine. Recombination may occur where there are two different chains in close contact, and often (but not always) this will be at an interface between two phases. On recombination, electrons and holes will form an exciton, which will eventually decay via photon emission. An efficient geometry could have a hole carrier matrix with a surface segregated or wetting layer of the electron carrier at the cathode. The surface segregated layer must be large enough to prevent recombination too close to the cathode, because this would quench photoemission. However, a diffuse interface could allow diffusion of the electrons into the hole-carrying matrix, where an exciton may eventually be formed. Diffuse (graded) interfaces have been shown [157] to be appropriate in the fabrication of LEDs because sharp interfaces can inhibit carrier motion. This means that, although the principle of operation of photovoltaic devices and LEDs is similar, the practicalities of designing the optimal structure are somewhat different; we present a *possible* idealised structure in Fig. 26(b). It must be emphasised, however, that this is a rather new area of research and these issues are not yet fully resolved; it is quite possible that the similar structure to that for a photovoltaic device would work just as well in an LED.

Given the above, it should be clear that phase separation into non-continuous domains in the bulk of the film is undesirable. This would inhibit charge transport to the electrodes and thereby lower the device efficiency. Blends are needed where the electrodes are wetted almost perfectly by the required component, but the interface between the two phases has the required properties; be it a graded interface, and/or one with a large interfacial area. The difficulty here is that these kinds of structures are normally hallmarks of very immiscible mixtures. In the future work concerned with optimising organic semi-conductor devices, it will therefore be necessary to not only understand the wetting and bulk properties of the materials, but also the interplay between the two. Such experiments are feasible if an appropriate technique such as nanotomography [41] is used.

One particularly useful blend for the fabrication of LEDs is that of poly(styrene sulphonic acid) (PSS) and poly(3,4-ethylene dioxythiophene) (PEDOT), which is marketed by Bayer AG (Leverkusen, Germany) as Baytron P™. The PSS/PEDOT mixture is used (with the PSS acting as a dopant to facilitate hole transport) in LEDs, when placed between an ITO substrate and an electroluminescent polymer layer. Knowledge of the wetting behaviour of such films is consequently particularly important. In a first experiment, particularly rough films were shown by XPS or ultraviolet photoelectron spectroscopy to have almost complete segregation of the PSS to the N_2 or vacuum (depending on treatment) surface [158]. More recent experiments on this blend have used NR measurements of surface segregation to obtain the surface composition profile [159]. These experiments are particularly illuminating because they make it possible for quantitative analysis of semi-conducting polymer films using the Schmidt and Binder [55] analysis. This will be particularly interesting because such rigid molecules are not usually considered in such a way; the rigidity alters the conformational entropy of these polymers, resulting in a very large step length for a random walk chain conformation.

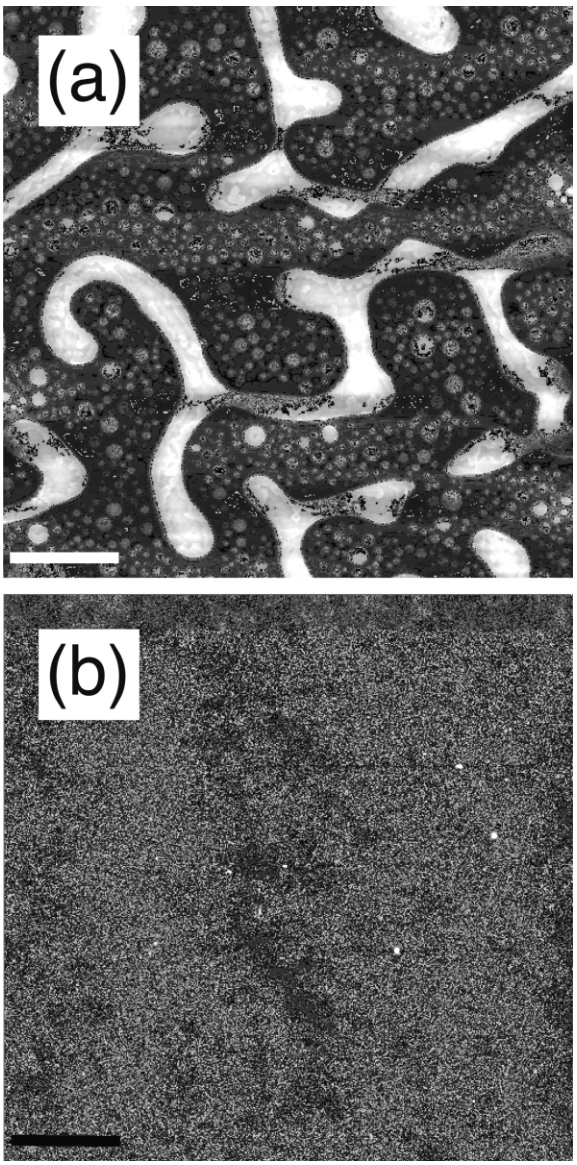

Fig. 27. SFM images of a thin film blend of PFB and F8BT with equal mass ratio [160,161]. The film in (a) was spun cast from xylene, whilst that in (b) was spun cast from chloroform. The height range is 350 nm in (a) and 30 nm in (b) and the scale bar for both figures is 10 μm. Reproduced with permission of Dr A.C. Arias [161].

Other experiments have been performed on a mixture of a green–yellow emitter (poly(9,9-dioctylfluorene-*alt*-benzothiadiazole), F8BT) mixed with PFB, an alternating copolymer of dioctylfluorene and triarylamine. Such a blend is particularly useful for photovoltaic structures. These experiments concerned controlling the amount of mixing of the two components (in a 1:1 by weight mixture cast from xylene) by heating the spin coater. At higher temperatures (close to 368 K), phase separation in the film occurred on a finer length scale, and led to better device performance. Similarly, further work on this theme using the same blend system considered the effect of casting solvent, as well as the method of casting (drop casting under a solvent atmosphere and spin coating on a heated and non-heated substrate) [160]. Again, it was concluded that phase separation on shorter length scales produced better device performance. As an example, we show in Fig. 27 the morphologies obtained by casting from chloroform and xylene solutions [161]. The blend cast from xylene has large-scale phase separation clearly visible, and is observed to produce less efficient device performance. The importance of controlling solvent evaporation was stressed in a later paper [162].

One can therefore attribute improved photovoltaic devices and LEDs to better control and limitation of phase separation in the bulk of the film. Further work on LED morphology concerned LEDs fabricated with blends of poly(9,9-dioctylfluorene) (PFO) and F8BT [163]. Here, it was shown that small phase-separated structures can be obtained by exposing the films to acetone, which is a poor solvent for both components. The authors proposed a possible explanation for the observed behaviour by suggesting that enhanced polymer diffusion could help to drive the demixing before the final morphology by either swelling of the film surface by the acetone, or by a preferential interaction between the acetone and one of the components of the blend.

The present challenge for scientists working with organic polymer semi-conductors is therefore to use their expertise, with the thermodynamics of thin polymer blend films, to solve the problems of creating the best device morphologies. The difficulties that arise are that the ‘model’ blends discussed in the earlier part of this review are not semi-conducting polymers, which are rigid and often display crystallinity. Physicists can no longer rely on tuning parameters such as composition of a random copolymer, because such changes will seriously affect the properties of the material. Nevertheless, the self-assembly of polymer blends to form organic devices shows great promise. As we indicated above, ‘traditional’ polymer physics is not all that is required to create the optimum device because the optimum morphology is still not understood. This means that the goal is not necessarily to create a particular morphology, such as one of those indicated in Fig. 26, but to first find out what the best morphology actually is. However, despite these challenges, the momentum in this new field is such that one can expect major progress to be made sooner rather than later.

4. Spreading and dewetting

The above discussion concerned polymer blends. In this section, we discuss the wetting behaviour of homopolymer

thin films on surfaces. In order to fully understand homopolymer wetting, one also needs to know the circumstances under which a film breaks up (dewetting). There is an enormous amount of work on the subject, which is well beyond the scope of this article. The interested reader will find further information in the reviews by de Gennes [10], Krausch [164] and Findenegg and Herminghaus [165] as well as the more recent article by Seemann et al. [166]. In this section we limit ourselves to a few examples illustrating some important ideas, as well as future directions that will be significant.

4.1. Spreading

The wetting transition, which was discussed above for polymer blends, is also important in thin films of homopolymers. As an example we consider the experiments by Maas et al., who studied the wetting behaviour of a PS film on a grafted PS layer (brush) [167]. The brush was created by the strong spontaneous adsorption of the polar poly(2-vinyl pyridine) (PVP) block of a PS-*block*-PVP diblock copolymer to an oxidised silicon substrate. The authors observed both stable and unstable homopolymer films depending on the grafting density of the brush layer. For low grafting densities the films were unstable, while for higher grafting densities stable films were found. For very large grafting densities, the PS homopolymer film suffers conformational restrictions and autophobic dewetting occurs [168]. The instability at low grafting densities was caused by a large repulsion of the PS homopolymer with the PVP block of the copolymer. However, for grafting densities within the range studied in this work both droplets and stable thin PS layers were observed in the same film corresponding to a wetting transition. However, droplets were also observed to be in local equilibrium with somewhat thicker layers, which was unexpected, demonstrating the complexities involved in the study of wetting.

We have mentioned before in this review the importance of wetting to industrial applications. A good example of work in this direction concerns the enhancement of wetting in small molecule liquids by the addition of polymers [169]. The issue considered here is the use of pesticides on plants, which are well known for their ability to cause water to bounce off their leaves. Past methods of dealing with this problem involve the use of organic solvents, which wet the surface more readily. However, the use of such toxic materials is best avoided for environmental reasons. By adding a water-soluble polymer, poly(ethylene oxide) (PEO), it was possible to change the behaviour of a droplet on hitting a surface. The polymer additive changes the liquid flow from simple Newtonian to a non-Newtonian behaviour. On hitting a hydrophobic surface, a droplet of a Newtonian fluid begins to coat that surface as its weight counters any repulsion due to the incompatible surface energies. However, as the energy due to gravity is dissipated, the surface tension causes the droplet to retract again, a process which may occur so rapidly as to reject some water through a rebound, causing loss. The addition of polymer may slow down this retraction by lowering the surface tension and/or by changing the viscosity of the fluid. The surface tension of the liquid was not significantly altered by the presence of a small amount of polymer additive. However, rheological experiments showed that the elongational viscosity of the solution was greatly increased by the polymeric additive, slowing the retraction and thereby increasing the effectiveness of the surface coating.

The spreading of polymer films from solution into ordered structures is a powerful and simple method to create polymer nanostructures. As an example silicon and aluminium nanotubes were placed in a polymer solution so that the polymer could coat the nanotube templates [170]. After coating, the nanotube templates could be removed by etching in aqueous KOH solution. Polytetrafluoroethylene, PS, and PMMA nanotubes were all created in this way.

The opposite situation, whereby a droplet can be made completely incompatible with a surface should also be possible. This has already been achieved with a fluorinated powder additive to a water mixture causing complete hydrophobicity with a glass substrate [171]. In contrast to the above situation, in this case the additive segregates to the surface of the fluid and changes in surface tension dominate over rheological effects. Another study by the same group has shown how lithographed surfaces can be used to create nearly spherical droplets ‘pearl drops’ [172]. This is due to the observation that, depending on the interaction between the fluid and the substrate, a microscopically ‘spiked’ surface can dramatically worsen (or improve) wettability.

4.2. Dewetting

As we have pointed out above, if one is to understand how a polymer wets a surface, it is necessary to understand what causes a polymer films to *dewet* surfaces. However, the amount of published work essentially means that dewetting deserves a review in its own right, and we restrict ourselves here to a summary of some of the most important aspects of dewetting.

4.2.1. Spinodal dewetting

One of the first quantitative studies of the dewetting of polymer films is also probably the simplest experiment. Reiter [173] used optical microscopy to observe the break-up of PS films on silicon substrates as a function of film thickness. In these experiments, Reiter pointed out that the break-up of the films could be reasonably well explained as a spinodal process (spinodal dewetting) [106,174], whereby long-range van der Waals forces cause an amplification of film thickness fluctuations eventually resulting in film break-up. Intuitively, it may be difficult to see how long-range van der Waals forces can cause film break-up since they are always attractive, and would seem to encourage film stability. However, if the attractive interaction between

a film and surrounding medium is weaker than the substrate and the surrounding medium, then the film will break-up. The details of the simple calculation of the attractive energy between two planar surfaces are reviewed elsewhere [175] and the result is (per unit area at a separation x)

$$W_{\mathrm{vdW}} = -\frac{A_{\mathrm{H}}}{12\pi x^2}, \tag{13}$$

where A_{H} is the Hamaker constant describing the interaction between the two surfaces. Different authors use a different sign convention for the corresponding forces and the reader is therefore advised caution. The dispersive forces driving the dewetting are counterbalanced by the inherent energy cost having a large interface. As a result of the competition between these two terms, a dominant wavelength λ emerges, which grows faster than any other unstable wavelength [174]. Films are, however, stable to thickness fluctuations below a critical wavelength, given by $\lambda/2$. Should the polymer film be confined to an area smaller than the dominant wavelength, then the spinodal dewetting is suppressed [176]. Spinodal dewetting is not, however, a phenomenon unique to polymer films and has been convincingly identified earlier in thin metal films [177].

The identification of spinodal dewetting as a mechanism for the break-up of polymer films has been further pinned down by SFM measurements of PS films on silicon [178]. In these experiments, the authors determined the fastest growing length λ as a function of film thickness. In this case the experiments showed uniformly distributed surface undulations in contrast to the random distribution of holes observed by Reiter [173]. There have been several other studies of the dewetting of PS from silicon substrates [166, 179–190], although not all of these are attributable to spinodal dewetting. NR measurements on the interface in bilayers of PMMA on PS [52] showed convincingly that the fastest growing length scale had the expected inverse square behaviour on PMMA film thickness. Moreover, their results were not inconsistent with the expected inverse sixth power behaviour of the rise time of the instability on the PMMA film thickness. These results were obtained by analysing the off-specular reflection; specular reflectivity was used to describe the surface and interfacial roughness as a function of time. Later work concerned in situ NR measurements to investigate the time dependence of the spinodal dewetting [191].

An important aspect of spinodal dewetting, which may be exploited in future work, is the ability to create patterned structures with a given dominant length scale. This has already been extensively theoretically discussed [192–196]. Spinodal dewetting has already been used to create structured patterns [197], where the simple act of rubbing a substrate imposed a preferred orientation on the dewetting process and PMMA was observed to dewet from PS to form a corrugated structure (Fig. 28). This provides a clear analogy with surface-directed spinodal decomposition [5] because the nucleation point only triggers the dewetting or phase separation, but does not impose a length scale; the system itself chooses its own preferred length scale from the thermodynamics.

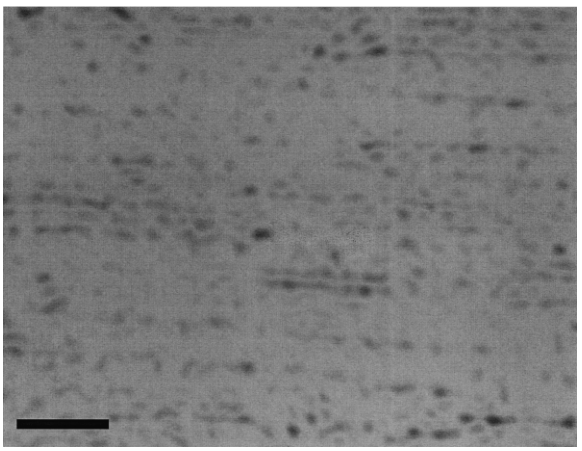

Fig. 28. Fifteen nanometre-thick of film of PMMA dewetting from a 300 nm film of PS (respective molecular weights of 112 and 259 kDa) after annealing at 423 K for 1 h. By imposing an orientation on the glass substrate (by gently rubbing it in one direction with a lens cleaning cloth) prior to spin coating and floating the PMMA film onto water, it is possible to create oriented dewetting [197]. The scale bar is 20 μm. Figure supplied by Dr A.M. Higgins.

Another means by which self-assembly due to spinodal dewetting can be used to create intricate patterns is due to chemical inhomogeneities in the substrate [192,193,198, 199]. In very thin films, where spinodal dewetting is a rapid process, such structure formation may well be quite common and difficult to control. As an example, we show in Fig. 29 the dewetting structure of a thin bilayer of PMMA on PS as measured by SFM. The origin of this instability may well be due to heterogeneity in the substrate. Theoretical work has shown how such patterns may form [192,193,199], and also that their formation can be much more rapid than the usual spinodal dewetting process. In this case, one might consider an imperfection, possibly only a few micrometres in size, on the silicon substrate causing a chemical heterogeneity. Only a small patch is necessary to induce a gradient in chemical potential along the substrate. This gradient will induce rupture in the film, in this case, the PS layer. The rim of the hole formed in the initial stages of rupture results in thickness fluctuations in the film, which can result in a spinodal mechanism taking over, with long-range pattern formation resulting. However, this discussion can only be the basis of a true explanation because the PS is sandwiched between PMMA and silicon, neither of which will be passive in the dewetting process. Further related theoretical work on this subject concerns chemical patterns on the substrate, rather than simple heterogeneities [200, 201]. We discuss experiments related to pattern formation on structured substrates in Section 5.

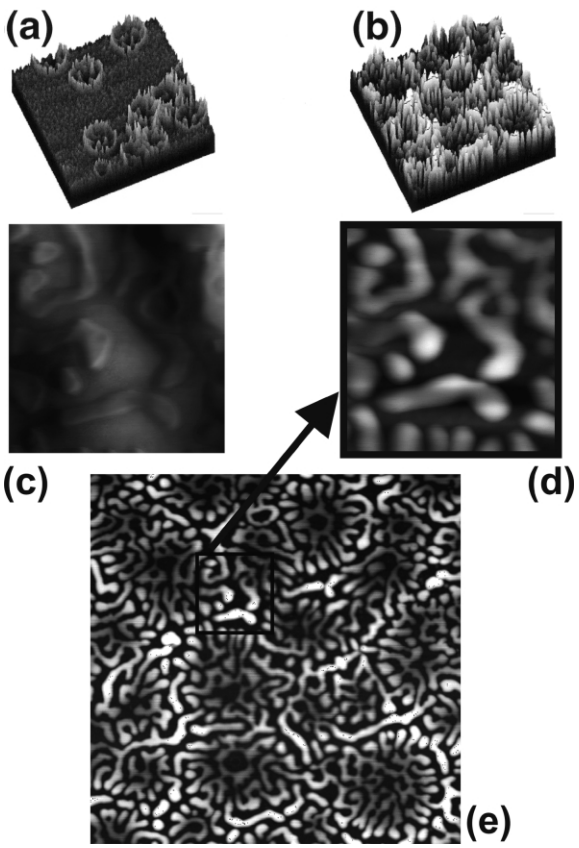

Fig. 29. Dewetting of a PMMA (M_w = 23.8 kDa, ~30 nm thick) film from PS (M_w = 166 kDa, originally ~15 nm thick) on silicon. The SFM images (a, b, d and e) were taken after the PMMA had been selectively removed with acetic acid. The dewetting structure was obtained after annealing for (a) 15 min and (b, c, d and e) 24 h at 443 K. In (a), the highest points are some 50 nm above the lowest regions of the film; the other height scales are (b and e) 100, (c) 40 and (d) 80 nm. The lateral scales are 10 μm × 10 μm (a and b) and 20 μm × 20 μm (e). In (d) we show a scan of part of the film in (e). The image in (c) is a scan over the same region as in (d) but before acetic acid washing (so the PMMA is still present on the surface).

The stability of polymer films on highly incompatible substrates has also been considered with thin films of polystyrene near its glass transition on PDMS-coated silicon substrates [202]. Although the PS film is close to its glass transition, the speed of film rupture is much more rapid than one would expect given the viscosity of the polymer in the bulk state. As well as the rapid kinetics, the shape of the hole also differs from previous experiments. Possible explanations of these results have been provided, with suggestions of mechanisms due to a plastic deformation [203] or shear thinning [204].

Experiments concerning spinodal dewetting of polymer films need not be limited to the simple air (or inert gas or vacuum)/polymer film (or bilayer)/substrate geometry. There is also the possibility of immersing the entire system in a fluid (for example, water) to change the very nature of the polymer–substrate interactions. Such experiments have been performed successfully with thin films of PDMS on a silicon substrate compatibilised with a PDMS brush [205–208]. These experiments showed that the strength of the interaction was much larger than expected from calculations [207], and was even large enough to destroy the chemically grafted brush layers [206]. Further evidence of the remarkable strength of these interactions was observed when a PS film was placed on the PDMS in water as a surrounding medium [209]. In this case, the PS film was deformed due to the rupture of the PDMS brush below it. Another way to control the interaction of a polymer film with its substrate is to add a copolymer one component of which prefers the substrate, and the other the film. First experiments along these lines have recently been published [210]. These experiments are nice examples for a situation where the knowledge of surface segregation, discussed in the beginning of this article, is utilised to improve film stability against dewetting.

An interesting alternative to immersing a polymer film on a substrate into some liquid is to perform experiments on freestanding films. Experiments have been performed on hole growth and rupture in freestanding PDMS [211,212] and PS films [213], all of which show how viscoelastic behaviour plays an important role in the rupture of the films. Freestanding PS films were also studied after coating with thin layers of silicon oxide [214,215]. The films were annealed such that the PS remained in the molten state, whilst the SiO_x coating remained solid, causing a mechanical confinement of the films. Dispersion forces (i.e. van der Waals forces) cause the film to crumple, although the resistance provided by the SiO_x layers limits this effect. An optical microscopy image of a PS film coated with two SiO_x layers is shown in Fig. 30. The minimisation of the total free energy confers the annealed film with its characteristic wavelength of ~6 μm. By equating the pressures induced in the film due to dispersion and bending forces, the authors were able to derive a simple scaling law, which was supported by their data and showed that the wavelength of the instability behaved as

$$\lambda \propto \frac{L^{3/4}}{x + 2L}, \tag{14}$$

where L is the thickness of the two SiO_x capping layers and x is the thickness of the PS film. The constant of proportionality depends on the Young's modulus and Poisson's ratio of the capping layer as well as the Hamaker constant for the system. Although these films were freestanding, the issue of dewetting in a deformable medium (such as the SiO_x or the other layers used in the above study) is an important issue that has been discussed both theoretically [216–218] and experimentally [209,218].

4.2.2. Nucleation and growth

In the above, experiments concerned with how long-range forces can cause a film to rupture and break-up were

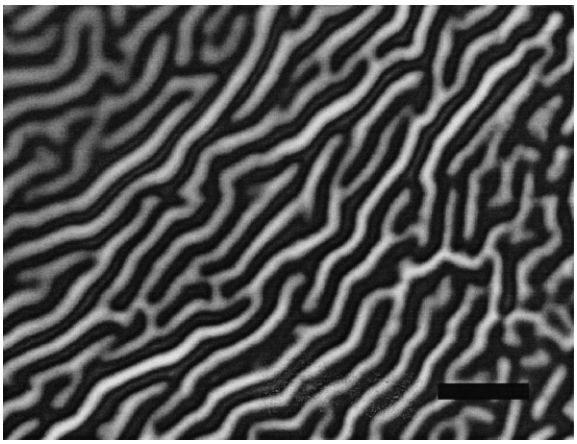

Fig. 30. Optical micrograph of a freestanding PS film capped by evaporated SiO_x layers [215] after annealing at 483 K for 3 h. The scale bar is 20 μm. Image provided by Professor K. Dalnoki-Veress.

briefly discussed. Many polymer films are metastable and break-up by the thermal nucleation of holes, or by nucleation at impurities or dust particles in the film or on the substrate. The key to whether or not a film is stable on a given substrate is given by Young's equation [219] for the spreading coefficient,

$$S = \gamma_B - (\gamma_{AB} + \gamma_A), \tag{15}$$

where γ_A, γ_B, and γ_{AB} are the surface energies of the polymer film, substrate, and film–substrate interface, respectively (Fig. 31). If the spreading coefficient is negative, then the film is unstable. Scaling laws have been presented to describe the behaviour of the dewetting speed as a function of film thickness [174], and these were developed and tested using films of PDMS on silicon substrates [220].

A particularly interesting subject is that of the dewetting from the interface between two liquids [164]. Although spinodal dewetting at liquid–liquid interfaces has also been experimentally [221] and theoretically [106] discussed, we restrict ourselves here to experiments on nucleated dewetting. In this case, the upper film will deform the lower film as it dewets, and one note that both the horizontal and vertical component of the capillary force must vanish at the

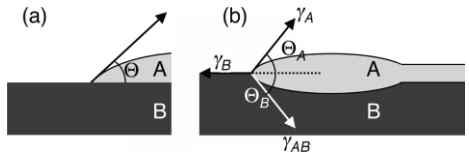

Fig. 31. Schematic diagram illustrating the criteria for dewetting on a (a) flat solid substrate and (b) deformable liquid substrate. If there is a finite contact angle, Θ the spreading coefficient (Eq. (15)) is negative and the film will dewet the substrate at equilibrium. In the case of a liquid substrate there are two contact angles, which can be used to describe the requirement that the vertical component of the capillary force must vanish at the contact line (Eq. (16)).

contact line. This is described by the von Neumann construction (Fig. 31(b)) and can be written in the limit of small contact angles as

$$\gamma_A \Theta_A = \gamma_{AB} \Theta_B, \tag{16}$$

where Θ_A and Θ_B are the contact angles defining the deformation into the upper and lower film, respectively. In order to study such deformation in films of PS on PMMA, the PS top layer was removed by selective dissolution in cyclohexane [34]. In these experiments, the dewetting speed was measured as a function of substrate viscosity, and it was found that the speed exhibited a minimum. The authors performed SFM measurements before and after selective dissolution of the PS, the latter giving insight into the shape of the initially buried PS/PMMA interface. They identified a crossover between a liquid substrate and a solid substrate. In the liquid substrate regime, the rim of the dewetting PS layer deforms the PMMA film (Fig. 31(b)), leading to holes growing as $t^{2/3}$ [106,222]. For larger PMMA molecular weight, the PMMA behaves like a solid substrate (Fig. 31(a)), i.e. the holes in the PS film grow rapidly in comparison to movement in the much higher viscosity PMMA substrate. In this case, a constant dewetting speed is observed in agreement with the theoretical expectation [174]. Further work on this system provided a quantitative investigation of the dewetting speed as a function of polymer molecular weight [223] and film thickness [224]. In Fig. 32, we show SFM scans of a PS film dewetting a PMMA lower layer, before (Fig. 32(a)) and after (Fig. 32(b)) cyclohexane etching. A line scan of the same hole before and after etching shows how one can obtain the complete three-dimensional morphology of the hole, revealing the PS–PMMA–N_2 contact line (Fig. 32(c)). In these studies, the dewetting speed is well explained by simple scaling theory [106]. However, experiments on bilayers of polycarbonate (PC) on a SAN copolymer are not in agreement with the theory. The discrepancies include a rate of hole growth in some films, which *increased* with annealing time [225,226]. It is quite possible that the interaction (miscibility) of the two layers plays an important role because it appears that PS and PMMA are more immiscible than PS and SAN.

4.2.3. Autophobicity

We return to our discussion of the wetting properties of homopolymer films on polymer brushes. As mentioned briefly above, there are situations when the polymer would want to dewet the brush itself for purely entropic reasons. Because the brush and film are of the same chemical species, one expects a certain miscibility between the two. However, depending on the molecular weights and the grafting density, it is possible that conformational restrictions will force the polymer to dewet a dense brush. These conformational restrictions can be relaxed by using shorter homopolymer chains, or lowering the grafting density. It has also been theoretically demonstrated that a bimodal brush

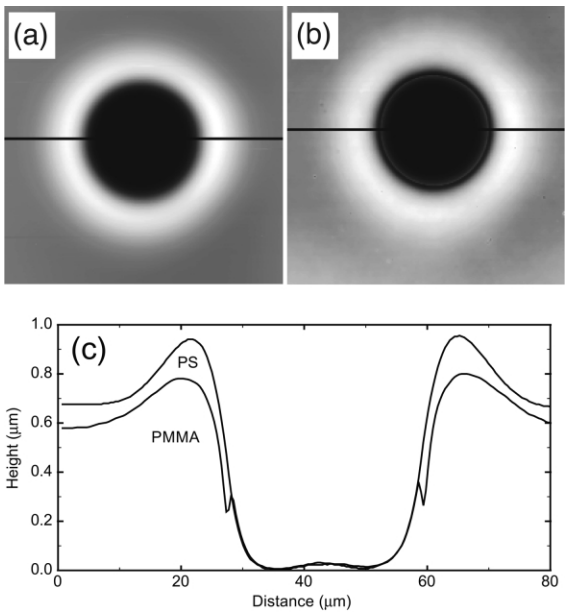

Fig. 32. (a) SFM image of a hole in a 270 nm film of PS ($M_w = 32$ kDa) dewetting from a 500 nm film of PMMA ($M_w = 31$ kDa) after annealing at 435 K for 990 min in nitrogen atmosphere. (b) The same hole as in (a) but after washing in cyclohexane to remove the upper PS layer. (c) Section through this hole; the black line in the SFM scans shows the location of the section. The large size of the hole means that the complete rim has not been imaged. These images form part of a study of dewetting at the polymer–polymer interface [224]. SFM images were provided courtesy of Dr C. Wang.

can suppress autophobic dewetting by broadening the brush/polymer interface [227].

Early experiments showed that PS films would entropically dewet a PS brush created by adsorption of a PS-*block*-PVP diblock copolymer [168] or PS chemically grafted to the silicon substrate [228,229]. Another study of such autophobic behaviour replaced the brush by a cross-linked film. In these studies [230,231], a polyolefin film was transferred onto a cross-linked film of the same material. Cross-linking was achieved by α-particle irradiation. For high enough cross-link densities, the authors observed complete wetting, which was attributed to roughening of the network surface. At moderate cross-linking densities autophobic dewetting was observed, whilst complete wetting was recovered at low cross-linking densities. Although the conclusions of these studies probably stand up, it should be pointed out that, compared to for example, proton-irradiated networks [232], such α-irradiated networks are very difficult to characterise [233] due to the effect of chain scission and radical formation. The high doses used (fluences of up to 10^{15} ions cm^{-2}), and the large energy loss of α-particles imply that the highly cross-linked systems are not chemically identical to the films placed on top of them.

The study of autophobic behaviour has now matured considerably and recent work includes quantitative studies; for example, the kinetics of dewetting of PDMS films from chemically identical brushes measured in situ [234,235]. In another study, it was shown how PS, end-terminated with a sulphonate group, can create a densely packed brush layer, from which the remainder of the end-terminated PS film autophobically dewets [236].

4.2.4. Other forms of dewetting

It has also been shown that polymer films can dewet *wettable* substrates [237]. In this case, PEP films were observed to dewet silicon substrates, when the film thickness became less than the polymer radius of gyration. This points to the importance of understanding the nature of the conformational entropy of a polymer chain in a thin polymer film, and whether or not it is the same as that in the bulk. Simple theory suggests that there is no entropy cost in having a chain at the surface [238], whilst more detailed work considers the small entropy cost due to chain ends [239]. Monte Carlo simulations also support the suggestion that there are deviations from the bulk conformation in thin films [240]. Recently, experiments have addressed this problem [241–245]. We shall return to this issue in the context of dewetting from corrugated substrates below [185]. It has also been theoretically demonstrated that fluctuations in density, perhaps due to composition fluctuations in a polymer blend, or a film close to a critical point, can initiate dewetting on a wettable substrate [246]. As yet, there has been no experimental demonstration of this mechanism.

Other mechanisms for dewetting are possible and we briefly mention some here. A Marangoni flow mechanism of dewetting has been proposed to explain dewetting in an immiscible oligomer blend [247]. After phase separation had commenced, this mixture dewetted inwards from the outside of the sample. Another unusual example concerned thick polybutadiene films placed on a liquid crystalline polymer [248] in which the dewetting behaviour depended on the phase of the liquid crystalline polymer below. The authors measured both the advancing (spreading) and receding (dewetting) contact angles [175] and observed that the receding contact angle dropped somewhat on passing from the smectic to the isotropic phase. The advancing contact angle, however, was found to be independent of temperature. Finally, it has recently been shown using bilayers of PS on PMMA on silicon substrates that electric fields can induce a spinodal instability that causes rupturing of the PS layer [249]. In these experiments, 60 V applied across two electrodes ~2 μm apart is enough to destabilise ~300 nm thick films of PS on similarly thick PMMA layers.

5. Pattern formation by structured substrates

So far we have largely dealt with the wetting properties of free surfaces and laterally homogeneous substrates. In recent years, however, the study of patterned substrates and,

in particular, the interplay between the length scales provided by the substrate pattern and the inherent length scale of the (de)wetting process has become an area of intensive research. Such substrate patterns may be topographical and/or chemical in nature. The idea of what may best be called 'structured wetting' dates back to the early 1990s, when Whitesides and co-workers demonstrated that microscopic liquid structures are created spontaneously in a liquid film on a substrate exhibiting lateral variations of surface energy [250,251]. In recent years, beautiful quantitative studies along these lines were reported by the Herminghaus group in Ulm [252]. These authors used a mask to enable the patterned deposition of a hydrophilic MgF_2 layer onto a hydrophobic silicone rubber. They showed that water follows the path of the hydrophilic component on the substrate and studied the stability of the resulting liquid structures as a function of the amount of water condensing onto the substrate. Along with the experimental work, theoretical calculations were performed which nicely agreed with the experimental observations [253].

The first reported use of patterned substrates for the creation of polymeric microstructures was by Krausch in 1995 [7]. The authors studied phase separation in a polymer blend in the presence of a laterally patterned substrate. Micron size metal lines were prepared lithographically on a silicon substrate. Thin films of a blend of PS and partially brominated PS were cast onto these substrates. The polymer domains formed on phase separation were found to align with the underlying line pattern, while laterally isotropic domain structures were observed on homogenous parts of the substrate. Later, Böltau et al. [137] continued work along these lines and carried the substrate driven domain alignment to some perfection. They studied various immiscible polymer blends (e.g. PS/PS_xBrS_{1-x} and PS/PVP) in the presence of lateral patterns of surface energy. By selective dissolution of one of the phases after phase separation was completed, they were able to transcribe a surface energy pattern into a topographic pattern in a polymer film. For perfect replication of the underlying structure, the inherent domain size formed during phase separation had to match the lateral size of the substrate pattern. Since the former is a function of the film thickness [135], for any given structure size on the substrate an optimum film thickness was identified. If the films were too thick, the domains were too large and did not follow the underlying grating. In thinner films, on the other hand, the domains are too small and recognise the small parts of the substrate pattern as homogenous substrates. Again, no pattern transfer was possible.

Another polymer blend, which has been shown to have its phase separation controlled by a surface energy pattern is a mixture of PB and PS [254]. In this work, thin ($\sim$70 nm) films of the blend were observed to follow a template created by microcontact printing of SAMs on silicon substrates. At about the same time Nisato et al. [255,256] reported on a similar study, which in addition to the work quoted above addressed the time development of the thin film domain structures in the presence of a laterally patterned substrate. Later work on two blends, PVP/PS_xBrS_{1-x} and PS/PVP, blends used dynamic SIMS and SFM to quantify the topography and morphology on a SAM microcontact printed onto gold [257]. Here, the effectiveness of pattern transfer as a function of the size of phase-separated domains was studied, with the best results being obtained when the pattern length scale is the same as that of the phase-separated morphology.

In the above-mentioned studies, the structural size of the patterned substrates was significantly larger than the molecular length scales of the (polymeric) liquid film. Given the rather large size of individual polymer molecules, it is tempting to study the wetting behaviour of thin polymer films on substrates exhibiting a lateral structure of comparable size. Various approaches have been reported aiming towards this direction. Obviously, the preparation of the patterned substrate becomes somewhat more involved when lateral scales of order 10 nm rather than microns are striven for. Electron beam lithography would in principle be able to create such structures, however, at high cost and on small areas only. Alternatively, self-organisation processes can be employed for substrate generation.

A quite elegant way to create a patterned substrate by self-organisation uses the well-established effects of surface reconstruction on silicon surfaces [258–260]. Here, surfaces of silicon single crystals are prepared with a surface orientation slightly off a low index crystal axis. Under suitable conditions (ultra-high vacuum annealing at around 1120 K), the surface develops facets of low index crystal planes. As an example, a silicon surface cut slightly off the $\langle 113 \rangle$ direction towards the $\langle 001 \rangle$ direction will develop a shallow sawtooth surface structure consisting of adjacent (113) and (114) facets. The angle between adjacent facets is 5.8°. When cooled to room temperature and exposed to air, a thin layer of native oxide forms on top of the facets, leaving the surface topography unchanged. An example of such a corrugated silicon substrate is shown in Fig. 33 [185]. Depending on the annealing time and temperature, the mean spacing between the corrugations along with their mean depth can be varied between some ten and some hundred nanometres. Such substrates were first used by Fasolka et al. to study their influence on the microdomain structure in diblock copolymer thin films [261]. Later, Rockford et al. showed that in addition to the topographical pattern, a chemical heterogeneity could be created on the corrugated silicon substrates by glancing angle metal evaporation [138, 262]. On these substrates, the authors studied the wetting behaviour of homopolymers, homopolymer blends, and diblock copolymers.

When a thin enough homopolymer film is coated on top of a corrugated substrate, the film is found to rupture into what may be called polymer 'nanochannels' (Fig. 34). This effect was first shown by Rehse et al. [185]. The results were

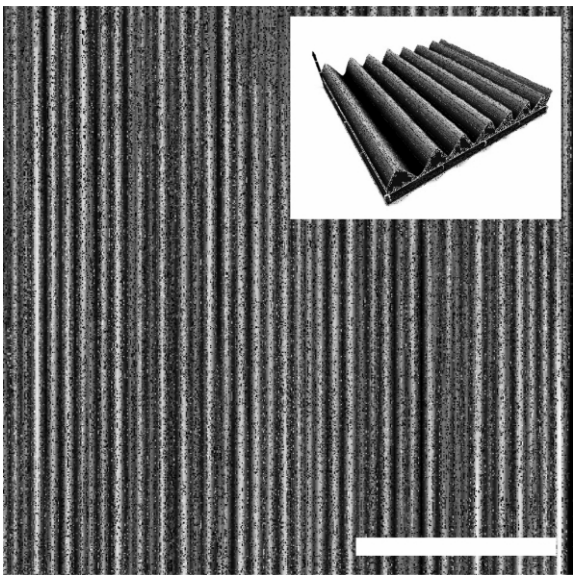

Fig. 33. SFM Tapping Mode™ topography image of a corrugated silicon surface of the type used for previous wetting experiments [138,185,261,262]. The scale bar is 4 μm, and the peak-to-valley distance (height) is ~5 nm. In the inset, a three-dimensional image of a 2 μm × 2 μm area is shown. Note that the height scale and the lateral scales are different, strongly exaggerating the aspect ratio of the surface structure. (These results are taken from the paper by Rehse et al. [185].) Reprinted with permission from Eur Phys J E 2001;4:69. © 2001 EDP Sciences [185].

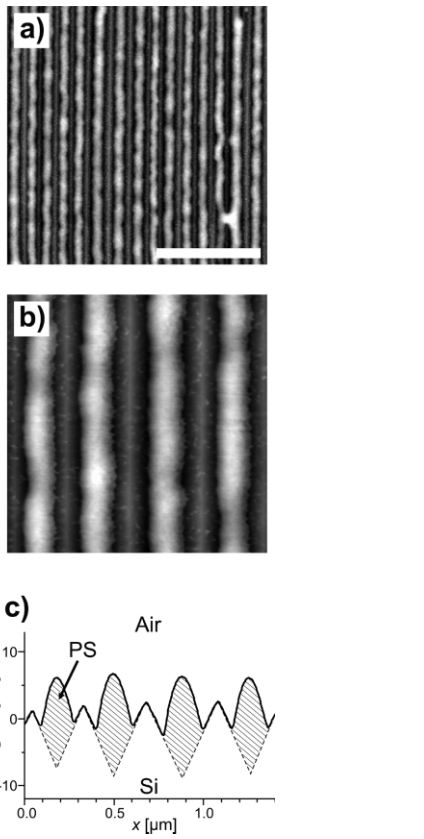

Fig. 34. (a and b) SFM TappingMode™ topography images (the scale bar is 2 μm) of a thin PS film (M_w = 100 kDa and average thickness, t_{av} = 5 nm) on a corrugated silicon substrate after annealing at 423 K for 3 h [185]. The film has broken into linear channels following the grooves of the substrate. The area shown in (b) is a 1.5 μm × 1.5 μm scan. (c) Average line scan along the horizontal taken from the image (b). The solid line is the experimental result. The dashed line depicts the position of the substrate surface. Reprinted with permission from Eur Phys J E 2001;4:69. © 2001 EDP Sciences [185].

surprising in that a PS film would only wet the corrugated substrate if the film thickness in the thinnest regions (t_{peak}, the thickness above the peaks of the corrugations) was more than about half of the chain radius of gyration. In Fig. 35 we show the stability phase diagram for thin PS films of differing M_w on these corrugated substrates as a function of t_{peak}. Above the line of stability, $t_{peak} = 0.55R_g$ the films remain stable after annealing, whereas for thicknesses smaller than $0.55R_g$, dewetting is observed. Test experiments on flat substrates, indicated by solid symbols in Fig. 35, exhibit the same behaviour, with thinner films dewetting the substrate and thicker ones remaining stable, although here there are not enough data to confirm a M_w dependence. Unstable films ruptured along the crests of the corrugation to form ordered nanochannels filling the valleys. The explanation of the stability phase diagram of these thin polymer films as a function of chain size is not wholly clear. Confinement effects appear to play a role, as was the case in the earlier experiments on topographically and chemically homogeneous substrates briefly mentioned above [237], but the effect of film preparation also needs to be considered. If a chemical heterogeneity is added to the topographical pattern by evaporation of Au on every other facet, the results look similar [138]. However, closer inspection of the ruptured films reveals that the nanochannels no longer fill the grooves symmetrically but preferentially cover the Au coated facets (Fig. 36) [185]. This effect can be understood given the wetting properties of PS on both SiO_x and Au, respectively [263].

Rockford et al. reported on quite interesting results regarding homopolymer blend thin films prepared on a corrugated and chemically patterned silicon substrate [138]. The chemical pattern is due to an evaporated gold layer on one side of each facet. The authors investigated the effect of the nanoscopic substrate pattern on the domain morphology of blends of PS and PMMA. On micron scales, an isotropic domain pattern appeared quite similar to a homogenous substrate with no preferential attraction to either of the two polymers. Here, the patterning resulted in a 'neutralisation' of the substrate, while homogenous surfaces of both SiO_x and Au are known to attract PMMA and PS, respectively [135]. After selective removal of the PMMA phase, however, the authors found that in the immediate vicinity

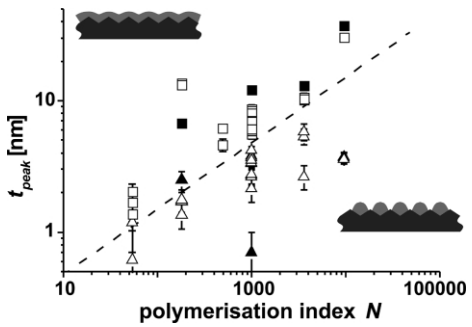

Fig. 35. Stability phase diagram for thin PS films on corrugated silicon substrates. Squares indicate stable PS films, while triangles refer to films where the formation of nano-channels was observed [185]. The dashed line indicates $t_{peak} = 0.55R_g$. The solid symbols indicate data taken from substrates with no corrugation. Reprinted with permission from Eur Phys J E 2001;4:69. © 2001 EDP Sciences [185].

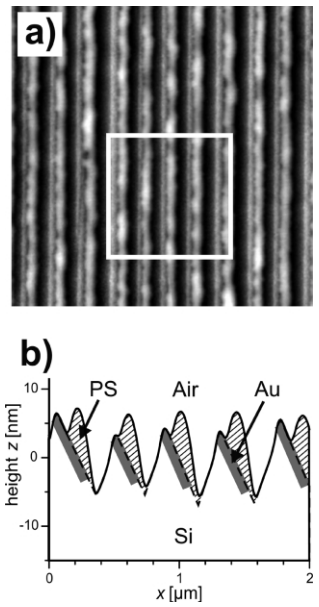

Fig. 36. (a) SFM TappingMode™ topography image of a thin PS film ($M_w = 100$ kDa, $t_{av} = 5$ nm) on a chemically patterned, corrugated silicon substrate after annealing at 423 K for 3 h [185]. Every other facet has been coated with a thin Au layer. The film has broken into linear channels following the grooves of the substrate. (b) Average line scan along the horizontal taken from the area inside the box indicated in image (a). The solid line is the experimental result. The dashed line depicts the position of the substrate surface. Reprinted with permission from Eur Phys J E 2001;4:69. © 2001 EDP Sciences [185].

of the substrate, laterally directed separation of PMMA and PS had taken place with PS selectively adsorbing onto the Au lines. Therefore, the presence of the nanoscopic grating indeed reduced the length scale of phase separation down to the molecular level.

Fukunaga et al. obtained similar results by using a quite different route of substrate patterning [264]. The authors adsorbed linear triblock copolymers of PS, PVP, and PtBMA onto the SiO_x surface of a silicon wafer. Since PVP strongly physisorbs on the polar substrate, the resulting film can be thoroughly washed to remove all loosely bound material. The resulting polymer brush consists of PS and PtBMA end blocks bound to the substrate by the PVP middle block. The PS and PtBMA blocks microphase separate and create a surface pattern of characteristic lateral spacing. The authors studied the wetting behaviour of thin films of a homopolymer blend of PS and PtBMA on such surfaces and observed that the domain size was significantly reduced in thin enough films (Fig. 37). A simple estimate of the interfacial energies involved predicts that the effect of the nanoscopically patterned substrate should influence the domain size up to a film thickness of about a quarter of the characteristic lateral spacing in agreement with the experimental observation. The authors also demonstrated that for thin enough films the effect of domain size reduction by the substrate is significantly more effective than the addition of PS-*block*-PtBMA copolymers acting as polymeric surfactants.

6. Outlook and conclusions

In this review much of what we have discussed concerns the fundamental physical processes that are important in the wetting behaviour of thin polymer films. Although there are still gaps in our knowledge, many of which have been alluded to elsewhere in this review, the subject is relatively well understood. In the section of dewetting, we discussed how various instability mechanisms could be used to generate pattern formation. The ways that patterned substrates could play a role in controlling the morphology of polymer films were discussed in the following section. We believe that such work will be more prevalent in the years to come as the fundamental understanding acquired during the previous 10 years, along with new fabrication procedures, is put to use. To conclude we summarise a few experiments that we believe will play an important role in future work involving the wetting of polymer films.

There are two directions to the research that we believe will dominate wetting phenomena in polymers in the years to come. We have described many relatively fundamental experiments, and it is now time to see how these can be applied, as an example, we have already discussed semi-conducting polymer blend films. Secondly, work will consider how wetting behaviour is altered in unusual geometries. As an example of the latter scenario, work is already starting to appear with confined polymers. For example, experiments have been performed where PS or SBS were confined to strips in a lithographed PDMS mask [265]. The polymer broke up, forming holes with a length scale of dewetting that was dependent on the size of the strips. Further experiments by these authors considered the

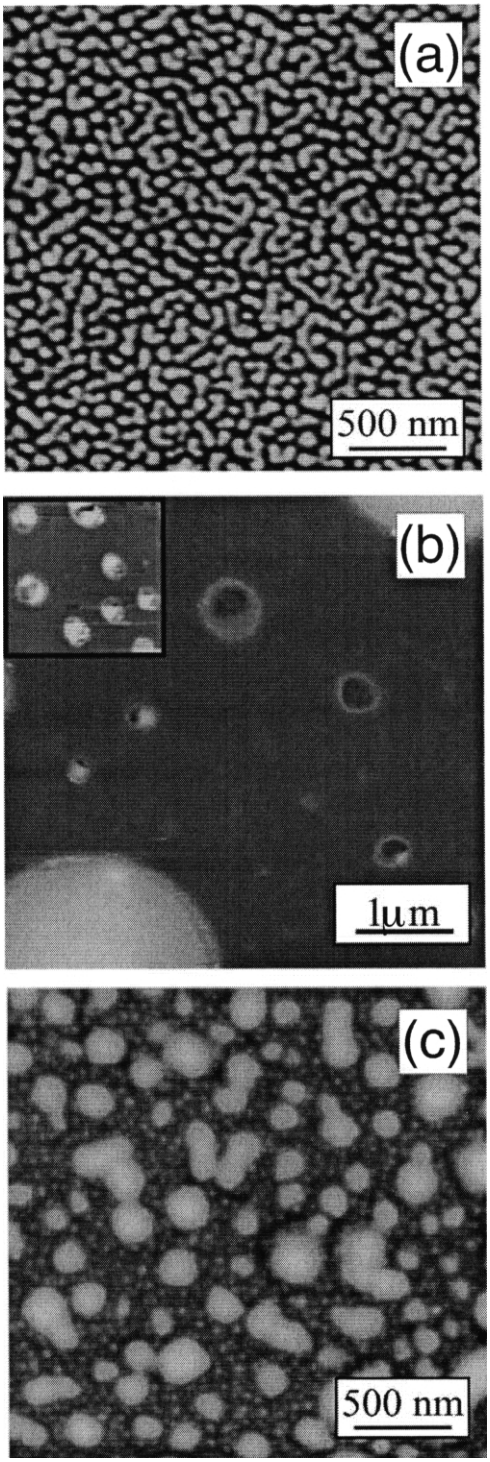

Fig. 37. (a) SFM TappingMode™ topography image of the surface of a 5 nm thick film of a PS-*block*-PVP-*block*-PtBMA triblock copolymer grafted onto a silicon wafer [264]. The respective molecular weights of the blocks are 51, 68, and 50 kDa. The height scale ranges between 0 and 5 nm. The r.m.s. roughness of the layer amounts to some 3 nm. (b) Topography image of a 20 nm thick film of a PS (M_w = 104 kDa)/PtBMA (M_w = 80 kDa) blend spun cast onto a plain silicon wafer (50% PS by weight). The height scale ranges between 0 and 50 nm. In the inset (top left corner) a larger area scan of the same sample is shown. (c) Topography image of a 20 nm thick film of a PS/PtBMA blend spun cast onto a silicon wafer coated with a graft layer of PS-*block*-PVP-*block*-PtBMA). The height scale ranges between 0 and 30 nm. Reprinted with permission from Langmuir 2000;16:3474. © 2000 American Chemical Society [264].

final morphology of blends of PS and PB annealed under PDMS masks [266]. Related experiments along the same lines were performed to create PMMA patterns after embossing in a silicon mask [267]. In a different experiment, blends of PMMA and SAN films were confined laterally on silicon substrates [268]. In this work the shapes of phase-separated domains depend upon the aspect ratio of the confinement (width and film thickness). For wider films, phase-separated domains are visible, whereas for films that are confined into thin strips, the domains are shaped more like capsules.

A recurring theme of research discussed in this review is that of self-assembly and pattern formation. A particularly interesting example of this is the use of electric fields to align polymers. Electric fields have a long-range behaviour, and can easily be tuned, which makes their use particularly desirable. Additionally, because thin films are being considered, only small potential differences can be used to generate large electric fields. We have already mentioned the use of electric fields in inducing dewetting, and it has also been shown that by placing a homopolymer film in an electric field, one can create uniform structures [269,270]. By using a patterned electrode one can select particular patterns [269]. These authors have performed similar experiments at polymer/oligomer and polymer/polymer interfaces [271,272]. Other related experiments were performed with copolymers; electric fields were used to align PS-*block*-PMMA to create PMMA cylinders in a matrix of PS [273]. A nice extension of this theme involves the use of ultra-violet irradiation to degrade the PMMA, whilst simultaneously cross-linking (i.e. fixing) the PS [274]. Rinsing in solvent (e.g. acetic acid) will remove the degraded PMMA leaving cylindrical nanopores, which, as an example, have been filled with cobalt to create magnetic nanostructures [275].

Another means of pattern formation that has been reported involves the annealing of polymer films above the glass transition typically ~100 nm below a mask, which is usually a silicon wafer coated with a surfactant monolayer to provide a low-energy surface [276,277]. In these initial experiments, thin films (between 100 nm and 2 μm) of PMMA were used. On cooling, the PMMA was observed to have risen against gravity, forming regularly spaced (a few micrometres) pillars in contact with the mask. The origin of this process is not yet understood although it may have electrostatic origins and could be related to some of the work involving pattern formation in stamps [267]; its use for

lithography should however be clear. It is difficult to see if a particular method of pattern formation will dominate in the coming years, because new methods are appearing with great regularity. As an example of a couple of other methods, the reader might like to consider the use of polyelectrolyte multi-layers [278] or the microbuckling of polymer films in water [279].

Acknowledgements

We thank Professors Jan Genzer, Russ Composto, Kari Dalnoki-Veress and Drs David Lidzey, Anthony Higgins, Ana Claudia Arias, Chun Wang, Peter Müller-Buschbaum, and Jakub Rysz for supplying data and figures, and for many useful comments. In particular we acknowledge Professor Andrzej Budkowski for a thorough critical reading of the manuscript. Figs. 2–4, 11, 12, 21 and 22 are reproduced with permission from EDP Sciences. The authors thank the Deutsche Forschungsgemeinschaft (SPP 1081) for generous financial support.

Appendix A. Mean-field theory of wetting

A.1. Theory of the wetting transition

The mathematics of the wetting transition is not difficult to follow as it involves a coupling of the theory of Cahn [56] with the Flory–Huggins lattice theory [57,58]. The theory of Cahn itself is simply a development of the van der Waals theory of capillarity [280]. Briefly, one writes the free energy of the binary mixture as a sum of the mixing entropy, enthalpy, and the surface energy. The (Gibbs) free energy of mixing per lattice site, G, for a polymer blend is given in the usual Flory–Huggins form as

$$\frac{G_{\text{bulk}}(\phi)}{k_{\text{B}}T} = \frac{\phi}{N_{\text{A}}}\ln\phi + \frac{1-\phi}{N_{\text{B}}}\ln(1-\phi) + \chi\phi(1-\phi), \tag{A1}$$

where N_{A} and N_{B} are the chain lengths. The difference in free energy caused by having a surface involves three terms: a surface energy term reflecting the benefit in having the component with the lower surface energy at the surface; a term dependent on the gradient in the free energy, which reflects the cost in having a composition gradient in the medium; and finally an energy cost in having a different surface composition to that in the bulk (ϕ_∞). These may be written as

$$\frac{\Delta G_{\text{surface}}(\phi)}{k_{\text{B}}T} = \Phi(\phi_{\text{s}}) + \int_0^\infty \left(g\left(\frac{\mathrm{d}\phi}{\mathrm{d}z}\right)^2 + \Delta f'(\phi)\right)\mathrm{d}z, \tag{A2}$$

and the cost in having the surface at a composition different from the bulk is given by

$$k_{\text{B}}T\Delta f'(\phi) = G(\phi) - G(\phi_\infty) - (\phi-\phi_\infty)\left(\frac{\partial G}{\partial\phi}\right)_{\phi_\infty}. \tag{A3}$$

The prefactor to the 'gradient squared term', g, represents the energy cost of having a composition gradient. Normally, g is assumed to be a constant, but in polymer systems it is calculated using the random phase approximation [90], and is given by

$$g = \frac{a^2}{36\phi(1-\phi)}. \tag{A4}$$

For very immiscible blends, the factor 1/36 is sometimes replaced by 1/24 [281]. The integral term in the surface free energy (Eq. (A2)) can be minimised by solving the Euler equation (this is a special case, in which the integrand does not contain z explicitly, see for example [282])

$$\Delta f'(\phi) = g\left(\frac{\mathrm{d}\phi}{\mathrm{d}z}\right)^2. \tag{A5}$$

Integrating the above (Eq. (A5)), we obtain the concentration profile

$$z = -\int_{\phi_{\text{s}}}^{\phi_\infty}\sqrt{\frac{g}{\Delta f'(\phi)}}\mathrm{d}\phi, \tag{A6}$$

which can be numerically solved using Eqs. (A1), (A3) and (A4).

By removing $(\mathrm{d}\phi/\mathrm{d}z)^2$ from Eq. (A2), using Eq. (A5), we arrive at the equilibrium surface free energy (with reduced dimensions of length)

$$\sigma = \Phi(\phi_{\text{s}}) + \int_{\phi_\infty}^{\phi_{\text{s}}}\frac{a}{3}\sqrt{\frac{\Delta f'(\phi)}{\phi(1-\phi)}}\mathrm{d}\phi, \tag{A7}$$

which, because it corresponds to thermodynamic equilibrium, yields the surface chemical potential, μ_{s}:

$$\mu_{\text{s}} = \frac{\mathrm{d}\Phi}{\mathrm{d}\phi_{\text{s}}} = -2\sqrt{g\Delta f'(\phi_{\text{s}})} = \frac{-a}{3}\sqrt{\frac{\Delta f'(\phi_{\text{s}})}{\phi_{\text{s}}(1-\phi_{\text{s}})}}. \tag{A8}$$

The importance of this surface chemical potential is revealed when both curves are plotted. This is the basis of the Cahn plot, or phase portrait, and is exemplified in Fig. 38. Eq. (A8) is solved when the curves cross. It can be seen that for particularly low values of $-\mathrm{d}\Phi/\mathrm{d}\phi_{\text{s}}$, there are three solutions to this equation. This means that partial and complete wetting can coexist. When there is only one solution, complete wetting is the only possible outcome. If the areas A and B are equal, there is a wetting transition.

Note that in Fig. 4 for the experiments of Rysz et al. [64], partial wetting occurs without an area B defined because they have a surface chemical potential with the solution $-\mathrm{d}\Phi/\mathrm{d}\phi_{\text{s}} = 0$ for $\phi < 1$. A consequence of this 'enrichment-depletion duality' [131] is that the polyolefin blend in

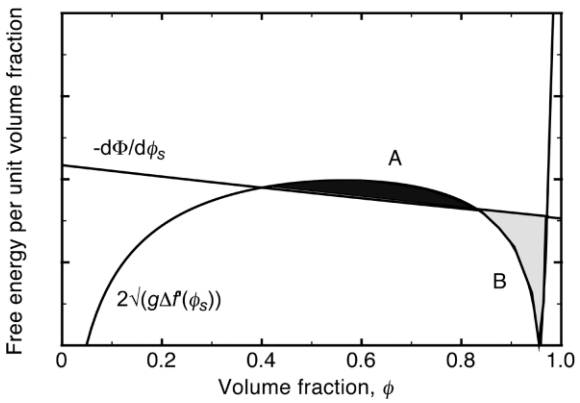

Fig. 38. Idealised phase portrait. If the area in A is less than that in B, total wetting represents the free energy minimum. If the area under A is greater than that under B, partial wetting is the more energetically favourable. When the two areas are equal, a wetting transition occurs.

this study could well be a good candidate for the observation of a second order wetting transition.

A.2. The approach to wetting

The approach to wetting was considered by Cahn [56], who discussed the possibility of prewetting in undersaturated systems. In such a case, a first order prewetting transition is possible whereby a mesoscopic (but finite) wetting layer could exist at the surface in equilibrium with a much smaller surface segregated layer.

The energy cost in having a surface segregated (or wetting) layer at a composition different from the bulk value is given by Eq. (A3), but one can also write this as a Taylor expansion around the upper coexistence volume fraction ϕ_β :

$$\Delta f'(\phi) = \Delta f'_{\min} + \tfrac{1}{2}(\phi - \phi_\beta)^2 \left(\frac{\partial^2 G}{\partial \phi^2}\right)_{\phi_\beta}. \tag{A9}$$

The first term corresponds to the distance of the tangent of the free energy curve at ϕ_∞ to the free energy at ϕ_β [56]. This distance is reached via an approximation

$$\Delta f'_{\min} = G(\phi_\infty) - G(\phi_\beta) - (\phi_\infty - \phi_\beta)\left(\frac{\partial G}{\partial \phi}\right)_{\phi_\infty}$$

$$\approx (\phi_\alpha - \phi_\infty)(\phi_\beta - \phi_\alpha)\left(\frac{\partial^2 G(\phi)}{\partial \phi^2}\right)_{\phi_\alpha}, \tag{A10}$$

where ϕ_α and ϕ_β are, respectively, the lower and upper coexistence volume fractions. Eq. (A10) can be justified because $(\partial G/\partial \phi)_{\phi_\infty} \approx (\phi_\infty - \phi_\alpha)(\partial^2 G/\partial \phi^2)_{\phi_\alpha}$ and we also replace $\phi_\infty - \phi_\beta$ with $\phi_\alpha - \phi_\beta$. For this to be possible we need to assume a symmetric or nearly symmetric blend. Cahn was primarily interested in binary metal alloys, for which, at coexistence $(\partial G/\partial \phi)_{\phi_\alpha} = (\partial G/\partial \phi)_{\phi_\beta} = 0$. For this reason the first order differential is missing from the Taylor expansion (Eq. (A9)).

We can now substitute Eq. (A9) into Eq. (A6) and obtain

$$\frac{l}{2} = -\sqrt{\frac{2g}{\left(\frac{\partial^2 G}{\partial \phi^2}\right)_{\phi_\beta}}} \int_{\phi_\infty}^{\phi_s} \frac{\mathrm{d}\phi}{\sqrt{\frac{2\Delta f'_{\min}}{\left(\frac{\partial^2 G}{\partial \phi^2}\right)_{\phi_\beta}} + (\phi - \phi_\beta)^2}}. \tag{A11}$$

In small molecule systems g can be treated as constant and the standard integral $\int \mathrm{d}u/\sqrt{a^2+u^2} = \ln(u + \sqrt{a^2+u^2})$ can be used to obtain

$$\frac{l}{2} = -\sqrt{\frac{2g}{\left(\frac{\partial^2 G}{\partial \phi^2}\right)_{\phi_\beta}}} \left(\tfrac{1}{2} \ln\left(\frac{2\Delta f'_{\min}}{\left(\frac{\partial^2 G}{\partial \phi^2}\right)_{\phi_\beta}} \right) - \ln\left((\phi_s - \phi_\beta) + \sqrt{(\phi_s - \phi_\beta)^2 + \frac{2\Delta f'_{\min}}{\left(\frac{\partial^2 G}{\partial \phi^2}\right)_{\phi_\beta}}} \right) \right). \tag{A12}$$

If we assume that $\Delta f'_{\min} \ll \Delta f'(\phi_s)$, which is valid in symmetric systems near saturation, we can allow $\phi_s - \phi_\beta$ to dominate the last term in the root of Eq. (A12) (inspection of Eq. (A9) should confirm this).

Neglecting $\Delta f'_{\min}$, we can substitute Eq. (A9) into Eq. (A8) to obtain

$$2(\phi_s - \phi_\beta) = \sqrt{\frac{2\mu_s^2}{g\left(\frac{\partial^2 G}{\partial \phi^2}\right)_{\phi_\beta}}}, \tag{A13}$$

which we can substitute into Eq. (A12) to yield

$$\frac{l}{2} = \sqrt{\frac{g}{2\left(\frac{\partial^2 G}{\partial \phi^2}\right)_{\phi_\beta}}} \left(\ln \frac{\mu_s^2}{g} - \ln \Delta f'_{\min} \right). \tag{A14}$$

As $\phi_\infty \to \phi_\alpha$, the size of the prewetting layer, l diverges logarithmically. As has been pointed out earlier, g is a function of ϕ and so Eq. (A11) can only be solved numerically. However, as a first approximation it is perfectly acceptable, and was used by Geoghegan et al. [6] to fit their adsorption isotherm for a d-PS/PαMS blend, although this will not be the ideal way to extract a value for μ_s. Earlier simulations demonstrated the validity of this approximation for d-PS/h-PS blends [83]. For a more quantitative analysis, the approach used for segregation in polyolefin blends is recommended [66].

A.3. Surface segregation

The form for the surface energy in polymer mixtures has been presented by different authors in different forms to account for differing results. The simplest, and most commonly used, is that due to Schmidt and Binder [55], which contains two terms

$$\Phi_s = -\mu_1\phi_s - \frac{s\phi_s^2}{2}, \tag{A15}$$

which are the leading terms in a Taylor expansion of the bare surface energy. It is necessary that $\mu_1 + s/2 > 0$ and ϕ_s be small, which can result in corrections for nearly complete wetting of the surface by one of the phases when surface entropy terms become important [88,283]. (Another approach [91], which is based on the Gibbs adsorption equation, is discussed briefly in Sections 3.3.2 and 3.3.4.) The two terms in the Schmidt and Binder form have physical meaning: μ_1 is a surface chemical potential difference (not to be confused with μ_s) and $s/2$ is a surface interaction parameter accounting for both the change in dimensionality and the different interactions from the bulk. We write the surface energy difference between the two components as

$$\Delta\gamma = \frac{k_B T}{b^3}\left(\mu_1 + \frac{s}{2}\right), \tag{A16}$$

with b being the size of a lattice unit. The surface interaction parameter s can be related to the bulk interaction parameter by [284–286]:

$$s = -b\chi. \tag{A17}$$

Differentiating Eq. (A15) with respect to ϕ_s, and substituting this, Eqs. (A3), (A4), (A16) and (A17) into Eq. (A8), we obtain

$$\frac{b^3\Delta\gamma}{k_B T} - b\chi\left(\phi - \tfrac{1}{2}\right) = \frac{a}{3}\sqrt{\frac{G(\phi) - G(\phi_\alpha) - (\phi - \phi_\alpha)\Delta\mu_\alpha}{k_B T\phi(1-\phi)}}, \tag{A18}$$

where $\Delta\mu_\alpha = (\partial G/\partial\phi)_{\phi_\alpha}$ and any composition dependence of ϕ has been neglected. The composition profile is obtained from Eq. (A6) and is recast in the Flory–Huggins form here to give the volume fraction-depth profile

$$z = \frac{a\sqrt{k_B T}}{6}\int_{\phi_s}^{\phi_\infty}\frac{d\phi}{\sqrt{G(\phi) - G(\phi_\infty) - \phi(1-\phi)\Delta\mu_\infty}}, \tag{A19}$$

where $\Delta\mu_\infty = (\partial G/\partial\phi)_{\phi_\infty}$. Similarly, the surface excess is given by

$$z^* = \frac{a\sqrt{k_B T}}{6}\int_{\phi_s}^{\phi_\infty}\frac{(\phi - \phi_\infty)d\phi}{\sqrt{G(\phi) - G(\phi_\infty) - \phi(1-\phi)\Delta\mu_\infty}}. \tag{A20}$$

References

[1] Bhatia QS, Pan DH, Koberstein JT. Preferential surface adsorption in miscible blends of polystyrene and poly(vinyl methyl ether). Macromolecules 1988;21:2166–75.

[2] Jones RAL, Kramer EJ, Rafailovich MH, Sokolov J, Schwarz SA. Surface enrichment in an isotopic polymer blend film. Phys Rev Lett 1989;62:280–3.

[3] Cahn JW. Phase separation by spinodal decomposition in isotropic systems. J Chem Phys 1965;42:93–9.

[4] Hashimoto T. Dynamics in spinodal decomposition of polymer mixtures. Phase Trans 1988;12:47–119.

[5] Jones RAL, Norton LJ, Kramer EJ, Bates FS, Wiltzius P. Surface-directed spinodal decomposition. Phys Rev Lett 1991;66:1326–9 ibid p. 3087.

[6] Geoghegan M, Ermer H, Jüngst G, Krausch G, Brenn R. Wetting in a phase separating polymer blend film: quench depth dependence. Phys Rev E 2000;62:940–50.

[7] Krausch G. Surface induced self assembly in thin polymer films. Mater Sci Engng 1995;R14:1–94.

[8] Budkowski A. Interfacial phenomena in thin polymer films: phase coexistence and segregation. Adv Polym Sci 1999;148:1–111.

[9] Stamm M. Polymer interfaces on a molecular scale: comparison of techniques and some examples. Adv Polym Sci 1992;100:357–400.

[10] de Gennes PG. Wetting: statics and dynamics. Rev Mod Phys 1985;57:827–63.

[11] Binder K. Phase transitions of polymer blends and block copolymer melts in thin films. Adv Polym Sci 1999;138:1–89.

[12] Müller M, Binder K, Albano EV. Phase equilibria in thin polymer films. Int J Mod Phys B 2001;15:1867–903.

[13] Puri S, Frisch HL. Surface-directed spinodal decomposition: modelling and numerical simulations. J Phys: Condens Matter 1997;9:2109–33.

[14] Fasolka MJ, Mayes AM. Block copolymer thin films: physics and applications. Annu Rev Mater Res 2001;31:323–55.

[15] Jones RAL, Richards RW. Polymers at surfaces and interfaces. Cambridge: Cambridge University Press; 1999.

[16] Schwarz SA, Wilkens BJ, Pudensi MAA, Rafailovich MH, Sokolov J, Zhao X, Zhao W, Zheng X, Russell TP, Jones RAL. Studies of surface and interface segregation in polymer blends by secondary ion mass spectrometry. Mol Phys 1992;76:937–50.

[17] Bernasik A, Rysz J, Budkowski A, Kowalski K, Camra J, Jedliński J. Three-dimensional information on the phase domain structure of thin films of polymer blends revealed by secondary ion mass spectroscopy. Macromol Rapid Commun 2001;22:829–34.

[18] Gray KH, Gould S, Leasure RM, Musselman IH, Lee JJ, Meyer TJ, Linton RW. Three-dimensional characterization of conducting polymer arrays using secondary ion mass spectrometry. J Vac Sci Technol, A 1992;10:2679–84.

[19] Composto RJ, Walters RM, Genzer J. Application of ion scattering techniques to characterize polymer surfaces and interfaces. Mater Sci Engng 2002;R38:107–80.

[20] Geoghegan M. MeV ion beam profiling of polymer surfaces and interfaces. In: Richards RW, Peace SK, editors. Polymer surfaces and interfaces III. Chichester: Wiley; 1999. p. 43–73.

[21] Geoghegan M, Jones RAL, Clough AS, Penfold J. The morphology of as-cast films of a polymer blend: dependence on polymer molecular weight. J Polym Sci, Part B: Polym Phys 1995;33:1307–11.
[22] Mills PJ, Green PF, Palmstrøm CJ, Mayer JW, Kramer EJ. Analysis of diffusion in polymers by forward recoil spectrometry. Appl Phys Lett 1984;45:957–9.
[23] Genzer J, Rothman JB, Composto RJ. Improved hydrogen and deuterium depth profiling in polymers using low energy forward recoil spectrometry. Nucl Instr Meth B 1994;86: 345–54.
[24] Sokolov J, Rafailovich MH, Jones RAL, Kramer EJ. Enrichment depth profiles in polymer blends measured by forward recoil spectrometry. Appl Phys Lett 1989;54:590–2.
[25] Ermer H, Pfaff O, Straub W, Geoghegan M, Brenn R. Deuterium depth profiling in polymers using heavy ion elastic recoil detection. Nucl Instr Meth B 1998;134:237–48.
[26] Geoghegan M, Abel F. High resolution elastic recoil detection analysis of polystyrene depth profiles using carbon ions. Nucl Instr Meth B 1998;143:371–80.
[27] Chaturvedi UK, Steiner U, Zak O, Krausch G, Schatz G, Klein J. Structure at polymer interfaces determined by high-resolution nuclear reaction analysis. Appl Phys Lett 1990;56: 1228–30.
[28] Payne RS, Clough AS, Murphy P, Mills PJ. Use of the D(^{3}He,p)^{4}He reaction to study polymer diffusion in polymer melts. Nucl Instr Meth B 1989;42:130–4.
[29] Russell TP. X-ray and neutron reflectivity for the investigation of polymers. Mater Sci Rep 1990;5:171–271.
[30] Bucknall DG, Higgins JS. Neutron reflection studies of polymer–polymer interfaces. In: Hommell H, editor. Polymer surfaces and interfaces—a versatile combination: recent research developments in polymer science. Trivandrum, India: Research Signpost; 1998. p. 161–99.
[31] Penfold J, Thomas RK. The application of the specular reflection of neutrons to the study of surfaces and interfaces. J Phys: Condens Matter 1990;2:1369–412.
[32] Cleveland JP, Anczykowski B, Schmid AE, Elings VB. Energy dissipation in tapping-mode atomic force microscopy. Appl Phys Lett 1998;72:2613–5.
[33] Krausch G, Hipp M, Böltau M, Mlynek J, Marti O. High resolution imaging of polymer surfaces with chemical sensitivity. Macromolecules 1995;28:260–3.
[34] Lambooy P, Phelan KC, Haugg O, Krausch G. Dewetting at the liquid–liquid interface. Phys Rev Lett 1996;76:1110–3.
[35] Knoll A, Magerle R, Krausch G. Tapping mode atomic force microscopy on polymers: where is the true sample surface? Macromolecules 2000;34:4159–65.
[36] Pohl DW, Denk W, Lanz M. Optical stethoscopy: image recording with resolution $\lambda/20$. Appl Phys Lett 1984;44: 651–3.
[37] Betzig E, Trautmann JK. Near-field optics: microscopy, spectroscopy, and surface modification beyond the diffraction limit. Science 1992;257:189–95.
[38] Straub W, Bruder F, Brenn R, Krausch G, Bielefeldt H, Kirsch A, Marti O, Mlynek J, Marko JF. Transient wetting and 2D spinodal decomposition in a binary polymer blend. Europhys Lett 1995;29:353–8.
[39] Betzig E. Principles and applications of near-field scanning optical microscopy (NSOM). In: Pohl DW, Courjon D, editors. Near field optics. Dordrecht: Kluwer; 1993. p. 7–15.
[40] Laurer JH, Winey KI. Direct imaging of ionic aggregates in Zn-neutralized poly(ethylene-*co*-methacrylic acid) copolymers. Macromolecules 1998;31:9106–8.
[41] Magerle R. Nanotomography. Phys Rev Lett 2000;85: 2749–52.
[42] Konrad M, Knoll A, Krausch G, Magerle R. Volume imaging of an ultrathin SBS triblock copolymer film. Macromolecules 2000;33:5518–23.
[43] Ertl G, Küppers J. X-ray photoelectron spectroscopy (XPS). Low energy electrons and surface chemistry, Weinheim: VCH; 1985. p. 65–85.
[44] Short RD, Ameen AP, Jackson ST, Pawson DJ, O'Toole L, Ward AJ. TOF-SIMS in polymer surface studies. Vacuum 1993;44:1143–60.
[45] Ade H, Zhang X, Cameron S, Costello C, Kirz J, Williams S. Chemical contrast in X-ray microscopy and spatially resolved XANES spectroscopy of organic specimens. Science 1992;258:972–5.
[46] Ade H, Winesett DA, Smith AP, Qu S, Ge S, Sokolov J, Rafailovich MH. Phase segregation in polymer thin films: elucidations by X-ray and scanning force microscopy. Europhys Lett 1999;45:526–32.
[47] Slep D, Asselta J, Rafailovich MH, Sokolov J, Winesett DA, Smith AP, Ade H, Anders S. Effect of an interactive surface on the equilibrium contact angles in bilayer polymer films. Langmuir 2000;16:2369–75.
[48] Slep D, Asselta J, Rafailovich MH, Sokolov J, Winesett DA, Smith AP, Ade H, Strzhemechny Y, Schwarz SA, Sauer BB. Phase separation of polystyrene and bromo-polystyrene mixtures in equilibrium structures in thin films. Langmuir 1998;14:4860–4.
[49] Factor BJ, Russell TP, Toney MF. Surface-induced ordering of an aromatic polyimide. Phys Rev Lett 1991;66:1181–4.
[50] Durell M, Macdonald JE, Trolley D, Wehrum A, Jukes PC, Jones RAL, Walker CJ, Brown G. The role of surface-induced ordering in the crystallisation of PET films. Europhys Lett 2002;58:844–50.
[51] Müller-Buschbaum P, Stamm M. Correlated roughness, long-range correlations, and dewetting of thin polymer films. Macromolecules 1998;31:3686–92.
[52] Sferrazza M, Heppenstall-Butler M, Cubitt R, Bucknall DG, Webster J, Jones RAL. Interfacial instability driven by dispersive forces: the early stages of spinodal dewetting of a thin polymer film on a polymer substrate. Phys Rev Lett 1998;81:5173–6.
[53] Gardella Jr JA. Recent advances in ion and electron spectroscopy of polymer surfaces. Appl Surf Sci 1988;31: 72–102.
[54] Reich S, Cohen Y. Phase separation of polymer blends in thin films. J Polym Sci, Polym Phys Ed 1981;19:1255–67.
[55] Schmidt I, Binder K. Model calculations for wetting transitions in polymer mixtures. J Phys 1985;46:1631–44.
[56] Cahn JW. Critical point wetting. J Chem Phys 1977;66: 3667–72.
[57] de Gennes P-G. Scaling concepts in polymer physics. Ithaca: Cornell University Press; 1979.
[58] Flory PJ. Principles of polymer chemistry. Ithaca: Cornell University Press; 1953.
[59] Bruder F, Brenn R. Spinodal decomposition in thin films of a polymer blend. Phys Rev Lett 1992;69:624–7.
[60] Krausch G, Dai C-A, Kramer EJ, Marko JF, Bates FS.

Interference in spinodal waves in thin polymer films. Macromolecules 1993;26:5566–71.
[61] Krausch G, Dai C-A, Kramer EJ, Bates FS. Real space observation of dynamic scaling in a critical polymer mixture. Phys Rev Lett 1993;71:3669–72.
[62] Geoghegan M, Jones RAL, Clough AS. Surface directed spinodal decomposition in a partially miscible polymer blend. J Chem Phys 1995;103:2719–24.
[63] Nakanishi H, Pincus P. Surface spinodals and extended wetting in fluids and polymer solutions. J Chem Phys 1983; 79:997–1003.
[64] Rysz J, Budkowski A, Bernasik A, Klein J, Kowalski K, Jedliński J, Fetters LJ. Wetting transition in a binary polymer blend. Europhys Lett 2000;50:35–40.
[65] Scheffold F, Eiser E, Budkowski A, Steiner U, Klein J, Fetters LJ. Surface phase behavior in binary polymer mixtures. I. Miscibility, phase coexistence, and interactions in polyolefin blends. J Chem Phys 1996;104:8786–94.
[66] Scheffold F, Budkowski A, Steiner U, Eiser E, Klein J, Fetters LJ. Surface phase behavior in binary polymer mixtures. II. Surface enrichment from polyolefin blends. J Chem Phys 1996;104:8795–806.
[67] Steiner U, Klein J. Growth of wetting layers from liquid mixtures. Phys Rev Lett 1996;77:2526–9.
[68] Steiner U, Klein J, Eiser E, Budkowski A, Fetters LJ. Complete wetting from polymer mixtures. Science 1992;258: 1126–9.
[69] Steiner U, Klein J, Fetters LJ. Surface phase inversion in finite-sized binary mixtures. Phys Rev Lett 1994;72: 1498–501.
[70] Losch A, Salomonovich R, Steiner U, Fetters LJ, Klein J. Self-diffusion in melts of statistical copolymers—the effect of changes in microstructural composition. J Polym Sci, Part B: Polym Phys 1995;33:1821–31.
[71] Jones RAL. The wetting transition for polymer mixtures. Polymer 1994;35:2160–6.
[72] Müller M, Albano EV, Binder K. Symmetric polymer blend confined into a film with antisymmetric surfaces: interplay between wetting behavior and the phase diagram. Phys Rev E 2000;62:5281–95.
[73] Wiltzius P, Cumming A. Domain growth and wetting in polymer mixtures. Phys Rev Lett 1991;66:3000–3.
[74] Troian SM. Coalescence induced domain growth near a wall during spinodal decomposition. Phys Rev Lett 1993;71: 1399–402. see also the comment by Keblinski P, Ma WJ, Maritan A, Koplik J, Banavar JR. 1994;72:3738 and reply 1994;72:3739.
[75] Marko JF. Influence of surface interactions on spinodal decomposition. Phys Rev E 1993;48:2861–79.
[76] Tanaka H. Interplay between wetting and phase separation in binary fluid mixtures: roles of hydrodynamics. J Phys: Condens Matter 2001;13:4637–74.
[77] Puri S, Binder K. Surface effects on spinodal decomposition in binary mixtures and the interplay with wetting phenomena. Phys Rev E 1994;49:5359–77.
[78] Puri S, Binder K, Frisch HL. Surface effects on spinodal decomposition in binary mixtures: the case with long-ranged surface fields. Phys Rev E 1997;56:6991–7000.
[79] Lifshitz IM, Slyozov VV. The kinetics of precipitation from supersaturated solid solutions. J Phys Chem Solids 1961;19: 35–50.
[80] Puri S, Binder K. Power laws and crossovers in off-critical surface-directed spinodal decomposition. Phys Rev Lett 2001;86:1797–800.
[81] Jones RAL, Kramer EJ. Kinetics of formation of a surface enriched layer in an isotopic polymer blend. Phil Mag B 1990;62:129–37.
[82] Lipowsky R, Huse DA. Diffusion-limited growth of wetting layers. Phys Rev Lett 1986;57:353–6.
[83] Geoghegan M, Nicolai T, Penfold J, Jones RAL. Kinetics of surface segregation and the approach to wetting in an isotopic polymer blend. Macromolecules 1997;30:4220–7.
[84] Bates FS, Wignall GD. Nonideal mixing in binary blends of perdeuterated and protonated polystyrene. Macromolecules 1986;19:932–4.
[85] Budkowski A, Steiner U, Klein J. The effects of confinement and surface interactions on coexistence in a binary polymer mixture. J Chem Phys 1992;97:5229–38.
[86] Green PF, Doyle BL. Isotope effects on interdiffusion in blends of normal and perdeuterated polymers. Phys Rev Lett 1986;57:2407–10.
[87] Sauer BB, Dee GT. Molecular weight and temperature dependence of polymer surface tension: comparison of experiment with theory. Macromolecules 1991;24:2124–6.
[88] Zhao H, Zhao W, Sokolov J, Rafailovich MH, Schwarz SA, Wilkens BJ, Jones RAL, Kramer EJ. Determination of the concentration profile at the surface of d-PS/h-PS blends using high-resolution ion scattering techniques. Macromolecules 1991;24:5991–6.
[89] Genzer J, Composto RJ. Surface segregation amplification in miscible polymer blends near criticality. Europhys Lett 1997; 38:171–6.
[90] Strobl GR. The physics of polymers. Berlin: Springer; 1997.
[91] Norton LJ, Kramer EJ, Bates FS, Gehlsen MD, Jones RAL, Karim A, Felcher GP, Kleb R. Neutron reflectometry study of surface segregation in an isotopic poly(ethylenepropylene) blend: deviation from mean-field theory. Macromolecules 1995;28:8621–8.
[92] Budkowski A, Rysz J, Scheffold F, Klein J, Fetters LJ. Effect of deuterium substitution on the surface interactions in binary polymer mixtures. J Polym Sci, Part B: Polym Phys 1998;36: 2691–702.
[93] Budkowski A, Scheffold F, Klein J, Fetters LJ. Surface phase behavior in binary polymer mixtures. III. Temperature dependence of surface enrichment and of wetting. J Chem Phys 1997;106:719–27.
[94] Sariban A, Binder K. Critical properties of the Flory–Huggins lattice model of polymer mixtures. J Chem Phys 1987;86:5859–73.
[95] Geoghegan M, Russ T, Brenn R. Thermodynamic suppression of Brownian motion. Phys Rev Lett 2001;86:2581–4.
[96] Siggia ED. Late stages of spinodal decomposition in binary mixtures. Phys Rev A 1979;20:595–605.
[97] Krausch G, Kramer EJ, Bates FS, Marko JF, Brown G, Chakrabarti A. Surface-induced asymmetries during spinodal decomposition in off-critical polymer mixtures. Macromolecules 1994;27:6768–76.
[98] Tanaka H. Interplay between phase separation and wetting for a polymer mixture confined in a two-dimensional capillary: wetting induced domain ordering and coarsening. Europhys Lett 1993;24:665–71.
[99] Wang H, Composto RJ. Understanding morphology

evolution and roughening in phase-separating thin-film polymer blends. Europhys Lett 2000;50:622–7.
[100] Wang H, Composto RJ. Hydrodynamic-flow-driven wetting in thin film polymer blends: growth kinetics and morphology. Phys Rev E 2000;61:1659–63.
[101] Wang H, Composto RJ. Thin film polymer blends undergoing phase separation and wetting: identification of early, intermediate, and late stages. J Chem Phys 2000;113: 10386–97.
[102] Wang H, Composto RJ. Kinetics of surface and interfacial fluctuations in phase separating polymer blend films. Macromolecules 2002;35:2799–809.
[103] Heier J, Kramer EJ, Revesz P, Battistig G, Bates FS. Spinodal decomposition in a subsurface layer of a polymer blend film. Macromolecules 1999;32:3758–65.
[104] Rysz J, Ermer H, Budkowski A, Bernasik A, Lekki J, Juengst G, Brenn R, Kowalski K, Camra J, Lekka M, Jedliński J. Hydrodynamic-flow-driven phase evolution in a polymer blend film modified by diblock copolymers. Eur Phys J E 2001;5:207–19.
[105] Rysz J, Bernasik A, Ermer H, Budkowski A, Brenn R, Hashimoto T, Jedliński J. Surface-directed spinodal decomposition modified by a surface active copolymer. Europhys Lett 1997;40:503–8.
[106] Brochard Wyart F, Martin P, Redon C. Liquid/liquid dewetting. Langmuir 1993;9:3682–90.
[107] Hoppe H, Heuberger M, Klein J. Self-similarity and pattern selection in the roughening of binary liquid films. Phys Rev Lett 2001;86:4863–6.
[108] Jones RAL, Norton LJ, Kramer EJ, Composto RJ, Stein RS, Russell TP, Mansour A, Karim A, Felcher GP, Rafailovich MH, Sokolov J, Zhao X, Schwarz SA. The form of the enriched surface layer in polymer blends. Europhys Lett 1990;12:41–6.
[109] Geoghegan M, Jones RAL, Sivia DS, Penfold J, Clough AS. Experimental study of surface segregation and wetting in films of a partially miscible polymer blend. Phys Rev E 1996; 53:825–37.
[110] Jones RAL. Effect of long-range forces on surface enrichment in polymer blends. Phys Rev E 1993;47:1437–40.
[111] Genzer J, Faldi A, Composto RJ. Self-consistent mean-field calculation of surface segregation in a binary polymer blend. Phys Rev E 1994;50:2373–6.
[112] Rowlinson JS, Widom B. Molecular theory of capillarity. Oxford: Oxford University Press; 1982.
[113] Genzer J, Composto RJ. Effect of molecular weight on the interfacial excess, tension, and width in a homopolymer/ binary polymer blend system. Macromolecules 1998;31: 870–8.
[114] Aubouy M, Manghi M, Raphaël E. Interfacial properties of polymeric liquids. Phys Rev Lett 2000;84:4858–61. see also the comment by Kumar SK, Jones RL. 2001;87:179601 and reply 2001;87:179602.
[115] Helfand E. Theory of the homopolymer/binary-polymer-mixture interface. Macromolecules 1992;25:1676–85.
[116] Faldi A, Genzer J, Composto RJ, Dozier WD. Segregation at the interface between a homopolymer and a binary polymer blend. Phys Rev Lett 1995;74:3388–91.
[117] Brown HR. Effect of a diblock copolymer on the adhesion between incompatible polymers. Macromolecules 1989;22: 2859–60.
[118] Creton C, Kramer EJ, Hui C-Y, Brown HR. Failure mechanisms of polymer interfaces reinforced with block copolymers. Macromolecules 1992;25:3075–88.
[119] Benkoski JJ, Fredrickson GH, Kramer EJ. Effects of composition drift on the effectiveness of random copolymer reinforcement at polymer–polymer interfaces. J Polym Sci, Part B: Polym Phys 2001;39:2363–77.
[120] Dai C-A, Dair BJ, Dai KH, Ober CK, Kramer EJ, Hui C-Y, Jelinski LW. Reinforcement of polymer interfaces with random copolymers. Phys Rev Lett 1994;73:2472–5. see also the comment by Noolandi J, Shi A-C. 1995;74:2836 and reply 1995;74:2837.
[121] Gersappe D, Irvine D, Balazs AC, Liu Y, Sokolov J, Rafailovich M, Schwarz S, Peiffer DG. The use of graft-copolymers to bind immiscible blends. Science 1994;265: 1072–4.
[122] Deruelle M, Léger L, Tirrell M. Adhesion at the solid–elastomer interface: influence of the interfacial chains. Macromolecules 1995;28:7419–28.
[123] Geoghegan M, Clarke CJ, Boué F, Menelle A, Russ T, Bucknall DG. The kinetics of penetration of grafted polymers into a network. Macromolecules 1999;32:5106–14.
[124] Hester JF, Bannerjee P, Mayes AM. Preparation of protein-resistant surfaces on poly(vinylidene fluoride) membranes via surface segregation. Macromolecules 1999;32: 1643–4650.
[125] Yethiraj A. Entropic and enthalpic surface segregation from blends of branched and linear polymers. Phys Rev Lett 1995; 74:2018–21.
[126] Geoghegan M, Boué F, Menelle A, Abel F, Russ T, Ermer H, Brenn R, Bucknall DG. Surface segregation from polystyrene networks. J Phys: Condens Matter 2000;12:5129–42.
[127] Genzer J, Kramer EJ. Wetting of substrates with phase-separated binary mixtures. Phys Rev Lett 1997;78:4946–9.
[128] Genzer J, Kramer EJ. Pretransitional thinning of a polymer wetting layer. Europhys Lett 1998;44:180–5.
[129] Huang E, Rockford L, Russell TP. Nanodomain control in copolymer thin films. Nature 1998;395:757–8.
[130] Hariharan A, Kumar SK, Russell TP. Reversal of the isotope effect in the surface behavior of binary polymer blends. J Chem Phys 1993;98:4163–73.
[131] Budkowski A, Rysz J, Scheffold F, Klein J. Surface enrichment-depletion duality in a binary polymer blend. Europhys Lett 1998;43:404–9.
[132] Walheim S, Schäffer E, Mlynek J, Steiner U. Nanophase-separated polymer films as high-performance antireflection coatings. Nature 1999;283:520–2.
[133] Geoghegan M, Jones RAL, Payne RS, Sakellariou P, Clough AS, Penfold J. Lamellar structure in a thin polymer blend film. Polymer 1994;35:2019–27.
[134] Nesterov A, Horichko V, Lipatov Y. Phase separation of poly(vinyl acetate)–poly(methyl methacrylate) mixtures in thin films. Makromol Chem, Rapid Commun 1991;12: 571–4.
[135] Walheim S, Böltau M, Mlynek J, Krausch G, Steiner U. Structure formation via polymer demixing in spin-cast films. Macromolecules 1997;30:4995–5003.
[136] Walheim S, Böltau M, Steiner U, Krausch G. Phase separation in thin films of strongly incompatible polymer blends. In: Richards RW, Peace SK, editors. Polymer

surfaces and interfaces III. Chichester: Wiley; 1999. p. 75–99.
[137] Böltau M, Walheim S, Mlynek J, Krausch G, Steiner U. Surface-induced structure formation of polymer blends on patterned substrates. Nature 1998;391:877–9.
[138] Rockford L, Liu Y, Mansky P, Russell TP, Yoon M, Mochrie SGJ. Polymers on nanoperiodic heterogeneous surfaces. Phys Rev Lett 1999;82:2602–5.
[139] Tanaka K, Takahara A, Kajiyama T. Film thickness dependence of the surface structure of immiscible polystyrene/poly(methyl methacrylate) blends. Macromolecules 1996;29:3232–9.
[140] Dalnoki-Veress K, Forrest JA, Stevens JR, Dutcher JR. Phase separation morphology of spin-coated polymer blend thin films. Physica A 1997;239:87–94.
[141] Müller-Buschbaum P, O'Neill SA, Affrossman S, Stamm M. Phase separation and dewetting of weakly incompatible polymer blend films. Macromolecules 1998;31:5003–9.
[142] Zhang Newby B, Wakabayashi K, Composto RJ. Confinement induced stabilization in polymer blend thin films. Polymer 2001;42:9155–62.
[143] Wang H, Composto RJ, Hobbie EK, Han CC. Multiple lateral length scales in phase-separating thin-film polymer blends. Langmuir 2001;17:2857–60.
[144] Gutmann JS, Müller-Buschbaum P, Stamm M. Complex pattern formation by phase separation of polymer blends in thin films. Faraday Discuss 1999;112:285–97.
[145] Wendlandt M, Kerle T, Heuberger M, Klein J. Phase separation in thin films of polymer blends: the influence of symmetric boundary conditions. J Polym Sci, Part B: Polym Phys 2000;38:831–7.
[146] Flebbe T, Dünweg B, Binder K. Phase separation versus wetting: a mean field theory for symmetrical polymer mixtures confined between selectively attractive walls. J Phys II 1995;6:667–95.
[147] Karim A, Slawecki TM, Kumar SK, Douglas JF, Satija SK, Han CC, Russell TP, Liu Y, Overney R, Sokolov J, Rafailovich MH. Phase-separation induced surface patterns in thin polymer blend films. Macromolecules 1998;31:57–62.
[148] Svoboda P, Kressler J, Inoue T. Crystalline morphology in polymer blends via competition with spinodal decomposition. J Macromol Sci: Phys 1996;B35:505–25.
[149] Svoboda P, Keyzlarová L, Sáha P, Rybnikář F, Chiba T, Inoue T. Spinodal decomposition and succeeding crystallization in PCL/SAN blends. Polymer 1999;40:1459–63.
[150] Moffitt M, Rharbi Y, Li H, Winnik MA. Novel morphology evolution in thick films of a polymer blend. Macromolecules 2002;35:3321–4.
[151] Pron A, Rannou P. Processible conjugated polymers: from organic semiconductors to organic metals and superconductors. Prog Polym Sci 2002;27:135–90.
[152] Kawase T, Sirringhaus H, Friend RH, Shimoda T. Inkjet printed via-hole interconnections and resistors for all-polymer transistor circuits. Adv Mater 2001;13:2001.
[153] Sirringhaus H, Kawase T, Friend RH, Shimoda T, Inbasekaran M, Wu W, Woo EP. High-resolution inkjet printing of all-polymer transistor circuits. Science 2000;290:2123–6.
[154] van Hutten PF, Krasnikov VV, Hadziioannou G. Role of interfaces in semiconducting polymer optoelectronic devices. In: Salaneck WR, Seki K, Kahn A, Pireaux J-J, editors. Conjugated polymer and molecular interfaces. New York: Marcel Dekker; 2001. p. 113–52.
[155] Halls JJM, Pichler K, Friend RH, Moratti SC, Holmes AB. Exciton diffusion and dissociation in a poly(*p*-phenylenevinylene)/C_{60} heterojunction photovoltaic cell. Appl Phys Lett 1996;68:3120–2.
[156] Mullins WW, Sekerka RF. Stability of a planar interface during solidification of a dilute binary alloy. J Appl Phys 1964;35:444–51.
[157] Ho PKH, Kim J-S, Burroughes JH, Becker H, Li SFY, Brown TM, Cacialli F, Friend RH. Molecular-scale interface engineering for polymer light-emitting diodes. Nature 2000;404:481–4.
[158] Greczynski G, Kugler T, Salaneck WR. Characterization of the PEDOT–PSS system by means of X-ray and ultraviolet photoelectron spectroscopy. Thin Solid Films 1999;354:129–35.
[159] Jukes PC. Grazing incidence X-ray diffraction and neutron reflection studies of semi-crystalline polymer surfaces and interfaces. PhD Thesis. University of Sheffield; 2002.
[160] Arias AC, MacKenzie JD, Stevenson R, Halls JJM, Inbasekaran M, Woo EP, Richards D, Friend RH. Photovoltaic performance and morphology of polyfluorene blends: a combined microscopic and photovoltaic investigation. Macromolecules 2001;34:6005–13.
[161] Arias AC. Conjugated polymer phase separation and three-dimensional thin-film structure for photovoltaics. PhD Thesis. University of Cambridge; 2001.
[162] Arias AC, Corcoran N, Banach M, Friend RH, MacKenzie JD, Huck WTS. Vertically segregated polymer-blend photovoltaic thin-film structures through surface-mediated solution processing. Appl Phys Lett 2002;80:1695–7.
[163] Morgado J, Moons E, Friend RH, Cacialli F. De-mixing of polyfluorene-based blends by contact with acetone: electro- and photo-luminescence probes. Adv Mater 2001;13:810–4.
[164] Krausch G. Dewetting at the interface between two immiscible polymers. J Phys: Condens Matter 1997;9:7741–52.
[165] Findenegg GH, Herminghaus S. Wetting: statics and dynamics. Curr Opin Colloid Interf Sci 1997;2:301.
[166] Seemann R, Herminghaus S, Jacobs K. Gaining control of pattern formation of dewetting liquid films. J Phys: Condens Matter 2001;13:4925–38.
[167] Maas JH, Cohen Stuart MA, Leermakers FAM, Besseling NAM. Wetting transition in a polymer brush: polymer droplet coexisting with two film thicknesses. Langmuir 2000;16:3478–81.
[168] Liu Y, Rafailovich MH, Sokolov J, Schwarz SA, Zhong X, Eisenberg A, Kramer EJ, Sauer BB, Satija SK. Wetting behavior of homopolymer films on chemically similar block copolymer surfaces. Phys Rev Lett 1994;73:440–3.
[169] Bergeron V, Bonn D, Martin JY, Vovelle L. Controlling droplet deposition with polymer additives. Nature 2000;405:772–5. see also Klein J. Smart polymer solutions. Nature 2000;405:745.
[170] Steinhart M, Wendorff JH, Greiner A, Wehrspohn RB, Nielsch K, Schilling J, Choi J, Gösele U. Polymer nanotubes by wetting of ordered porous templates. Science 2002;296:1997.
[171] Aussillous P, Quéré D. Liquid marbles. Nature 2001;411:

924–7. see also Mahadevan L. Non-stick water. Nature 2001;411:895.
[172] Bico J, Marzolin C, Quéré D. Pearl drops. Europhys Lett 1999;47:220–6.
[173] Reiter G. Dewetting of thin polymer films. Phys Rev Lett 1992;68:75–8.
[174] Brochard Wyart F, Daillant J. Drying of solids wetted by thin liquid films. Can J Phys 1990;68:1084–8.
[175] Israelachvili JN. Intermolecular and surface forces. London: Academic Press; 1991.
[176] Suh KY, Park J, Lee HH. Controlled polymer dewetting by physical confinement. J Chem Phys 2002;116:7714–8.
[177] Bischof J, Scherer D, Herminghaus S, Leiderer P. Dewetting modes of thin metallic films: nucleation of holes and spinodal dewetting. Phys Rev Lett 1996;77:1536–9.
[178] Xie R, Karim A, Douglas JF, Han CC, Weiss RA. Spinodal dewetting of thin polymer films. Phys Rev Lett 1998;81: 1251–4.
[179] Jacobs K, Herminghaus S, Mecke KR. Thin liquid polymer films rupture via defects. Langmuir 1998;14:965–9.
[180] Karapanagiotis I, Evans DF, Gerberich WW. Leveling and dewetting processes of nanoindentation-induced defects on thin polymer films. Macromolecules 2001;34:3741–7.
[181] Karapanagiotis I, Evans DF, Gerberich WW. Nucleation processes for dewetting initiation of thin polymer films. Langmuir 2001;17:3266–72.
[182] Karapanagiotis I, Gerberich WW, Evans DF. Early dewetting stages of thin polymer films initiated by nanoindentation. Langmuir 2001;17:2375–9.
[183] Müller-Buschbaum P, Gutmann JS, Stamm M. Dewetting of confined polymer films: an X-ray and neutron scattering study. Phys Chem, Chem Phys 1999;1:3857–63.
[184] Müller-Buschbaum P, Vanhoorne P, Scheumann V, Stamm M. Observation of nano-dewetting structures. Europhys Lett 1997;40:655–60.
[185] Rehse N, Wang C, Hund M, Geoghegan M, Magerle R, Krausch G. Stability of thin polymer films on a corrugated substrate. Eur Phys J E 2001;4:69–76.
[186] Seemann R, Herminghaus S, Jacobs K. Dewetting patterns and molecular forces: a reconciliation. Phys Rev Lett 2001; 86:5534–7.
[187] Sharma A, Reiter G. Instability of thin polymer films on coated substrates: rupture, dewetting, and drop formation. J Colloid Interf Sci 1996;178:383–99.
[188] Seemann R, Herminghaus S, Jacobs K. Shape of a liquid front upon dewetting. Phys Rev Lett 2001;87:196101.
[189] Müller M, MacDowell LG, Müller-Buschbaum P, Wunnike O, Stamm M. Nano-dewetting: interplay between van der Waals- and short-ranged interactions. J Chem Phys 2001; 115:9960–9.
[190] Masson J-L, Green PF. Hole formation in thin polymer films: a two-stage process. Phys Rev Lett 2002;88:205504.
[191] Higgins AM, Sferrazza M, Jones RAL, Jukes PC, Sharp JS, Dryden LE, Webster J. The timescale of spinodal dewetting at a polymer/polymer interface. Eur Phys J E 2002;8: 137–43.
[192] Kargupta K, Konnur R, Sharma A. Instability and pattern formation in thin liquid films on chemically heterogeneous substrates. Langmuir 2000;16:10243–53.
[193] Kargupta K, Konnur R, Sharma A. Spontaneous dewetting and ordered patterns in evaporating thin liquid films on homogeneous and heterogeneous substrates. Langmuir 2001; 17:1294–305.
[194] Khanna R, Sharma A. Pattern formation in spontaneous dewetting of thin apolar films. J Colloid Interf Sci 1997;195: 42–50.
[195] Sharma A, Khanna R. Pattern formation in unstable thin liquid films. Phys Rev Lett 1998;81:3463–6.
[196] Sharma A, Khanna R. Pattern formation in unstable thin liquid films under the influence of antagonistic short- and long-range forces. J Chem Phys 1999;110:4929–36.
[197] Higgins AM, Jones RAL. Anisotropic spinodal dewetting as a route to self-assembly of patterned surfaces. Nature 2000; 404:476–8.
[198] Kargupta K, Sharma A. Templating of thin films induced by dewetting on patterned surfaces. Phys Rev Lett 2001;86: 4536–9.
[199] Konnur R, Kargupta K, Sharma A. Instability and morphology of thin liquid films on chemically heterogeneous substrates. Phys Rev Lett 2000;84:931–4.
[200] Kargupta K, Sharma A. Morphological self-organization by dewetting in thin films on chemically patterned substrates. J Chem Phys 2002;116:3042–51.
[201] Kargupta K, Sharma A. Dewetting of thin films on periodic physically and chemically patterned surfaces. Langmuir 2002;18:1893–903.
[202] Reiter G. Dewetting of highly elastic thin polymer films. Phys Rev Lett 2001;87:186101.
[203] Shenoy V, Sharma A. Dewetting of glassy polymer films. Phys Rev Lett 2002;88:236101.
[204] Saulnier F, Raphaël E, de Gennes P-G. Dewetting of thin polymer films near the glass transition. Phys Rev Lett 2002; 88:196101.
[205] Reiter G, Khanna R, Sharma A. Enhanced instability in thin liquid films by improved compatibility. Phys Rev Lett 2000; 85:1432–5.
[206] Reiter G, Sharma A, Casoli A, David M-O, Khanna R, Auroy P. Thin film instability induced by long-range forces. Langmuir 1999;15:2551–8.
[207] Reiter G, Sharma A, Khanna R, Casoli A, David M-O. The strength of long-range forces across thin liquid films. J Colloid Interf Sci 1999;214:126–8.
[208] Reiter G, Sharma A, Casoli A, David M-O, Khanna R, Auroy P. Destabilizing effect of long-range forces in thin liquid films on *wettable* substrates. Europhys Lett 1999;46:512–8.
[209] David MO, Reiter G, Sitthaï T, Schultz J. Deformation of a glassy polymer film by long-range intermolecular forces. Langmuir 1998;14:5667–72.
[210] Oslanec R, Costa AC, Composto RJ, Vlcek P. Effect of block copolymer adsorption on thin film dewetting kinetics. Macromolecules 2000;33:5505–12.
[211] Debrégeas G, de Gennes P-G, Brochard-Wyart F. The life and death of bare viscous bubbles. Science 1998;279: 1704–7.
[212] Debrégeas G, Martin P, Brochard-Wyart F. Viscous bursting of suspended films. Phys Rev Lett 1995;75:3886–9.
[213] Dalnoki-Veress K, Nickel BG, Roth C, Dutcher JR. Hole formation and growth in freely standing polystyrene films. Phys Rev E 1999;59:2153–6.
[214] Dalnoki-Veress K, Forrest JA, Dutcher JR. Mechanical confinement effects on the phase separation morphology of polymer blend thin films. Phys Rev E 1998;57:5811–7.

[215] Dalnoki-Veress K, Nickel BG, Dutcher JR. Dispersion-driven morphology of mechanically confined polymer films. Phys Rev Lett 1999;82:1486–9.
[216] Martin A, Rossier O, Buguin A, Auroy P, Brochard-Wyart F. Spinodal dewetting of thin liquid films at soft interfaces. Eur Phys J E 2000;3:337–41.
[217] Shenoy V, Sharma A. Pattern formation in a thin solid film with interactions. Phys Rev Lett 2001;86:119–22.
[218] Martin A, Buguin A, Brochard-Wyart F. Dewetting nucleation centers at soft interfaces. Langmuir 2001;17:6553–9.
[219] Young T. An essay on the cohesion of fluids. Phil Trans R Soc Lond 1805;95:65–87.
[220] Redon C, Brochard-Wyart F, Rondelez F. Dynamics of dewetting. Phys Rev Lett 1991;66:715–8.
[221] Segalman RA, Green PF. Dynamics of rims and the onset of spinodal dewetting at liquid/liquid interfaces. Macromolecules 1999;32:801–7.
[222] Jacobs K, Seemann R, Schatz G, Herminghaus S. Growth of holes in liquid films with partial slippage. Langmuir 1998;14:4961–3.
[223] Qu S, Clarke CJ, Liu Y, Rafailovich MH, Sokolov J, Phelan KC, Krausch G. Dewetting dynamics at a polymer–polymer interface. Macromolecules 1997;30:3640–5.
[224] Wang C, Krausch G, Geoghegan M. Dewetting at a polymer–polymer interface: film thickness dependence. Langmuir 2001;17:6269–74.
[225] Faldi A, Composto RJ, Winey KI. Unstable polymer bilayers. 1. Morphology of dewetting. Langmuir 1995;11:4855–61.
[226] Pan Q, Winey KI, Hu HH, Composto RJ. Unstable polymer bilayers. 2. The effect of film thickness. Langmuir 1997;13:1758–66.
[227] Edgecombe SR, Gardiner JM, Matsen MW. Suppressing autophobic dewetting by using a bimodal brush. Macromolecules 2002;35:6475–7.
[228] Reiter G, Auroy P, Auvray L. Instabilities of thin polymer films on layers of chemically identical grafted molecules. Macromolecules 1996;29:2150–7.
[229] Voronov A, Shafranska O. Synthesis of chemically grafted polystyrene brushes and their influence on the dewetting in thin polystyrene films. Langmuir 2002;18:4471–7.
[230] Kerle T, Yerushalmi-Rozen R, Klein J. Cross-link-induced autophobicity in polymer melts: a re-entrant wetting transition. Europhys Lett 1997;38:207–12.
[231] Kerle T, Yerushalmi-Rozen R, Klein J. Wetting and autophobicity of a polymer melt on a network of itself. Macromolecules 1998;31:422–9.
[232] Russ T, Brenn R, Abel F, Boué F, Geoghegan M. Reptation and interdiffusion in polystyrene networks. Eur Phys J E 2001;4:419–33.
[233] Klaumünzer S, Zhu QQ, Schnabel W, Schumacher G. Ion-beam-induced crosslinking of polystyrene—still an unsolved puzzle. Nucl Instr Meth B 1996;116:154–8.
[234] Reiter G, Khanna R. Kinetics of autophobic dewetting of polymer films. Langmuir 2000;16:6351–7.
[235] Reiter G, Khanna R. Real-time determination of the slippage length in autophobic polymer dewetting. Phys Rev Lett 2000;85:2753–6.
[236] Henn G, Bucknall DG, Stamm M, Vanhoorne P, Jérôme R. Chain end effects and dewetting in thin polymer films. Macromolecules 1996;29:4305–13.
[237] Zhao W, Rafailovich MH, Sokolov J, Fetters LJ, Plano R, Sanyal MK, Sinha SK, Sauer BB. Wetting properties of thin liquid polyethylene propylene films. Phys Rev Lett 1993;70:1453–6.
[238] Silberberg A. Distribution of conformations and chain ends near the surface of a melt of linear flexible macromolecules. J Colloid Interf Sci 1982;90:86–91.
[239] Semenov AN. Theory of long-range interactions in polymer systems. J Phys II 1996;6:1759–80.
[240] Müller M. Chain conformations and correlations in thin polymer films: a Monte Carlo study. J Chem Phys 2002;116:9930–8.
[241] Brûlet A, Boué F, Menelle A, Cotton JP. Conformation of polystyrene chain in ultrathin films obtained by spin coating. Macromolecules 2000;33:997–1001.
[242] Jones RL, Kumar SK, Ho DL, Briber RM, Russell TP. Chain conformation in ultrathin polymer films. Nature 1999;400:146–9.
[243] Jones RL, Kumar SK, Ho DL, Briber RM, Russell TP. Chain conformation in ultrathin polymer films using small-angle neutron scattering. Macromolecules 2001;34:559–67.
[244] Kraus J, Müller-Buschbaum P, Kuhlmann T, Schubert DW, Stamm M. Confinement effects on the chain conformation in thin polystyrene films. Europhys Lett 2000;49:210–6.
[245] Shuto K, Oishi Y, Kajiyama T. Non-equilibrium characteristics of a two-dimensional ultrathin film prepared by the water casting method. Polymer 1995;36:549–57.
[246] Wensink KDF, Jérôme B. Dewetting induced by density fluctuations. Langmuir 2002;18:413–6.
[247] Yerushalmi-Rozen R, Kerle T, Klein J. Alternative dewetting pathways of thin liquid films. Science 1999;285:1254–6.
[248] de Crevoisier G, Fabre P, Corpart J-M, Leibler L. Switchable tackiness and wettability of a liquid crystalline polymer. Science 1999;285:1246–9. see also Russell TP, Kim HC. Tack—a sticky subject. Science 1999;285:1219.
[249] Lin Z, Kerle T, Russell TP, Schäffer E, Steiner U. Electric field induced dewetting at polymer/polymer interfaces. Macromolecules 2002;35:6255–62.
[250] Abbott NL, Folkers JP, Whitesides GM. Manipulation of the wettability of surfaces on the 0.1- to 1-micrometer scale through micromachining and molecular self-assembly. Science 1992;257:1380–2.
[251] Biebuyck HA, Whitesides GM. Self-organisation of organic liquids on patterned self-assembled monolayers of alkanethiolates on gold. Langmuir 1994;10:2790–3.
[252] Gau H, Herminghaus S, Lenz P, Lipowsky R. Liquid morphologies on structured surfaces: from microchannels to microchips. Science 1999;283:46–9. see also Grunze M. Driven liquids. Science 1999;283:41.
[253] Swain PS, Lipowsky R. Wetting between structured surfaces: liquid bridges and induced forces. Europhys Lett 2000;49:203–9.
[254] Karim A, Douglas JF, Lee BP, Glotzer SC, Rogers JA, Jackman RJ, Amis EJ, Whitesides GM. Phase separation of ultrathin polymer-blend films on patterned substrates. Phys Rev E 1998;57:R6723–6.
[255] Ermi BD, Nisato G, Douglas JF, Rogers JA, Karim A. Coupling between phase separation and surface deformation modes in self-organizing polymer blend films. Phys Rev Lett 1998;81:3900–3.
[256] Nisato G, Ermi BD, Douglas JF, Karim A. Excitation of surface deformation modes of a phase-separating polymer

blend on a patterned substrate. Macromolecules 1999;32: 2356–64.
[257] Cyganik P, Bernasik A, Budkowski A, Bergues B, Kowalski K, Rysz J, Lekki J, Lekka M, Postawa Z. Phase decomposition in polymer blend films cast on substrates patterned with self-assembled monolayers. Vacuum 2001;63:307–13.
[258] Song S, Mochrie SGJ. Tricriticality in the orientational phase diagram of stepped Si(113) surfaces. Phys Rev Lett 1994;73: 995–8.
[259] Song S, Mochrie SGJ. Attractive step–step interactions, tricriticality, and faceting in the orientational phase diagram of silicon surfaces between [113] and [114]. Phys Rev B 1995;51:10068–84.
[260] Song S, Mochrie SGJ, Stephenson GB. Faceting kinetics of stepped Si(113) surfaces: a time resolved X-ray scattering study. Phys Rev Lett 1995;74:5240–3.
[261] Fasolka MJ, Harris DJ, Mayes AM, Yoon M, Mochrie SGJ. Observed substrate topography-mediated lateral patterning of diblock copolymer films. Phys Rev Lett 1997;79:3018–21.
[262] Rockford L, Mochrie SGJ, Russell TP. Propagation of nanopatterned substrate templated ordering of block copolymers in thick films. Macromolecules 2001;34:1487–92.
[263] Russell TP, Coulon G, Deline VR, Miller DC. Characteristics of the surface-induced orientation for symmetric diblock PS/PMMA copolymers. Macromolecules 1989;22:4600–6.
[264] Fukunaga K, Elbs H, Krausch G. Thin film phase separation on a nanoscopically patterned substrate. Langmuir 2000;16: 3474–7.
[265] Suh KY, Lee HH. Anistropic hole formation in thin polymer films confined by walls. J Chem Phys 2001;115:8204–8.
[266] Yoo PJ, Suh KY, Lee HH. Short- and long-range interactions in thin films of polymer blends in microchannels. Macromolecules 2002;35:3205–12.
[267] Schift H, Heyderman LJ, Auf der Maur M, Gobrecht J. Pattern formation in hot embossing of thin polymer films. Nanotechnology 2001;12:173–7.
[268] Zhang Newby B, Composto RJ. Phase-morphology map of polymer-blend thin films confined to narrow strips. Phys Rev Lett 2001;87:098302.
[269] Schäffer E, Thurn-Albrecht T, Russell TP, Steiner U. Electronically induced structure formation and pattern transfer. Nature 2000;403:874–7.
[270] Schäffer E, Thurn-Albrecht T, Russell TP, Steiner U. Electrohydrodynamic instabilities in polymer films. Europhys Lett 2001;53:518–24.
[271] Lin Z, Kerle T, Baker SM, Hoagland DA, Schäffer E, Steiner U, Russell TP. Electric field induced instabilities at liquid/liquid interfaces. J Chem Phys 2001;114:2377–81.
[272] Lin Z, Kerle T, Russell TP, Schäffer E, Steiner U. Structure formation at the interface of liquid/liquid bilayer in electric field. Macromolecules 2002;35:3971–6.
[273] Thurn-Albrecht T, DeRouchey J, Russell TP, Jaeger HM. Overcoming interfacial interactions with electric fields. Macromolecules 2000;33:3250–3.
[274] Thurn-Albrecht T, Steiner R, DeRouchey J, Stafford CM, Huang E, Bal M, Tuominen M, Hawker CJ, Russell TP. Nanoscopic templates from oriented block copolymer films. Adv Mater 2000;12:787–91.
[275] Thurn-Albrecht T, Schotter J, Kästle GA, Emley N, Shibauchi T, Krusin-Elbaum L, Guarini K, Black CT, Tuominen MT, Russell TP. Ultrahigh-density nanowire arrays grown in self-assembled diblock copolymer templates. Science 2000;290:2126–9.
[276] Chou SY, Zhuang L. Lithographically induced self-assembly of periodic polymer micropillar arrays. J Vac Sci Technol, B 1999;17:3197–202.
[277] Deshpande P, Sun X, Chou SY. Observation of dynamic behavior of lithographically induced self-assembly of supramolecular periodic pillar arrays in a homopolymer film. Appl Phys Lett 2001;79:1688–90.
[278] Yang SY, Rubner MF. Micropatterning of polymer thin films with pH-sensitive and cross-linkable hydrogen-bonded polyelectrolyte multilayers. J Am Chem Soc 2002;124:2100–1.
[279] Sharp JS, Jones RAL. Micro-buckling as a route towards surface patterning. Adv Mater 2002;14:799–802.
[280] van der Waals JD. Thermodynamische theorie der kapillarität unter Voraussetzung stetiger Dichteänderung. Z Phys Chem 1894;13:657–725. translated into English by Rowlinson JS. J Stat Phys 1979;20:197–244.
[281] Fredrickson GH. Theoretical methods for polymer surfaces and interfaces. In: Sanchez IC, editor. Physics of polymer surfaces and interfaces. Boston: Butterworth–Heinemann; 1992. p. 1–28.
[282] Riley KF. Mathematical methods for the physical sciences. Cambridge: Cambridge University Press; 1974. p. 332–40.
[283] Cohen SM, Muthukumar M. Critical wetting in two-component polymer blends. J Chem Phys 1989;90:5749–55.
[284] Hariharan A, Kumar SK. Surface segregation in binary polymer mixtures: a lattice model. Macromolecules 1991;24: 4909–17.
[285] Jerry RA, Nauman EB. Phase transitions in thin films of a binary mixture. Phys Lett A 1992;167:198–204.
[286] Jones RAL, Kramer EJ, Rafailovich M, Sokolov J, Schwarz SA. Surface enrichment in polymer blends: simple theory and an experimental test. In: DeKoven BM, Rosenberg R, Gellman AJ, editors. Interfaces between polymers, metals, and ceramics. Pittsburgh: Materials Research Society; 1989. p. 133–41.